Report No. OR 8394
Copy No.
Date: October 1966

RESEARCH ON OPTICAL PROPERTIES OF SINGLE CRYSTALS OF BETA PHASE SILICON CARBIDE

Summary Technical Report
5 May 1965 Through 5 June 1966

Dr. P. B. Pickar
Dr. J. S. Ziomek
H. D. Tiller

Project No.: FI-5-24955-01-GG-NG

Army MCMS Code No.: 5023.11.14200

Martin Marietta Corporation
Orlando, Florida

Contract No. DA-28-017-AMC-2002(A)

Prepared for

Engineering Sciences Laboratory
Feltman Research Laboratories
Picatinny Arsenal
Dover, New Jersey

Report No. OR 8394
Copy No.
Date: October 1966

RESEARCH ON OPTICAL PROPERTIES OF SINGLE CRYSTALS OF BETA PHASE SILICON CARBIDE

Summary Technical Report
5 May 1965 Through 5 June 1966

Dr. P. B. Pickar
Dr. J. S. Ziomek
H. D. Tiller

Project No.: FI-5-24955-01-GG-NG

Army MCMS Code No.: 5023.11.14200

Martin Marietta Corporation
Orlando, Florida

Contract No. DA-28-017-AMC-2002(A)

Prepared for

Engineering Sciences Laboratory
Feltman Research Laboratories
Picatinny Arsenal
Dover, New Jersey

FOREWORD

This summary technical report was prepared for the Engineering Sciences Laboratory, Feltman Research Laboratories, Picatinny Arsenal, Dover, New Jersey, by Martin Company, Martin-Marietta Corporation, Orlando, Florida. It describes work performed during the period 5 May 1965 through 5 June 1966, on Contract DA-28-017-AMC-2002(A) on Optical Properties of Beta Silicon Carbide.

The work was done in the Physical Sciences Laboratory, with support from the Design and Development group and, in particular, C. Joyce. The chief contributors to the program and their main interests, in addition to P. B. Pickar, J. S. Ziomek and H. D. Tiller, were D. A. Ringers, crystal growing; K. J. Russel, infrared and visible electroluminescence spectroscopy; D. L. Boone, absorption and reflection spectroscopy; W. D. Fountain, photoluminescence; and A. A. Boczar, hall voltage measurements and diode fabrication. We wish to acknowledge the services of M. Trache and J. Kitsen of the Prototype Model Shop for their contributions to the design and construction of special research equipment.

ABSTRACT

This research work on Beta Silicon Carbide dealt with several different attributes of this material. These studies included: 1) the electroluminescent spectra of point contact and alloyed junction diodes under forward and reverse bias in the visible and near infrared region; 2) square and sine wave modulation of this electroluminescence; 3) photostimulated emission at liquid nitrogen temperature under ultraviolet pumping; 4) absorption spectra in the visible and near infrared region at several different temperatures; 5) reflection spectra at room temperature at two angles of incidence. From these measurements at 5000 Å, the absorption coefficient was found to be on the order of $10^5 cm^{-1}$.

The method for preparing the samples for use in electroluminescent, absorption and reflection experiments is discussed.

Hall measurements on equivalent samples of β-SiC crystals used in this study showed electron carrier concentrations between 10^{17} and $10^{18}/cm^3$. Resistivities of these samples were found to be on the order of 0.1 to 1.0 ohm-cm.

Preliminary cyclotron resonance experiments employing 70 kMc excitation with super conducting magnets gave an "effective" mass of $m^*/m = 0.41 \pm 0.04$.

Preliminary data on the effect of neutron radiation on electrical diodes is discussed. Comparisons are made with several silicon diodes.

Extensive X-ray diffraction studies using both single crystal rotation techniques and Weissenberg techniques have been used to determine that the crystals under investigation were monocrystals.

Results from absorption and reflection data can, in gross features, be described in terms of the band model for this material.

CONTENTS

ILLUSTRATIONS

TABLES

I. ELECTROLUMINESCENT EMISSION STUDIES

A. EXPERIMENTAL ARRANGEMENT

1. Sample Preparation

a. Point Contact Diodes

The crystals used in the point contact electroluminescent studies were first selected from a group of crystals whose electron carrier concentration was estimated to be on the order of $2 \times 10^{18}/cm^3$. The major dopant in these crystals was nitrogen. These crystals were then ground into rectangular parallelepiped configurations by means of specially constructed jigs in a faceting machine. The crystals were first ground with 6μ diamond paste and then subsequently polished with 0.5μ diamond paste followed with Linde "A" polishing. The average size of these crystals was 1.5 mm wide by 1.5 mm thick by 2 mm long.

After the crystals were ground, they were etched in a solution of $HF\text{-}HNO_3$ to remove surface contaminants. Then they were given a final rinse in triply distilled deionized water and then in alcohol. After the final cleaning, the crystals were mounted in the holder (Figure 1). The crystals were mechanically held in place by the tungsten whisker under a force of several grams.

The point contact was made from 0.38 mm diameter tungsten wire etched down to 0.10 to 0.15 mm in diameter.

The temperature of the crystal when in operation was monitored by a thermocouple as seen in Figure 1.

b. Alloyed Junction Diodes

These crystals were ground, polished, and cleaned the same as those for the point contact diodes. They also had the same carrier concentration as the point contact diodes.

As shown in Figure 2, these crystals were mounted on the molybdenum posts 3/32 inch diameter by 1/4 inch long, which had first been ground on a lapping machine and then ultrasonically cleaned.

Using specially designed graphite susceptors to hold the molybdenum posts in an RF heated vacuum (10^{-6} torr) furnace, the crystals were bonded to the molybdenum posts by means of a gold-tantalum alloy. After this operation the crystals were again thoroughly cleaned. The last operation was the alloying of a junction into the base N type crystal of β-SiC. The alloying took place in the same furnace that was used for bonding the crystal to the post. An alloy of aluminum-silicon was used to produce the junction by heating at approximately 1200-1400°C for times varying from a few minutes to a few hours. After this operation the crystal was again cleaned and placed in the holder as shown in Figure 2. The electrical connection was made to the alloyed junction by means of an ultrasonic bonder. Two, 5, and 10 mil aluminum wires were used in these experiments with similar results (i.e. optical emission spectra).

2. Emission Spectra in the Visible and Near Infrared

Emission spectra of the optical diodes were recorded in the visible and near infrared using the equipment shown in Figure 3. The diodes were placed in a room temperature water cooled mount (or in a liquid nitrogen cooled mount) and then put in front of the entrance slit of the Perkin-Elmer Model 99 Monochromator. This monochromator uses a fused quartz prism with the dispersion curve given in Figure 4. The diodes were placed about 2 to 3 inches from the monochromator entrance slit, and the diode current was supplied by a constant current source (the current driver in Figure 3). Figure 5 shows a schematic circuit of the current driver.

The output of the monochromator was allowed to fall on an external detector. Two different photomultipliers were used as the external detectors. An RCA C-7268 photomultiplier (which has very high sensitivity) was used for most of the visible spectral measurements. Figure 6 shows the relative spectral sensitivity of this photomultiplier. The relative sensitivity of the entire monochromator system, which includes effects of prism dispersion and photomultiplier spectral sensitivity, was obtained by running the spectrum of a National Bureau of Standards (NBS) quartz-iodine tungsten filament standard lamp. By comparing this spectrum with the calibration of the standard lamp the relative sensitivity of the monochromator system was found (Figure 7). The output of the photomultiplier was applied to a Princeton Applied Research Model CR-4 low noise amplifier. The output of this amplifier went to a Princeton Applied Research Model JB-5 lock-in amplifier whose output was fed to a Leeds & Northrup Speedomax G recorder.

An RCA 7102 photomultiplier (liquid nitrogen cooled) was used to cover a range of wavelengths from the visible out to 1.2 to 1.3μ. Figure 8 is

the relative sensitivity curve for the RCA 7102 photomultiplier. The relative sensitivity of the monochromator system using the liquid nitrogen cooled RCA 7102 photomultiplier is shown in Figure 9. This was obtained by recording the spectrum of the NBS quartz-iodine standard and comparing it with the calibration curve of the standard.

The Perkin-Elmer Model 99 Monochromator also has an internally mounted lead sulfide cell detector for use in the 0.7 to 2.8μ region. Figure 10 is a block diagram of the equipment used to record the spectra when using the lead sulfide detector. The relative sensitivity of the lead sulfide cell is shown in Figure 11.

3. Emission Spectra in the Infrared

Infrared emission spectra of the silicon carbide diodes were taken using a standard Beckman IR-9 instrument. The diode (either point contact or alloyed junction) was mounted on a water cooled base in the sample compartment of the instrument. The instrument was operated in the single beam mode with a constant slit width. The spectral range covered was from 2.5 to 25μ.

4. Spectral Irradiance in the Visible

Spectral irradiance of the optical diode was measured using the equipment shown in Figure 3, with the addition that the optical diode on a water cooled mount was placed inside a 7 inch integrating sphere. The exit port of this sphere was placed in front of the entrance slit of the monochromator. A magnesium oxide coating was used on the inside of the integrating sphere. The secondary irradiance (that due to reflection from the sphere walls) of a source inside the sphere is proportional to the radiant flux of the source. The secondary spectral irradiance of the optical diode is then compared with the secondary spectral irradiance of a source of radiant flux calibrated against the NBS quartz-iodine standard of spectral irradiance. Fron this the spectral irradiance of the optical diode can be found. Light from a comparison lamp (GE type 328) was allowed to fall on a hole of known radius in the surface of the integrating sphere to furnish a source of radiant flux with which to compare the light from the diode. The comparison lamp was at a known distance from the hole and was operated at 200 mA current.

5. Sine Wave, Square Wave, and Pulse Response Tests

Figure 12 is a block diagram of equipment used in the sine and square wave response tests. The current modulator produced a sine or square wave of current through the diode depending on whether the square wave generator or sine wave generator was used. (Some of the data was obtained

with a Tektronix 555 oscilloscope and Type H plug-ins instead of the plug-in shown in Figure 12.)

For measurements in the visible the RCA C-7268 photomultiplier was used. In this case the diode was placed directly in front of the RCA C-7268 photomultiplier. For measurements in the near infrared an RCA 7102 photomultiplier was used. An optical filter was placed between the diode and the photomultiplier. For measurements in the infrared out to about 3μ the lead sulfide detector was used. It was removed from the monochromator and the diode placed directly in front of it. The Fluke 405B high voltage supply was not used with the lead sulfide detector.

In the square wave measurement the desired frequency was chosen, the square wave displayed on the oscilloscope and a picture taken of the display. In the sine wave measurements the peak-to-peak value of the current was set at the desired value on top of a dc bias. This value of current was held constant as the frequency was increased and the peak-to-peak value of the photomultiplier output (which was proportional to the photomultiplier current) was measured.

Sine wave modulation of the infrared output was examined using the equipment shown in Figure 12 except that the detector was a Texas Instrument Ge:Hg 76TC2 mercury doped germanium detector which is sensitive to radiation in the wavelength range of 2 to 14μ. The diode was placed in front of the Irtran II window on the detector.

Figure 13 illustrates the equipment used to try to detect pulses of infrared radiation due to pulses of current through the diode. The diode was placed in front of the Irtran II window of the detector and rectangular pulses of current injected into the diode with the diode pulser. The Hewlett Packard Pulse Generator furnished the rectangular pulse to the diode pulser. Figure 14 is the schematic circuit for the diode pulser. The signal from the mercury doped germanium detector and a signal proportional to the current pulse were displayed on the oscilloscope. In all of the sine wave, square wave, and pulse measurements the diode was on a room temperature water cooled mount.

6. Junction Capacitance Measurements

Qualitative values of junction capacitance for a few alloyed junction diodes were measured using an Electro Scientific Industries, Inc. Model 290A universal impedance bridge. Because of the relatively high leakage of the diodes, only one value of reverse voltage was used for each diode measurement. No external equipment was used with the bridge.

B. EXPERIMENTAL RESULTS AND DISCUSSION

1. Point Contact Diode Emission Spectra

a. Visible and Near Infrared

Emission spectra in the visible have been taken for many samples of silicon carbide using a point contact configuration, the point being tungsten wire etched to a fine point. Because samples from many different growth runs have been used, the emission spectra in the visible have about as many differences as there have been crystals used. However, in most instances, these differences have been in degree of luminescent intensity at a particular emission wavelength rather than in the position in energy of the emissi n band. One series of curves for a point contact diode was given in the second quarterly report and are reprcduced here (Figure 15). Figures 16 and 17 are plots of the recorder tracings of another point contact diode, these curves being representative of the behavior of many of the crystals used. Both figures are for the same crystal, the only difference between the two figures being the gain setting of the Princeton Applied Research JB-5 amplifier. The slit setting of the monochromator was the same for both figures. The diameter of the tungsten probe that actually contacted the crystal was approximately 0.1 mm in diameter. From this the current densities can be calculated. Table I is a summary of characteristics for Figures 16 and 17. The temperatures given were taken from a thermocouple mounted in the copper block on which the crystal was resting, the thermocouple being approximately 5 mm from the crystal. The crystal itself, and especially the top surface of the crystal, is certainly at a higher temperature, but this difference was not determined.

Some of the point contact diodes were run at near liquid nitrogen temperature. Figure 18 is a tracing of one crystal at or somewhat above room temperature and at near liquid nitrogen temperature. The current for both curves is the same but the voltage had to be increased at liquid nitrogen temperature. The difference in intensity of the two curves has no significance because of the difference in gain settings of the instrument.

It should be noted that all of these curves were taken directly from the recorder tracings and, therefore, have not been corrected for the monochromator system's sensitivity characteristics. The curves necessary for this correction are given elsewhere in this report (Figures 6 and 7).

To observe any possible electroluminescent emission bands in the near infrared (1 to 3μ), the same monochromator system was used with

TABLE I

Point Contact Emission Spectra Data

Curve No.	I(mA)	I/A (A/cm^2)	(Arbitrary Units) Amp Gain	Temp (°C)
1	10	130	1.0	20
2	20	260	1.0	20
3	30	390	1.0	20
4	40	520	1.0	20
5	10	130	0.5	17
6	20	260	0.5	18
7	50	650	0.5	21
8	70	910	0.5	25
9	100	1300	0.5	32
10	140	1800	0.5	37
11	160	2100	0.5	42
12	180	2300	0.5	47

the exception of the detector; a lead sulfide detector supplied by Perkin-Elmer Corporation being substituted for the photomultiplier tube. It was found that the diodes did emit in this region. However, it had to be determined if this was luminescent emission or merely "black body" radiation. Figure 19 shows, among other things, a typical emission with wavelength tracing obtained in 1 to 3μ region using a point contact diode. Plotted on the same scale is an approximate sensitivity curve of a lead sulfide detector operating at room temperature. Also shown are two other curves: one a tracing, using a PbS detector, of a tungsten filament lamp and the other of a Perkin-Elmer Corporation globar source. All of these are for constant slit settings for each curve, although each curve may have a different slit setting from the others.

The depressions in the emission curves are due to atmospheric and quartz prism absorption. As would be expected, the tungsten source peaks nearer the visible, because of its higher color temperature, the globar peaking at lower energy. The diode emission curve consists of the one maxima only, this being at lower energy than the other two sources. No other emission bands have been observed in this spectral region. On the basis of a comparison of the diode emission "band" and the emission observed from the tungsten and globar sources, it is concluded that in the region of 1 to 3μ, and in the sensitivity limit of the monochromator system, there is no detectable electroluminescent emission. This conclusion is substantiated in the case of the alloyed junction diodes by frequency response measurements.

b. Infrared

Figure 20, Curve (c), shows a typical trace obtained on the Beckman IR-9 infrared spectrophotometer of a silicon carbide point contact diode. This graph is representative of the many crystals studied. The spectrophotometer was operated in a single beam mode and at the slit width noted in the figure. Curve (c) of Figure 20 is a trace from the instrument, in the single beam mode, from the raw data, and no corrections have been made for the varying sensitivity of the instrument with wavelength. A discussion of this representative curve is included in a following section on infrared emission of alloyed junction diodes.

2. Alloyed Junction Diodes

a. Emission spectra

1) Visible and Near Infrared

Using the RCA C-7268 photomultiplier with the experimental arrangement shown in Figure 3, electroluminescent spectra were obtained for two diodes under reverse bias and using room temperature water cooling. The spectra of the diodes are uncorrected for the response of the photomultiplier and monochromator. Figure 21 is the spectrum of L-104 and Figure 22 is the spectrum of L-110. Using the same apparatus, forward bias electroluminescent spectra were obtained for L-110 for several values of current through the diode. Again the diode was on a room-temperature water cooled mount. Figure 23 shows the forward bias spectra of L-110.

The forward and reverse bias spectra of diode L-110 were recorded using the liquid nitrogen cooled RCA 7102 photomultiplier. This detector allows observation of the spectra in the near infrared. The diode was in a room temperature water colled mount. Figure 24 is the reverse bias spectrum of diode L-110. Figure 25 is the forward bias spectra from diode L-110 for different currents through the diode.

Using the lead sulfide detector and the equipment shown in Figure 10, the spectrum of diode L-102 was recorded for an input power to the diode of 12.8 watts. The diode was under reverse bias and in a room temperature water cooled mount. Figure 26 is the spectrum obtained for diode L-102.

Using the apparatus shown in Figure 3, including the RCA C-7268 photomultiplier detector, the change of optical diode spectrum with temperature was investigated. Diode L-113 was placed in a mount capable of

being cooled by either water or liquid nitrogen. The diode mount is fastened to a copper plate which forms the bottom of the center container of a metal dewar. The diode can be placed to emit through either a quartz or an Irtran II window, both being mounted in the outer wall of the dewar. The quartz window was used in this experiment. Figure 27 is a spectrum of L-113 with the dewar filled with room temperature water. The spectrum in Figure 28 was run for L-113 with the dewar filled with liquid nitrogen. The change in optical output is readily apparent. The low temperature run shows the spectrum shape slightly changed and the diode to be a more intense source for approximately the same input power.

The spectra in the preceding paragraph in this section are not corrected for the detector and monochromator response.

2) Infrared

Figure 20, Curve (d), is a tracing of the graph obtained on the IR-9 spectrophtometer of a typical alloyed junction diode. Curve (c) of the same figure is the emission of a point contact diode. The graphs of the apparent infrared emission from the two types of diodes appear similar. To get an idea of how the sensitivity of the instrument varied with wavelength, a graph was taken (Curve (b) Figure 20), in the single beam mode at a constant slit width, of the Nernst glower used as an emission source in the IR-9. It can be seen that it is very similar to the two diode emission curves. The Nernst glower curve peaks (due to dispersion and grating efficiencies) at an apparent wavelength of 3 to 3.5μ, the exact value being dependent on its color temperature. The vertical sections of all of the curves are easily explained since they occur at the order breaks of the instrument gratings, these being 5, 8.333 and 15μ. The depressions in the three emission curves at about 4.3, 6, and 6.6μ are due to atmospheric absorption. Curve (a) of Figure 20 is a plot of the IR-9 dispersion. To a rough approximation, higher values of dispersion will indicate a higher effective "gain" of the instrument for a constant slit width. Also shown in Figure 20 are the first and second order blaze frequencies for the two gratings used in the IR-9. Taking all of the preceding into consideration, it is concluded that the only detectable and reproducible emission from either the point contact or alloyed junction diode in the region 2.5 to 25μ is the "black body" emission peaking in the range of 2.5 to 5μ. This conclusion is further substantiated by the experiments on frequency modulation discussed in a later section.

b. Spectral Irradiance

Using the equipment shown in Figure 3, including the RCA C-7268 photomultiplier, with the addition that the diode is on a room temperature

water cooled mount inside a 7 inch integrating sphere, spectral irradiance of the diodes was measured. The secondary irradiance (that due to reflection from the sphere walls) of a source inside the sphere is proportional to the radiant flux of the source. The secondary spectral irradiance of the optical diode is then compared with the secondary spectral irradiance of a source of radiant flux (the comparison lamp) calibrated against the NBS quartz-iodine standard of spectral irradiance. In this manner the spectral irradiance of the optical diode can be found. Figure 29 shows the spectral irradiance found for L-104 under reverse bias with 16.5 watts input power. Calculating the area under the curve, the total power emitted by the diode in the 350 to 750 millimicron region can be found. This amounts to 0.256 microwatts for L-104.

c. Sine Wave, Square Wave, and Pulse Response Tests

Square wave modulation of L-109 was investigated using the apparatus shown in Figure 12. Figure 30 shows the square wave modulation for four frequencies. Peak diode current was 200 mA reverse bias. The lower trace is the diode current; increasing current is downward. The upper trace is proportional to the photomultiplier current. The rise time can be seen to be approximately 0.25 microsecond from the picture taken at 200 kc.

Square wave modulation of diode L-119 was investigated for both forward and reverse bias. Figure 31 is the square wave modulation of L-119 under forward bias. The upper beam is the current, increasing downward. A 800 mA peak-to-peak 60 cycle square wave was used. The lower beam is proportional to the photomultiplier output. The rise time is approximately 10 milliseconds for the forward bias case. The rise time bias behavior is likely to be temperature dependent. Figure 32 is the square wave modulation of L-119 under reverse bias. The upper beam is the current increasing downward. A 200 mA peak-to-peak, 50 kc square wave, was used. The lower beam is proportional to the photomultiplier current. The rise time of the lower trace is 4 microseconds and the decay time is 9 microseconds for reverse bias.

Sine wave modulation experiments were performed on diode L-120 using the apparatus shown in Figure 12. Forward and reverse bias cases were studied. For forward bias, the current through the diode was 48 mA peak-to-peak on a 350 mA dc bias. Figure 33 is a plot of photomultiplier current versus frequency. The current through the diode was 100 mA peak-to-peak on a 100 mA dc bias for the reverse bias measurement. Figure 34 is a plot of photomultiplier current versus frequency for reverse bias. From the two graphs the modulation under forward bias is poor compared with the reverse bias case.

Using the experimental arrangement shown in Figure 12 and the RCA 7102 photomultiplier, sine wave modulation measurements were made on diode L-104. In this case, however, Corning glass filters were inserted between the diode and the detector. The purpose of these filters was to prevent the shorter wavelengths of diode emission from reaching the detector. Table II gives the approximate bands of radiation that the photomultiplier-filter combination will respond to.

TABLE II

Corning Filter Transmission Bands

Filter No.	Bands (μ)
CS 2-64	0.64 to 1.2
CS 2-64 + 4-77	0.67 to 1.2
CS 7-69	0.71 to 1.12
CS 7-56	0.82 to 1.2

The transmission curves for the Corning filters are shown in Figure 35. The current through L-104 was 400 mA peak-to-peak on top of 300 mA dc reverse bias. Figures 36 and 37 are graphs of the photomultiplier current versus frequency, using the various filters. The high frequency response (falling off) is probably due to the measuring equipment. From this experiment the diode emission in the near infrared appears to be modulatable.

Sine wave modulation measurements were made on L-102 using the apparatus shown in Figure 12 with the lead sulfide detector. However, the phtomultiplier current was down considerably at 100 c/s and was essentially zero past 1000 c/s. The source of the signal was therefore assumed to be thermal.

Sine wave modulation of the emission from diode L-104 was examined using the equipment shown in Figure 12, except that the detector was the mercury doped germanium detector. The results were like those of the lead sulfide test, that is, the photomultiplier output was down considerably at 100 c/s and was zero past 1000 c/s. The source of the signal was therefore assumed to be thermal.

Modulation of diode emission in the infrared was tried unsuccessfully as mentioned above (emission could not be modulated at high frequencies) and electroluminescent emission in the infrared wavelength region 2 to 14μ had not been observed so an experiment was performed using the apparatus shown in Figure 13 to see if a pulse of current through

the diode would produce a corresponding pulse from the detector. A pulse width of about 15 microseconds was used; the pulse repetition rate was 50 p/s. Reverse bias currents of up to 4 A peak and forward bias currents up to 8 A peak were passed through diode L-121. For neither forward nor reverse bias was a pulse in phase with the current pulse received from the mercury doped germanium detector. Thus, no detectable electroluminescent emission existed in the infrared region covered by the detector (2 to 14μ).

d. Junction Capacitance Measurements

Information about the diode junction width or the length of the space charge region of the diode may be deduced from capacitance measurements of the junction at low reverse voltages. For a parallel plate capacitor:

$$C = \frac{KA}{4\pi\gamma L} \text{ (fds)}$$

where

C = capacitance in farads
K = dielectric constant of the material
A = area of the junction
γ = constant equal to 9×10^{11} cm/fd
L = width of the space charge region in cm.

Therefore

$$L = \left(\frac{K}{4\pi\gamma}\right)\left(\frac{A}{C}\right)$$

If we approximate the dielectric constant of silicon carbide as 10, we get

$$L \simeq 0.9 \times 10^{-12}\left(\frac{A}{C}\right) \text{ fd/cm}$$

using this expression (values of C varied from 400 to 4000 pf, values of A varied from 10^{-3} to 3×10^{-3} cm^2), values of L calculated varied from 0.01μ to about 0.1μ. These values must be taken as approximations only, due in part to the problem of relatively high reverse leakage current. Had it been possible to obtain capacitance values at more than one voltage, information about the junction gradient could have been deduced. However, it might be expected that the alloyed junctions used would have a high dopant gradient.

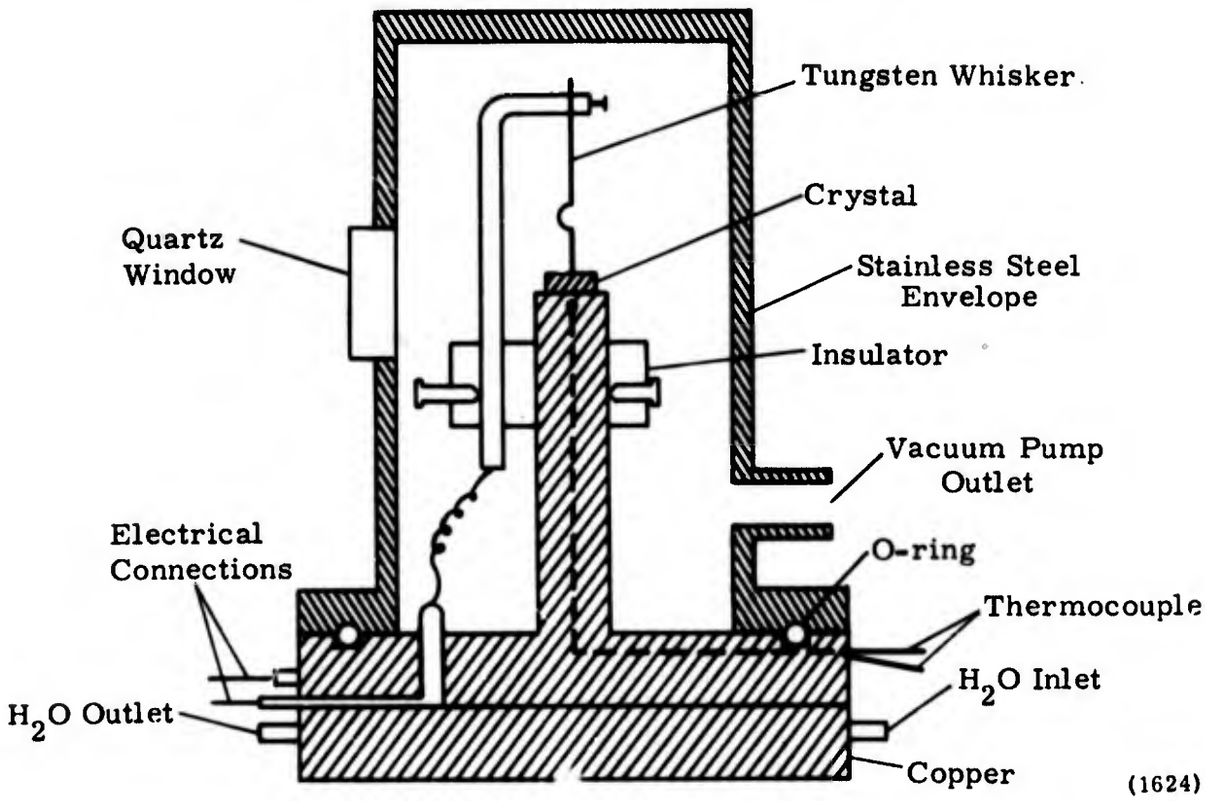

Figure 1. Point Contact Diode Mount

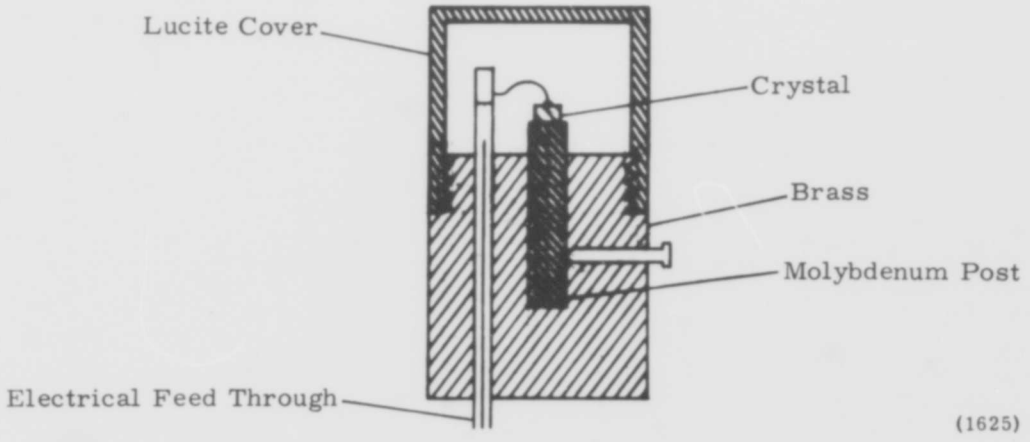

Figure 2. Alloyed Junction Diode Mount

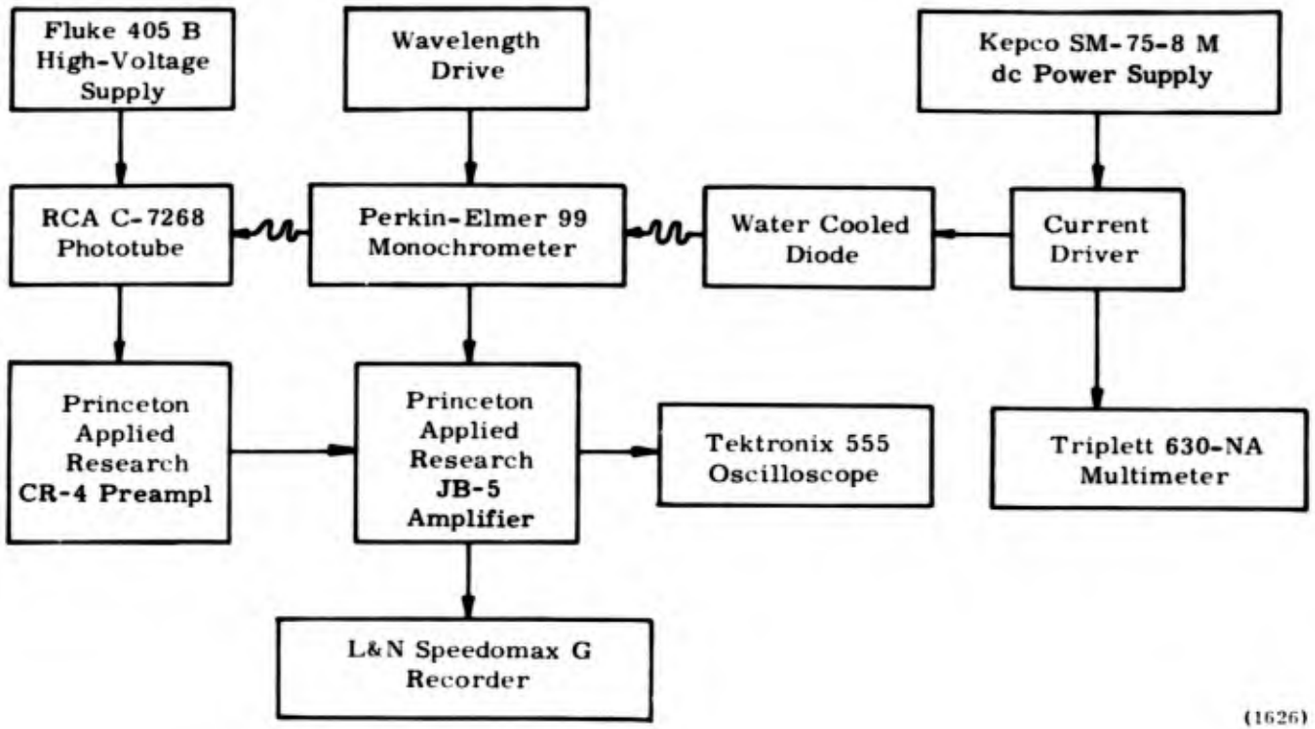

Figure 3. Spectrometer Diagram Using Photomultiplier Detector

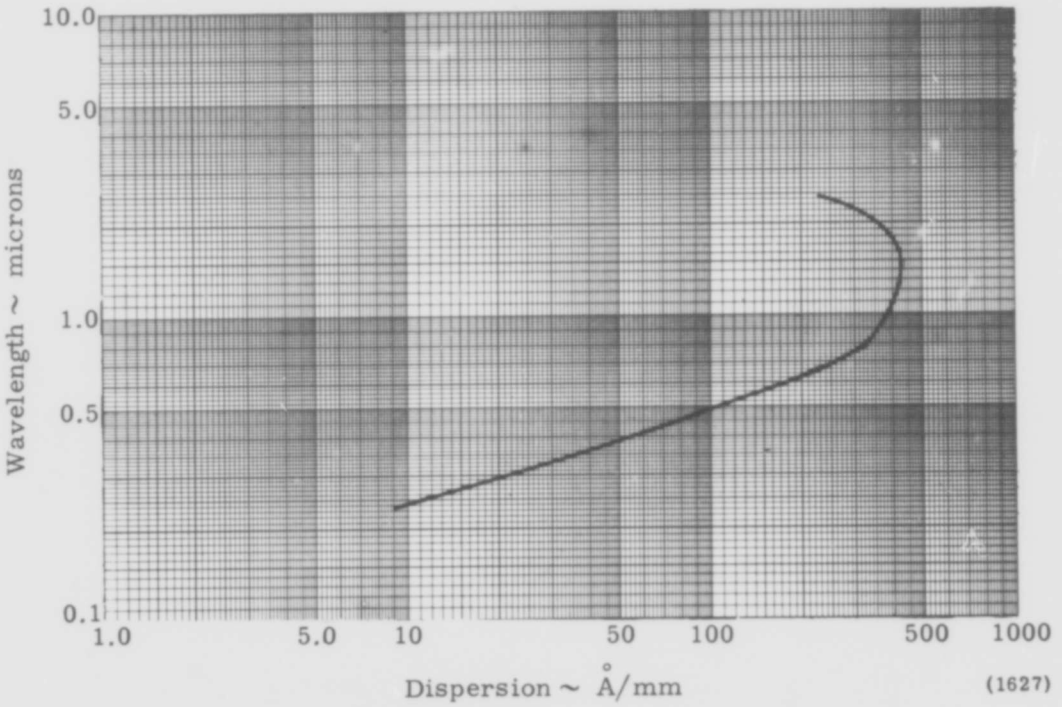

Figure 4. Linear Dispersion for Fused Quartz

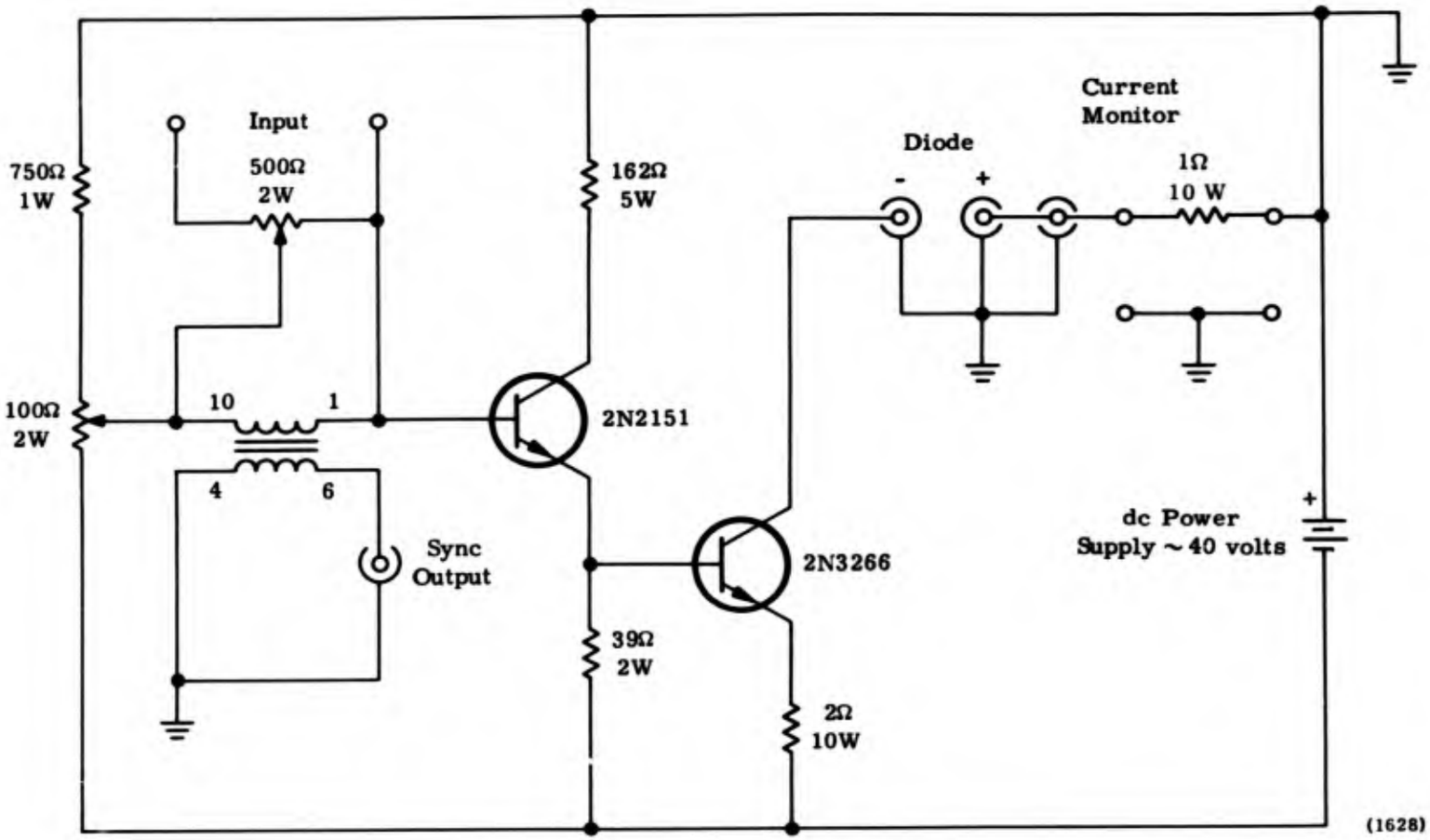

Figure 5. Current Modulator and Driver

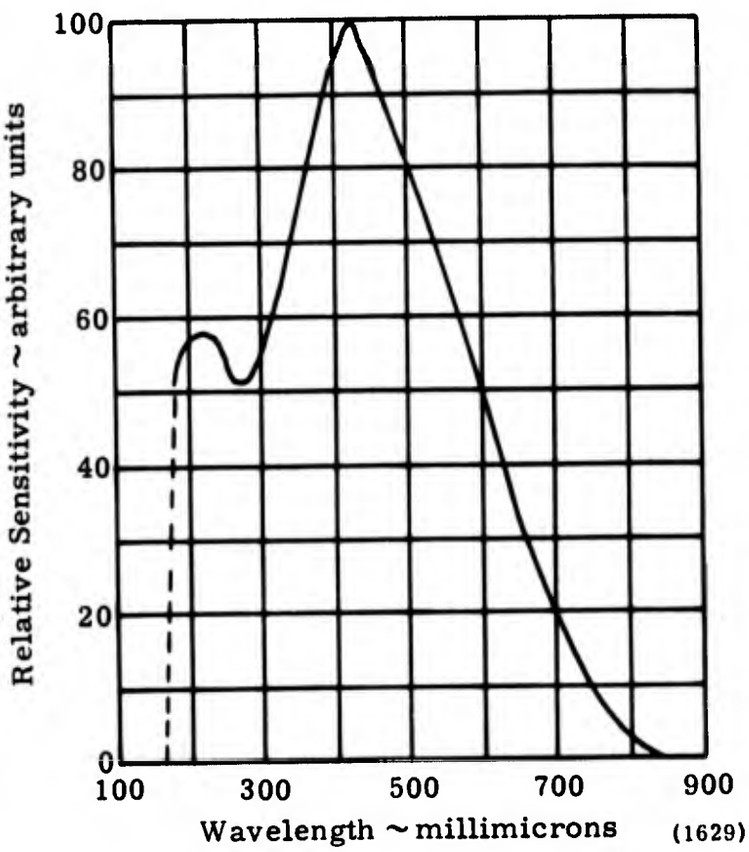

Figure 6. Relative Sensitivity of RCA C-7268 Photomultiplier

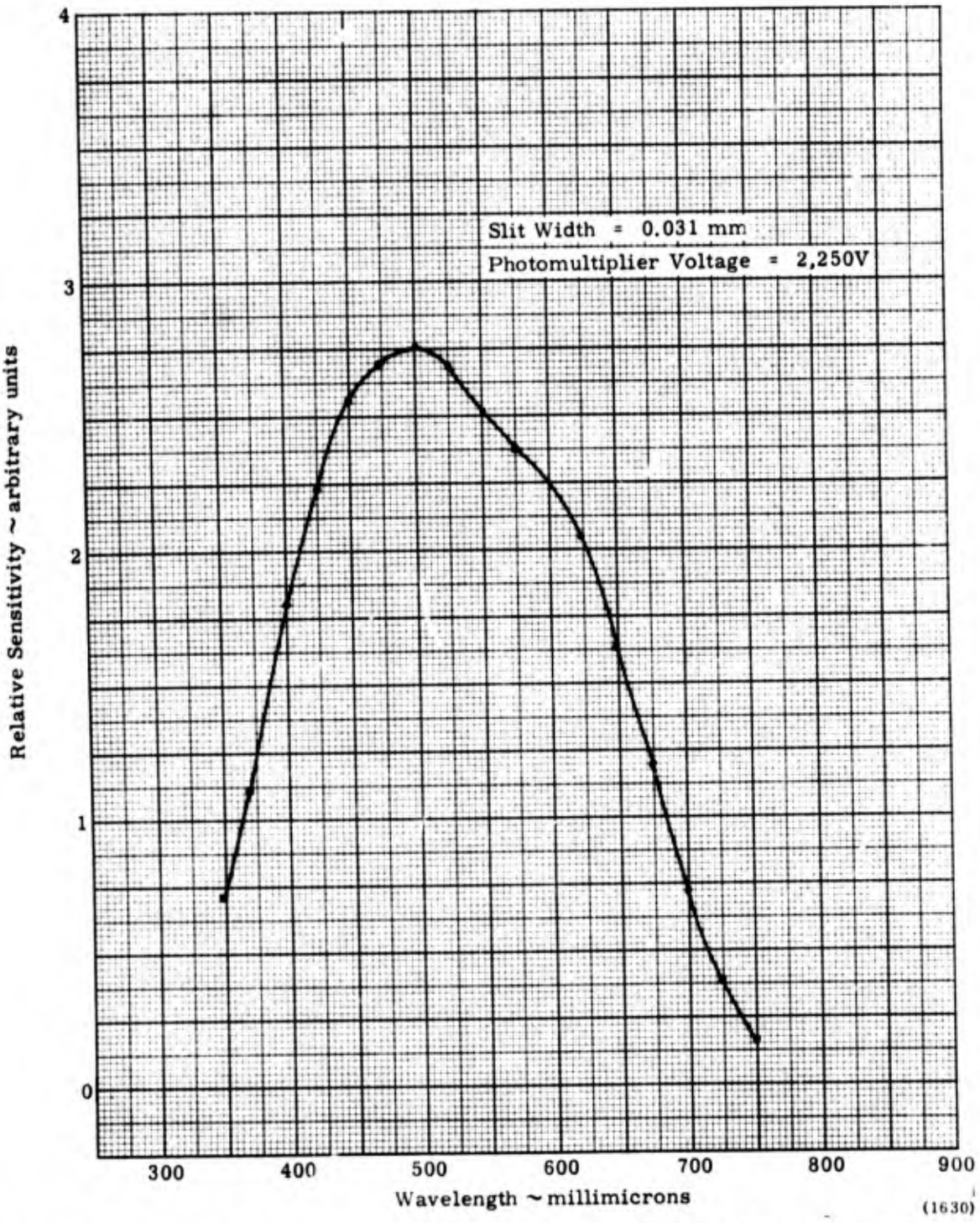

Figure 7. Relative Sensitivity of Monochromator and RCA C-7268 Photomultiplier

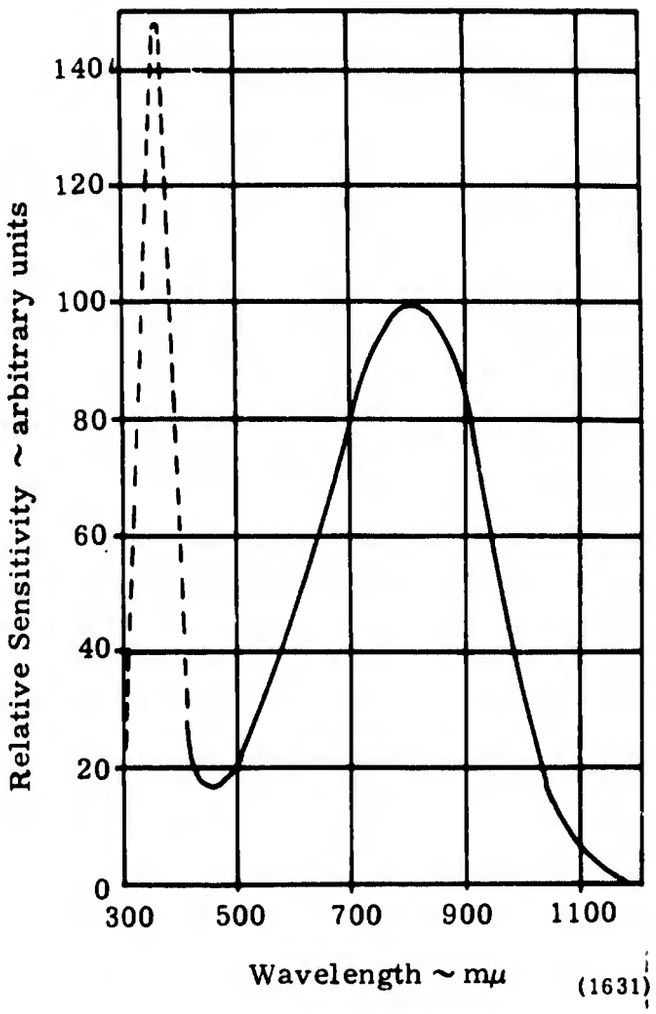

Figure 8. Spectral Sensitivity of RCA 7102 Photomultiplier

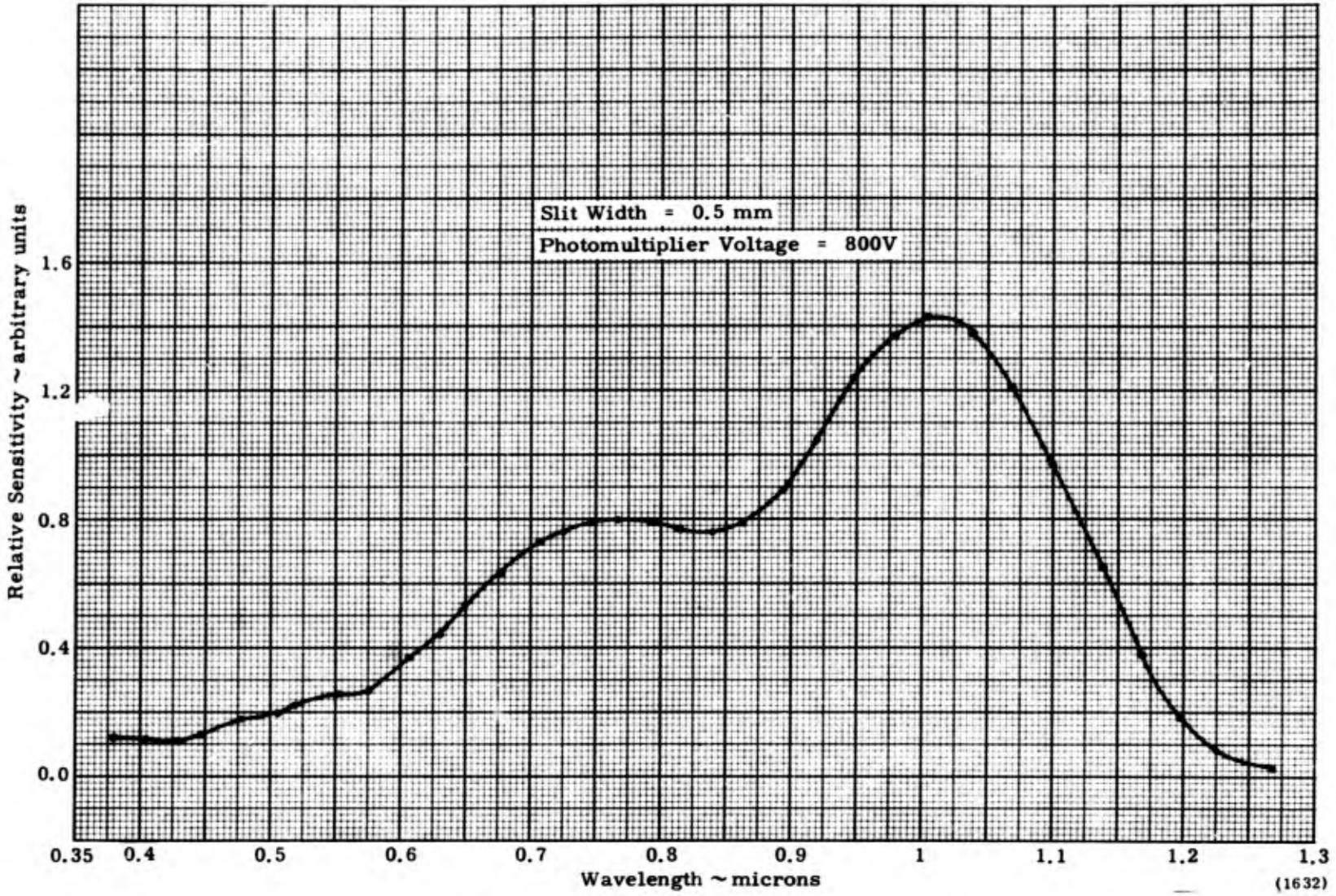

Figure 9. Relative Sensitivity of Monochromator and RCA 7102 Photomultiplier

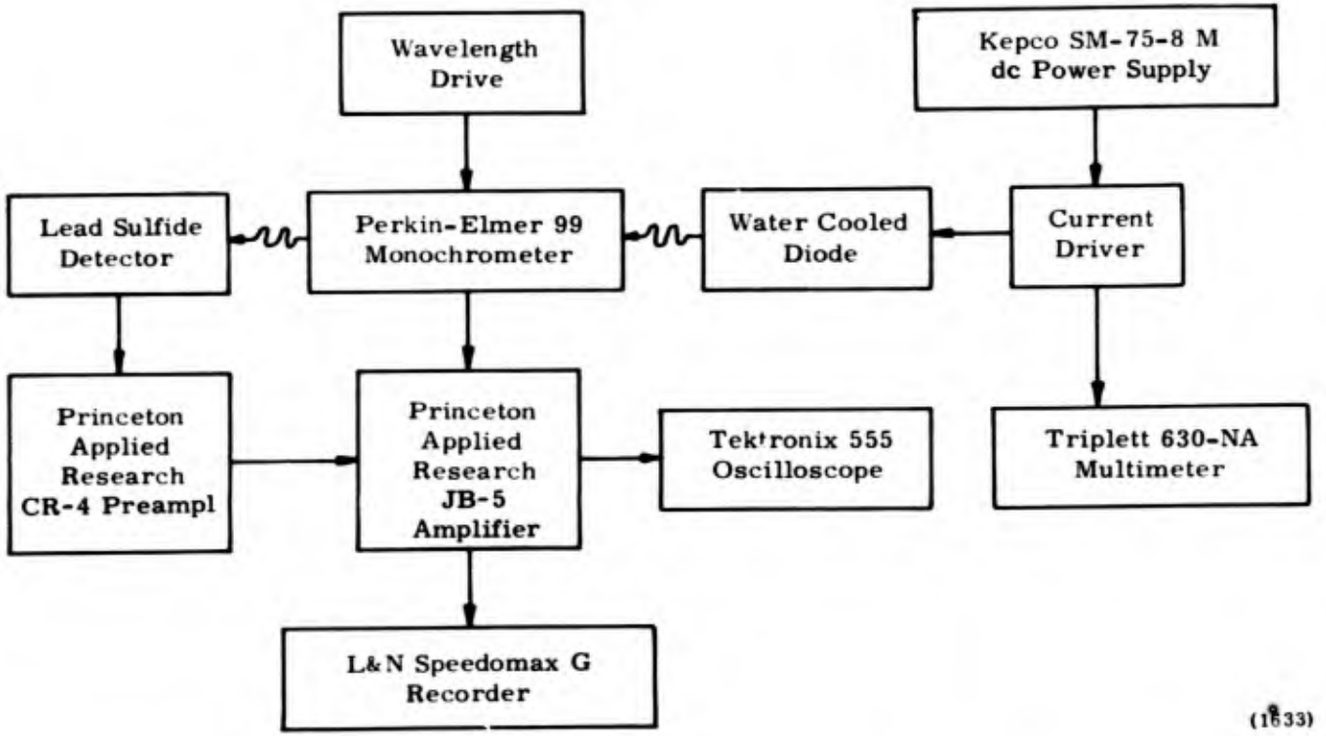

Figure 10. Spectrometer Diagram Using Lead Sulfide Detector

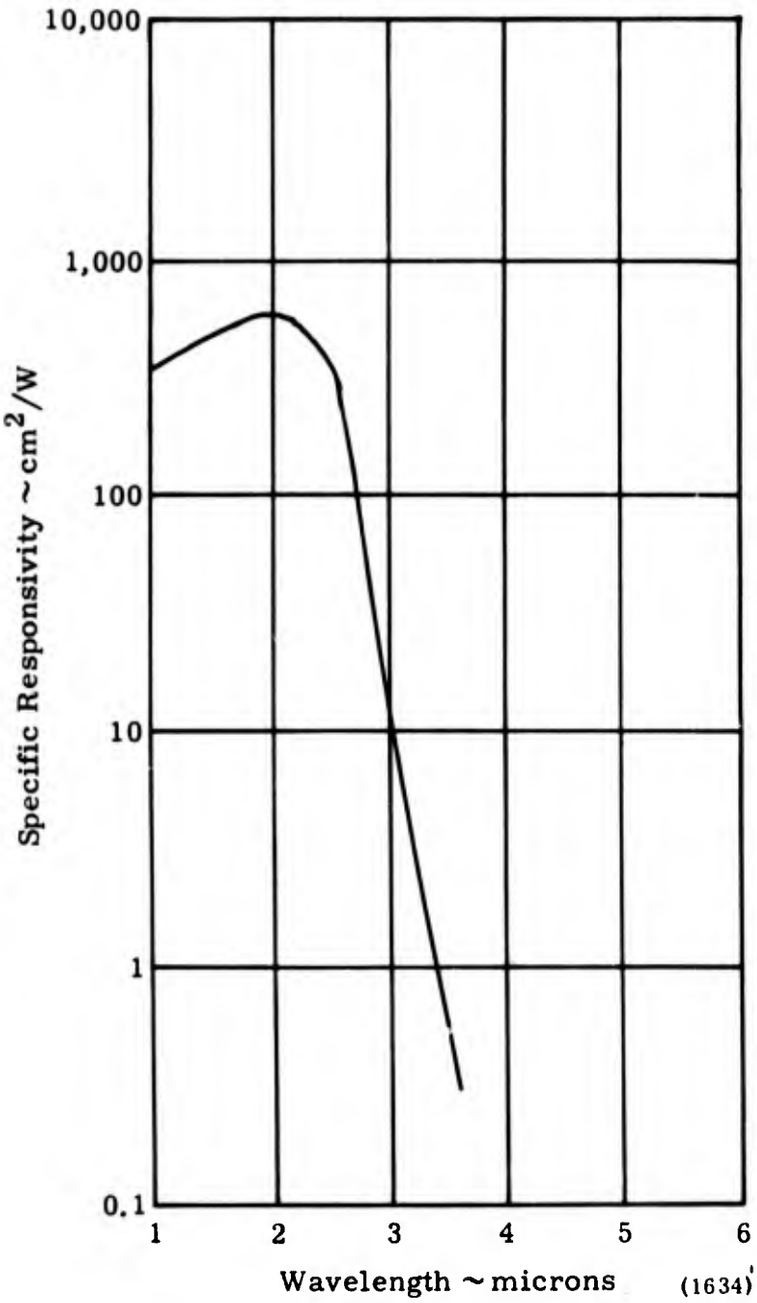

Figure 11. Relative Sensitivity of Lead Sulfide Detector

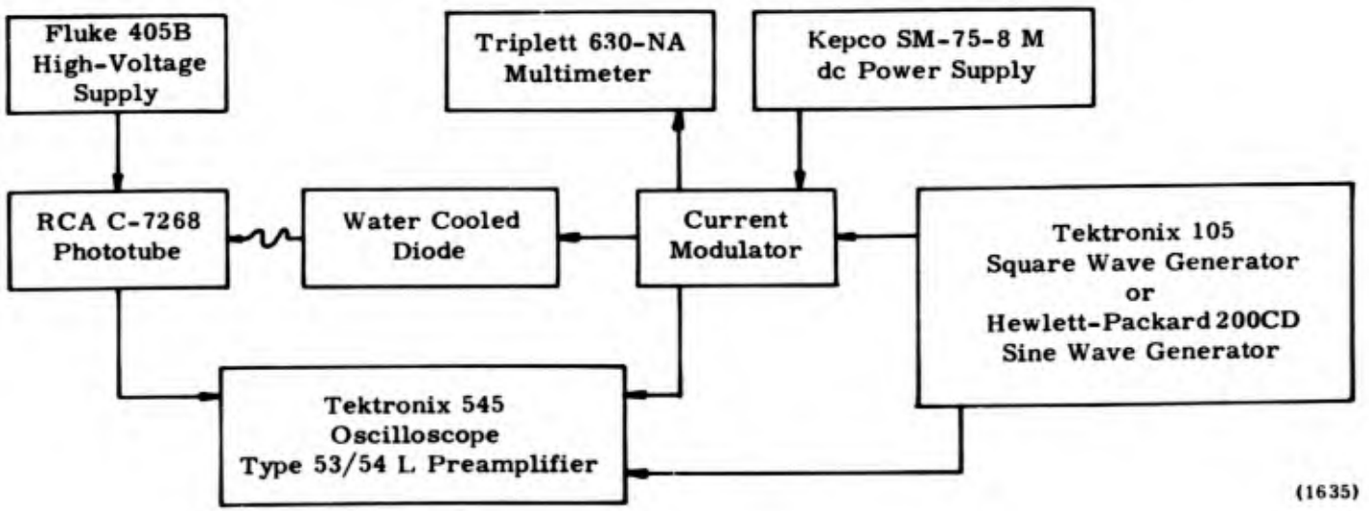

Figure 12. Sine-Wave Square-Wave Modulation

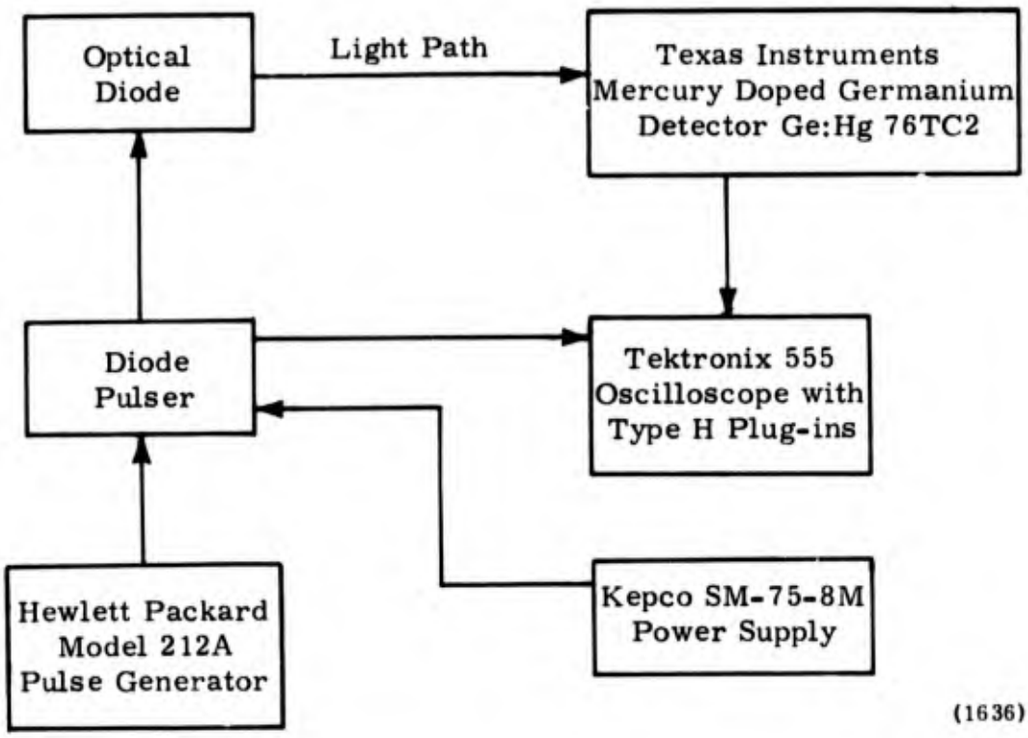

Figure 13. Pulse Response Equipment

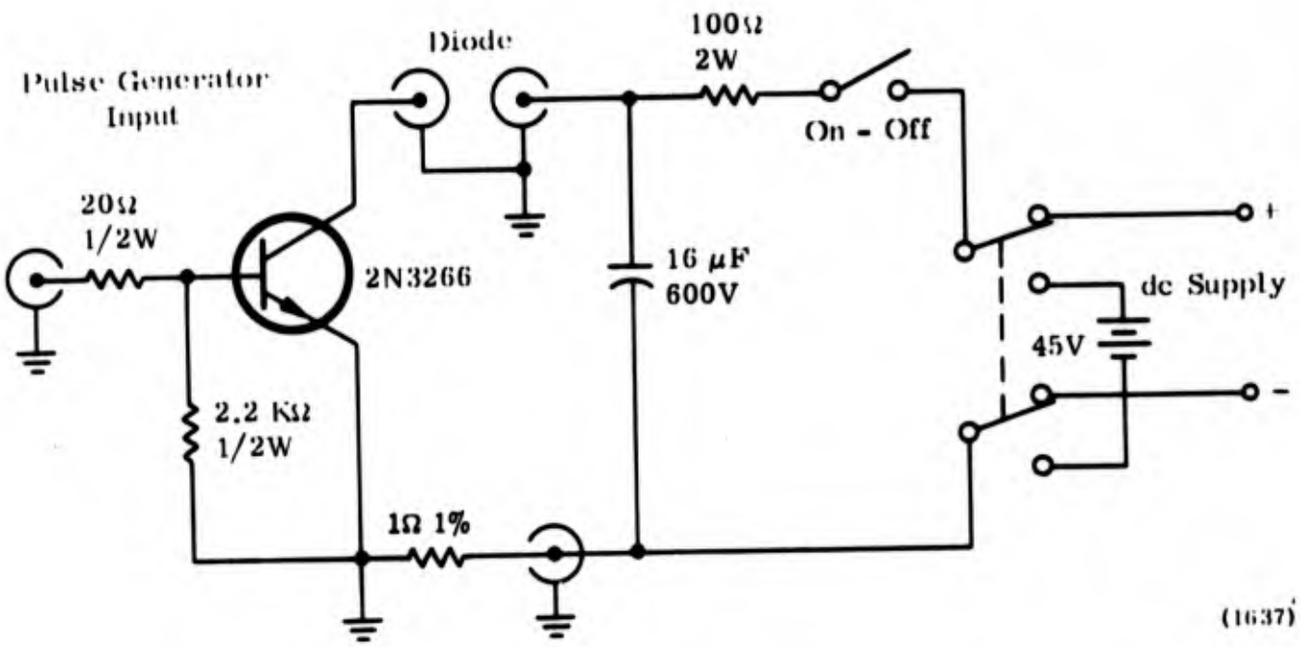

Figure 14. Diode Pulser

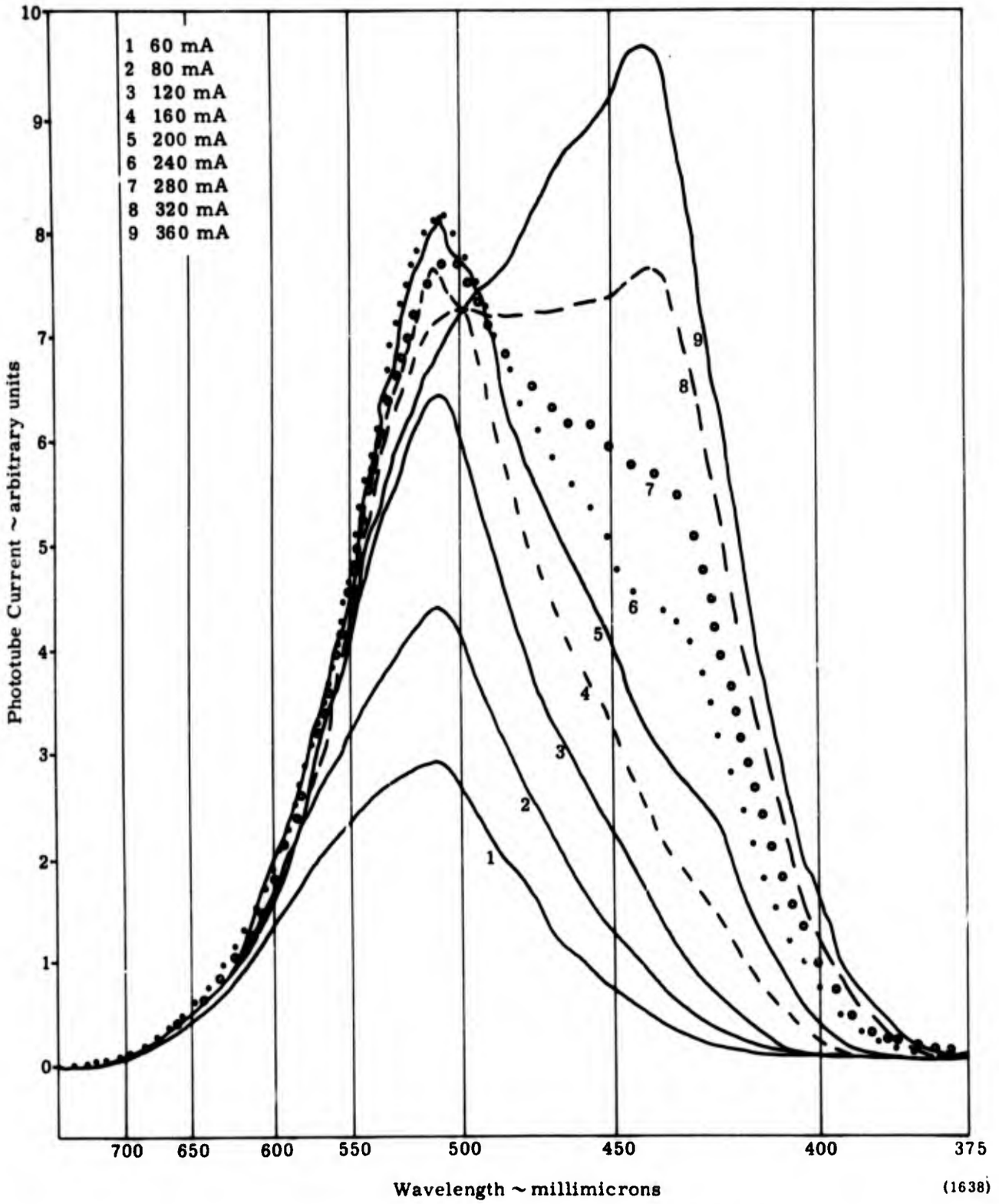

Figure 15. Point Contact Emission Spectra

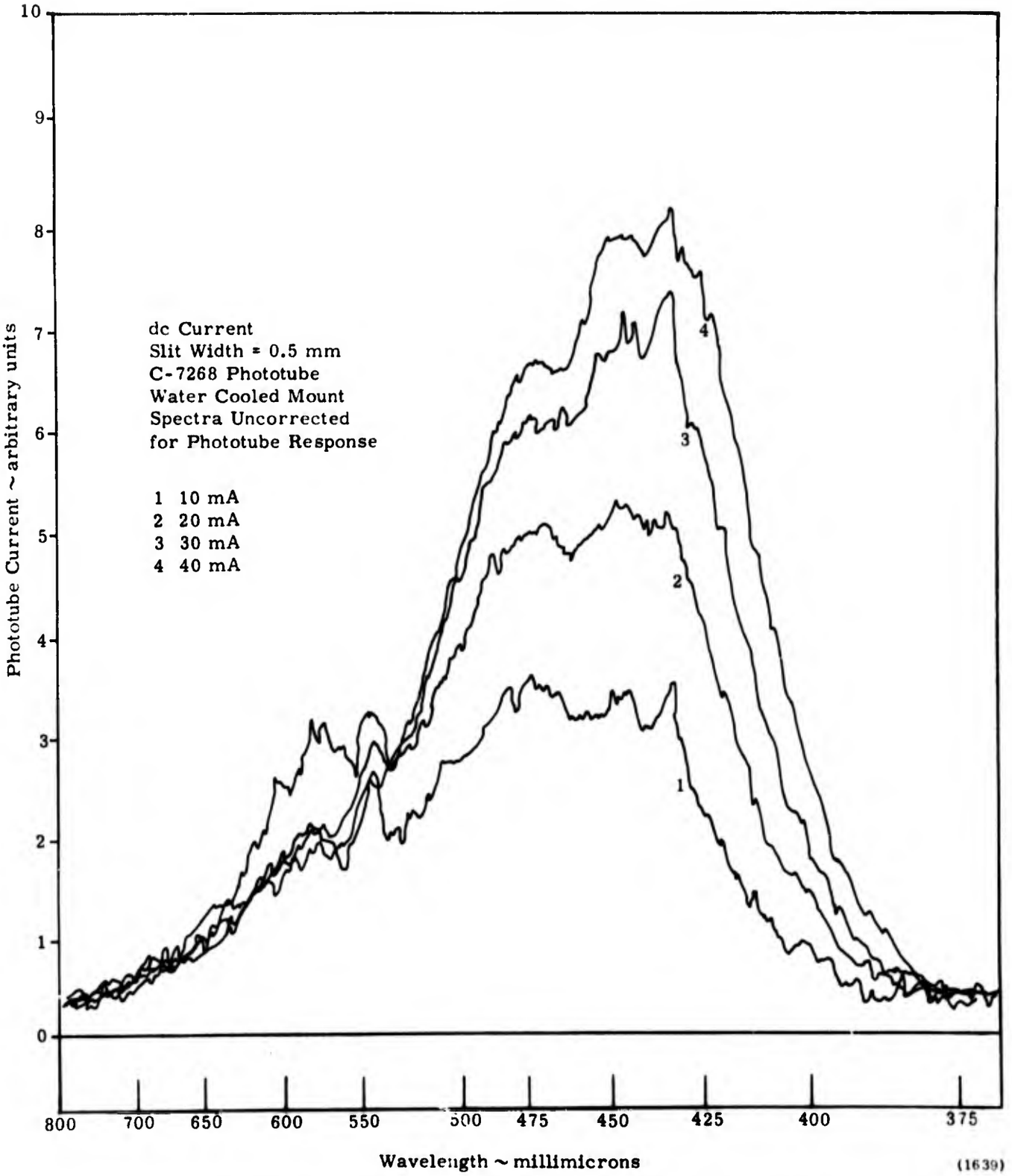

Figure 16. Point Contact Emission Spectra at Low Currents

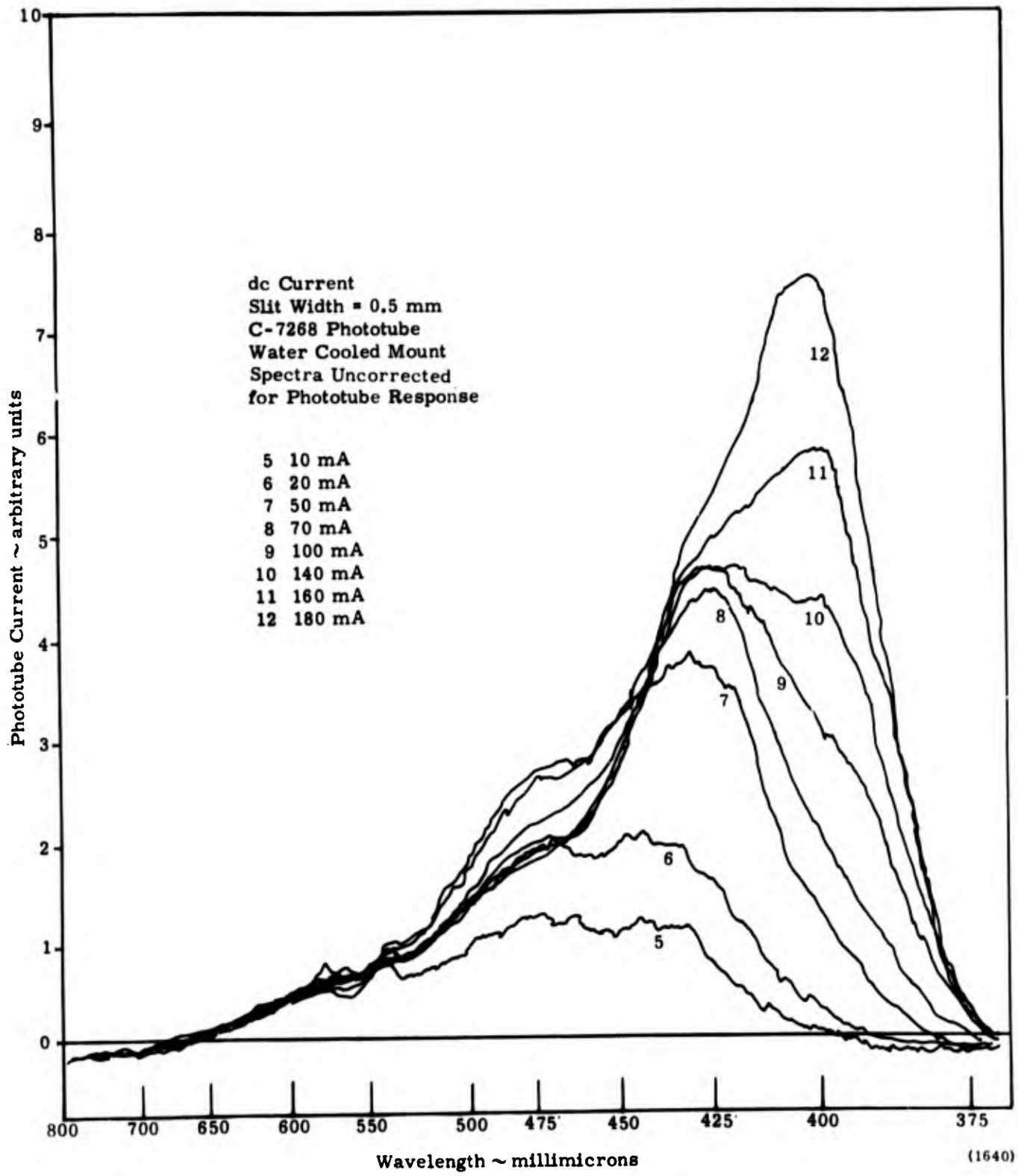

Figure 17. Point Contact Emission Spectra at High Currents

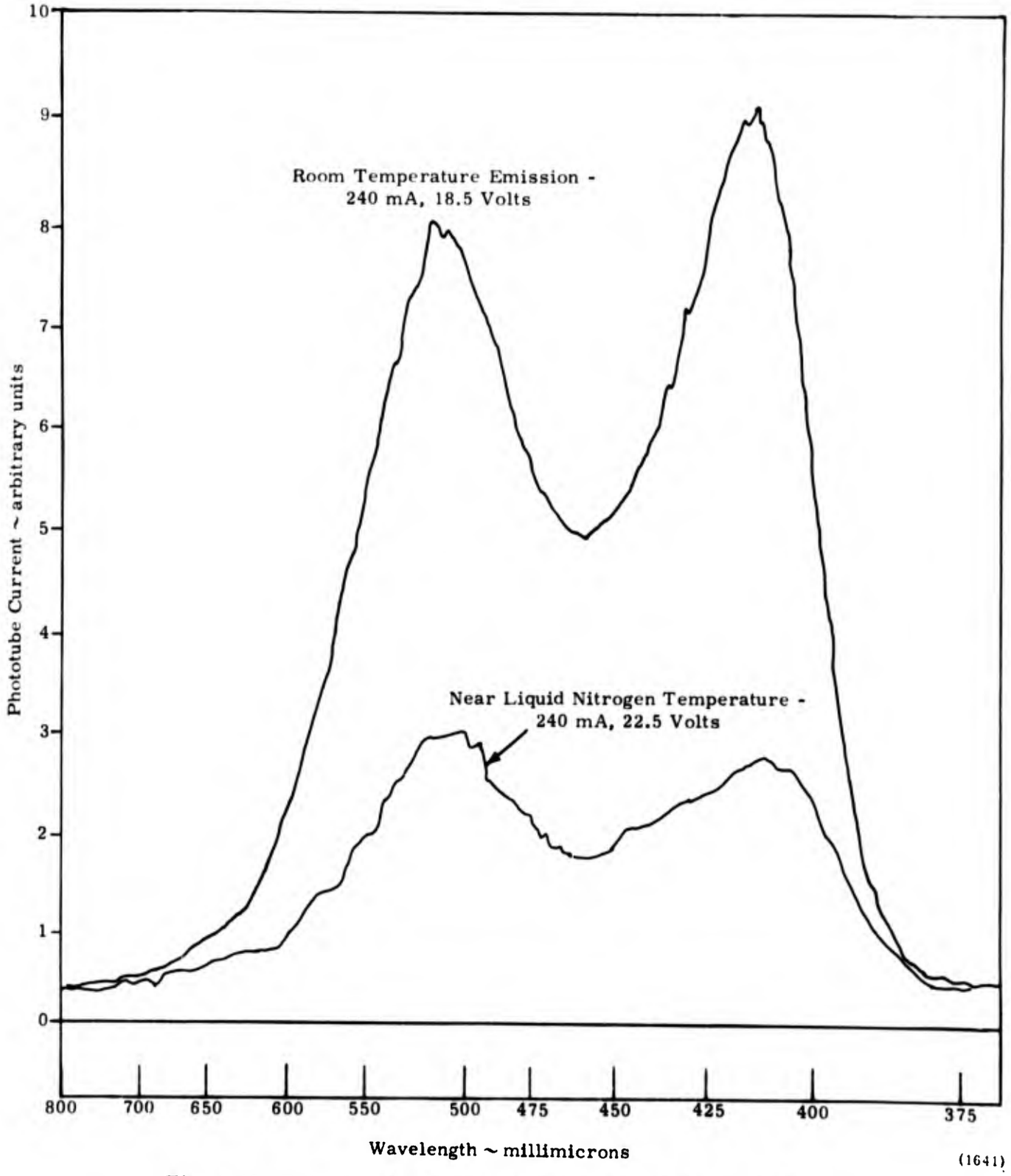

Figure 18. Point Contact Emission Spectra, Temperature Variation

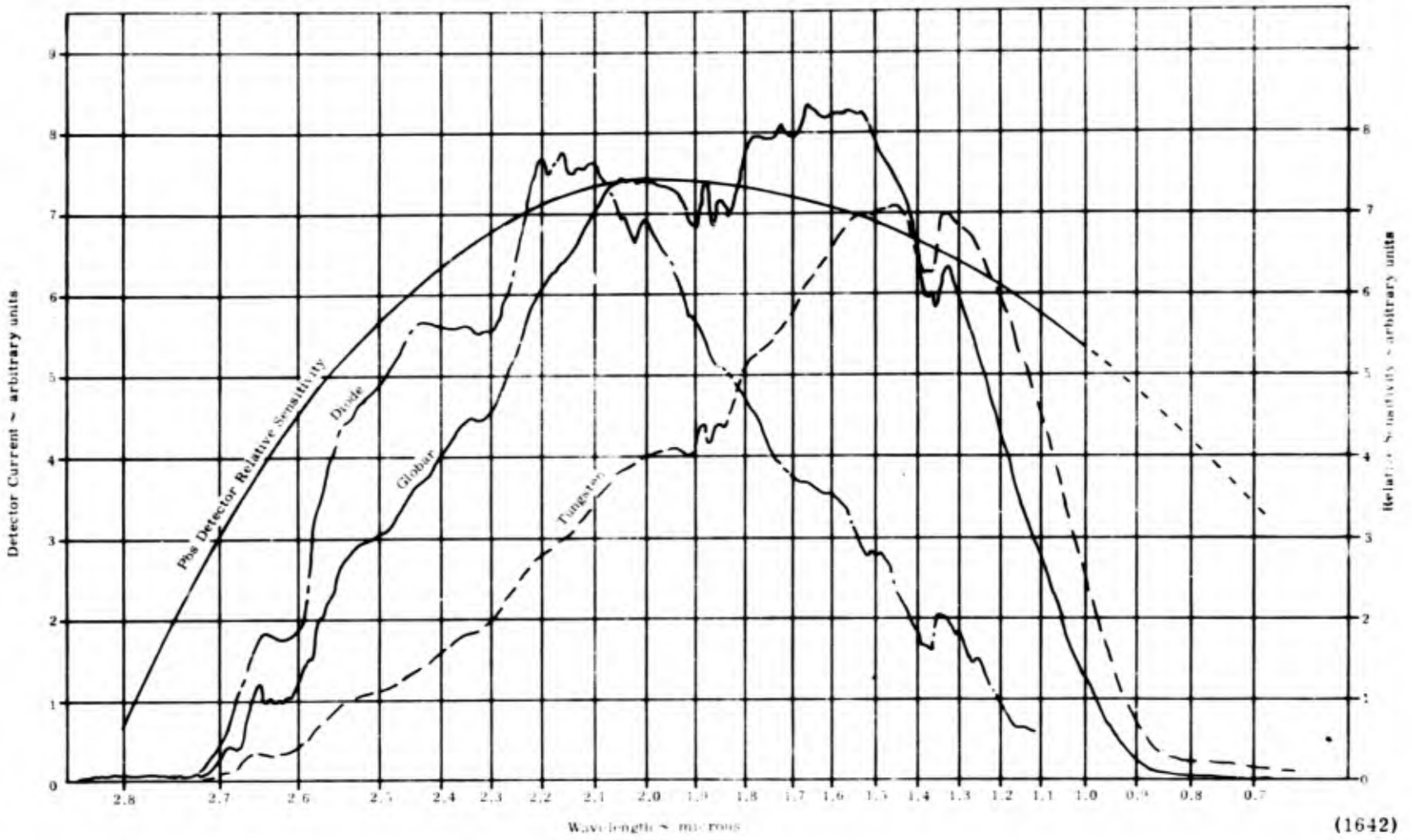

Figure 19. Near-Infrared Emission Spectra

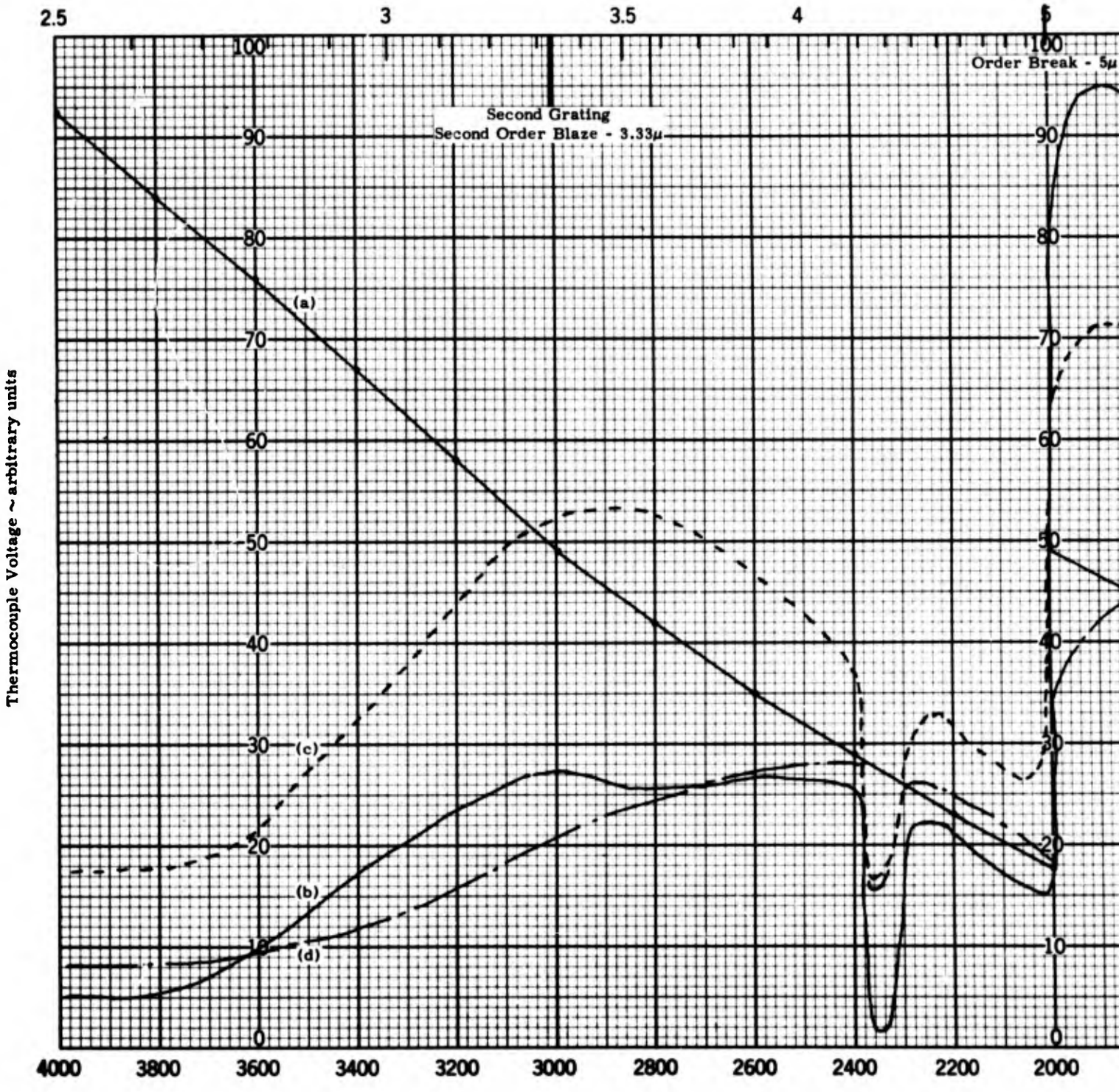
2.5
3
3.5
4
5
Second Grating
Second Order Blaze - 3.33μ
Order Break - 5μ
(a)
(b)
(c)
(d)
100
90
80
70
60
50
40
30
20
10
0
4000
3800
3600
3400
3200
3000
2800
2600
2400
2200
2000
Thermocouple Voltage ~ arbitrary units

A

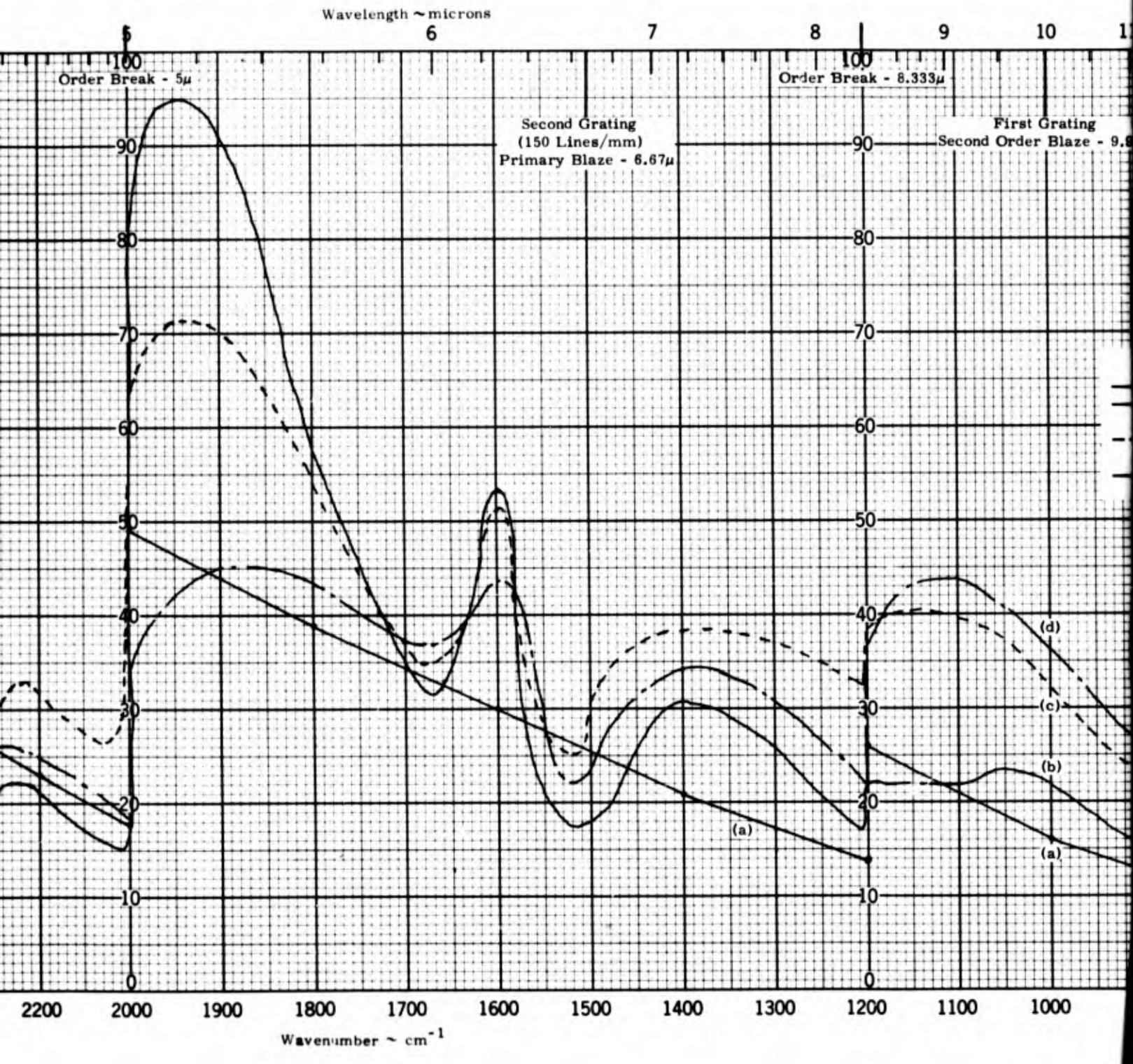
Wavelength ~ microns
5
6
7
8
9
10
Order Break - 5μ
Order Break - 8.333μ
Second Grating
(150 Lines/mm)
Primary Blaze - 6.67μ
First Grating
Second Order Blaze - 9.
100
90
80
70
60
50
40
30
20
10
0
(a)
(b)
(c)
(d)
2200
2000
1900
1800
1700
1600
1500
1400
1300
1200
1100
1000
Wavenumber ~ cm⁻¹

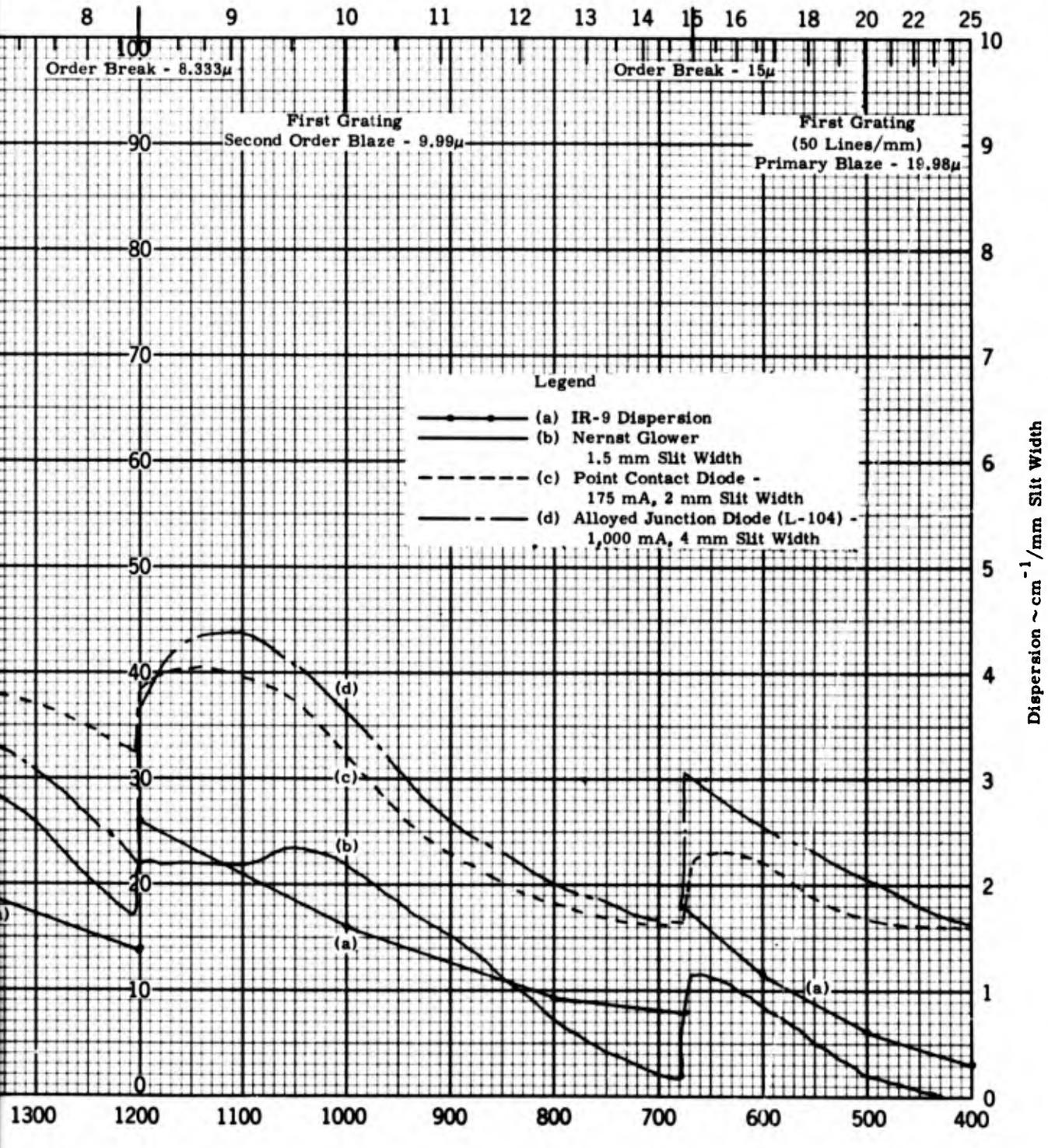

Figure 20. Infrared Emission Spectra

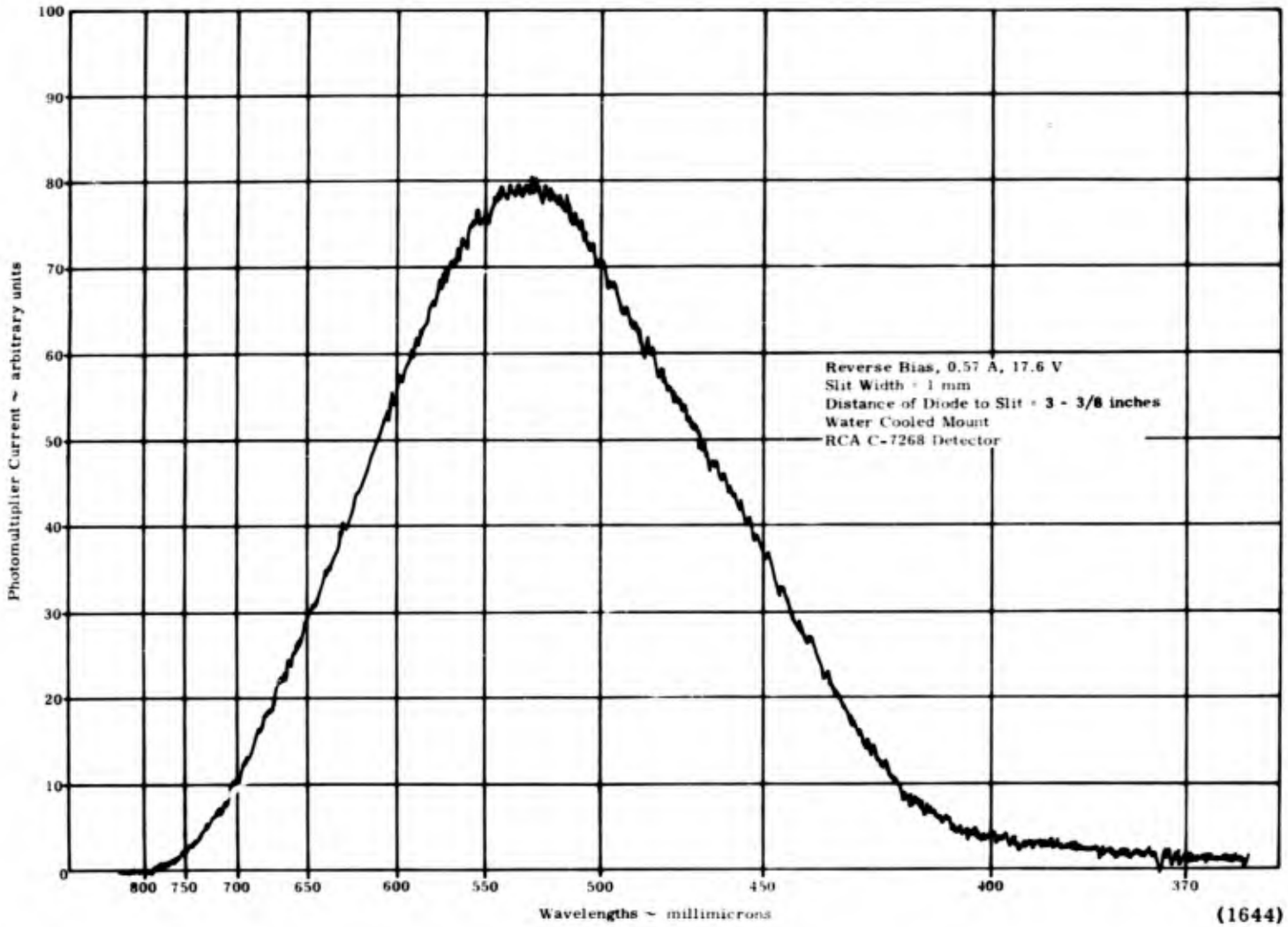

Figure 21. Spectrum of L-104, Reverse Bias, Using RCS C-7268

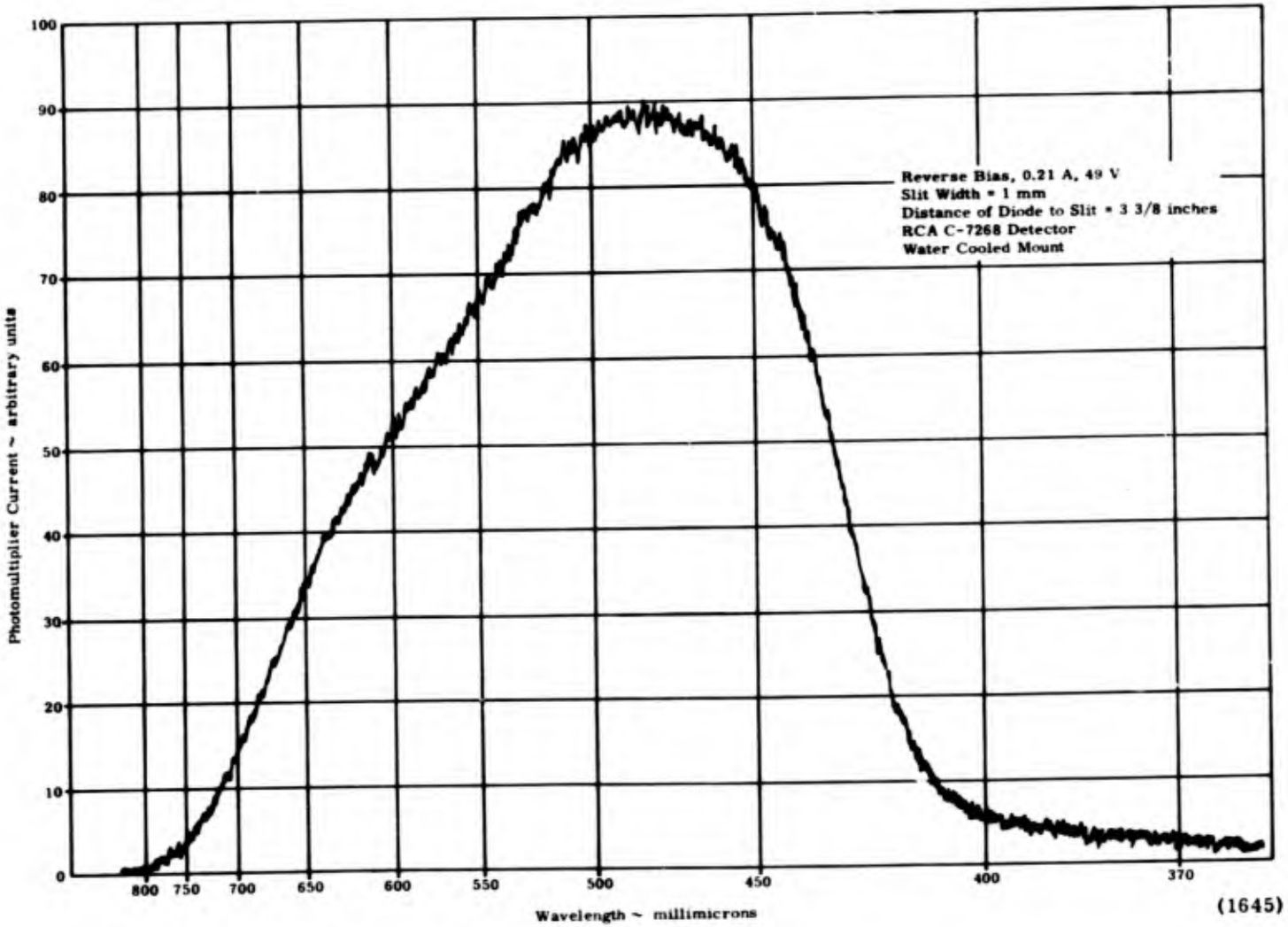

Figure 22. Spectrum of L-110, Reverse Bias, Using RCA C-7268

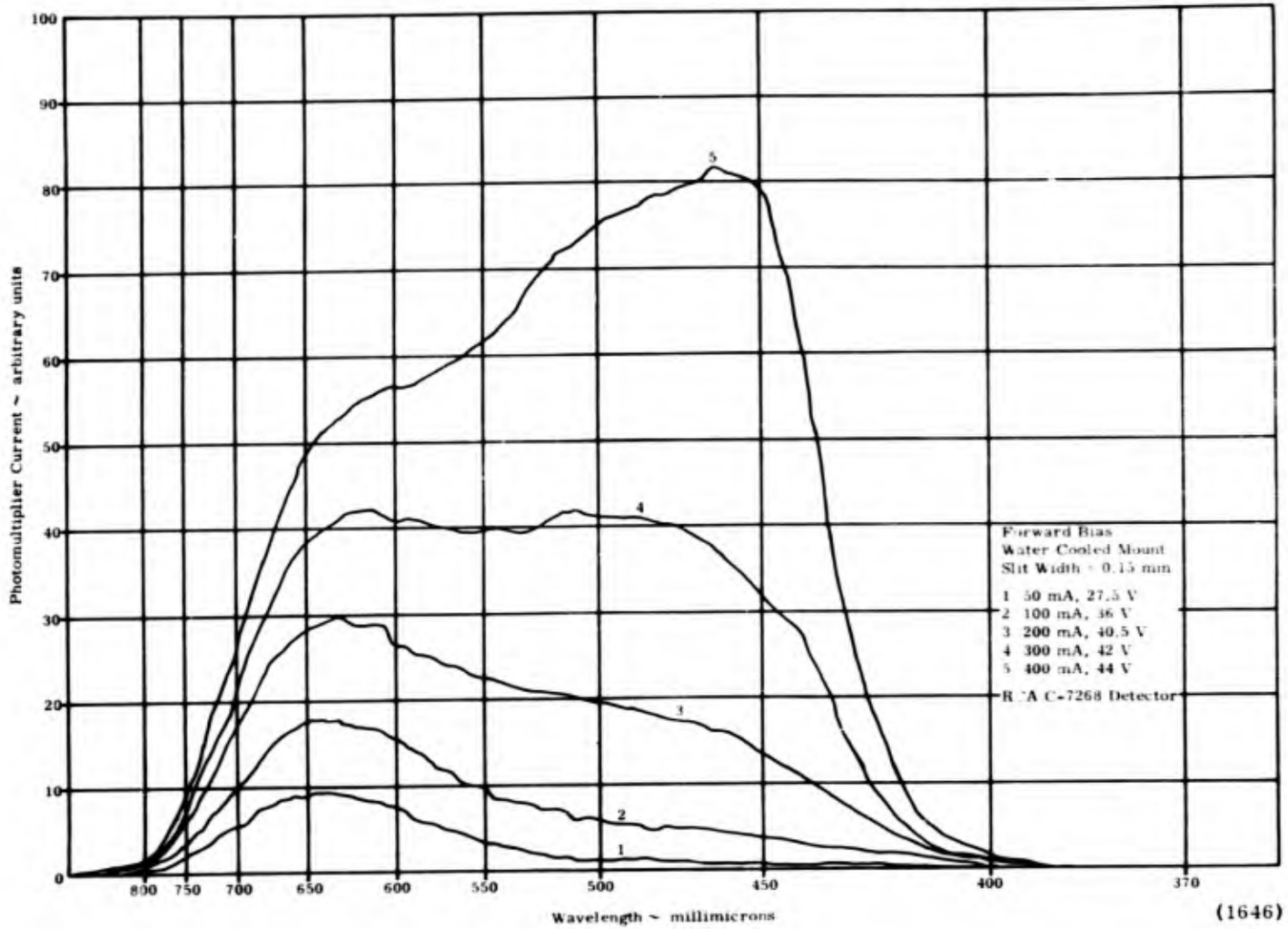

Figure 23. Spectra of L-110, Forward Bias, Using RCA C-7268

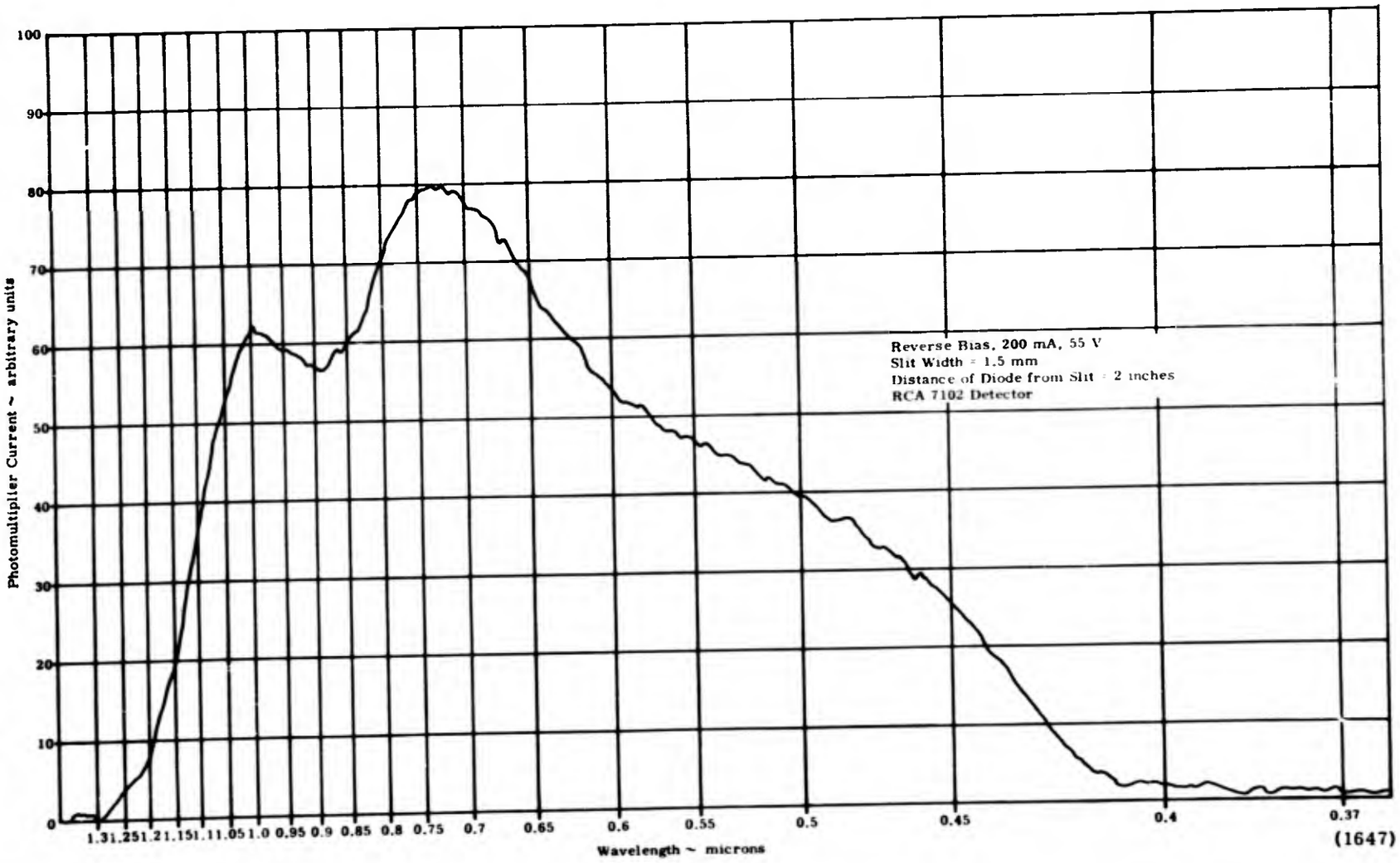

Figure 24. Spectrum of L-110, Reverse Bias, Using RCA 7102

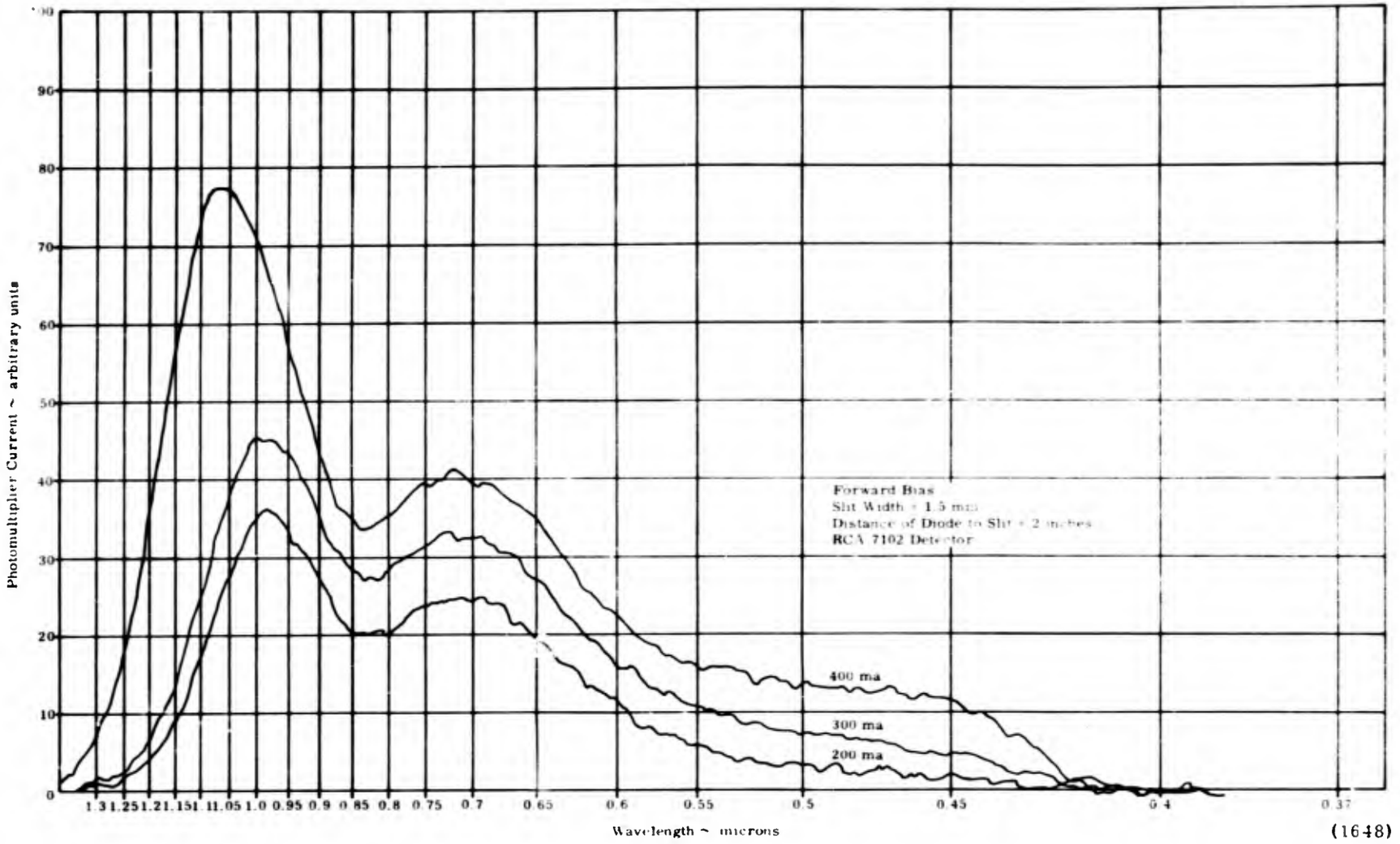

Figure 25. Spectra of L-110, Forward Bias, Using RCA 7102

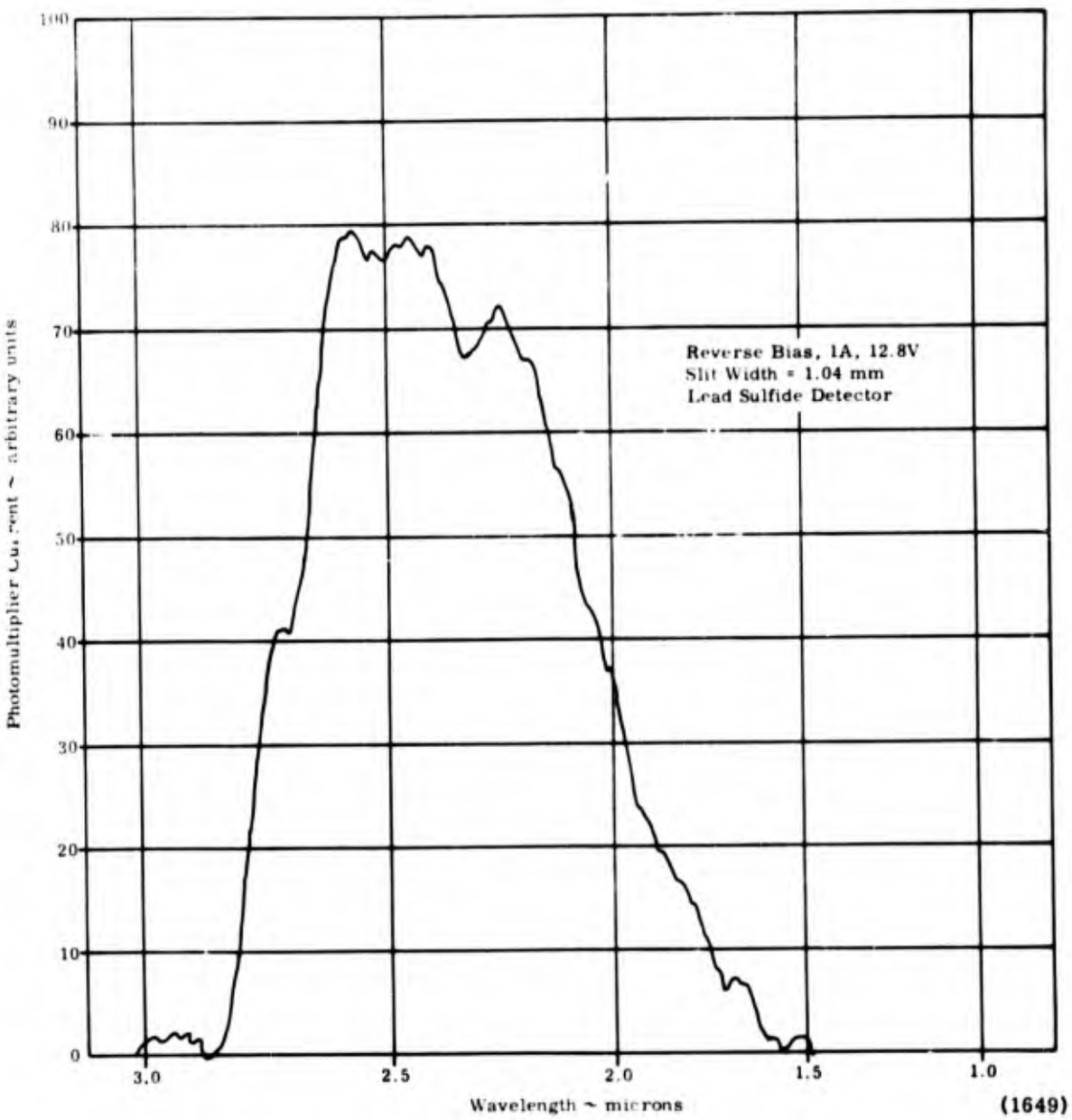

Figure 26. Spectrum of L-102, Using Lead Sulfide Detector

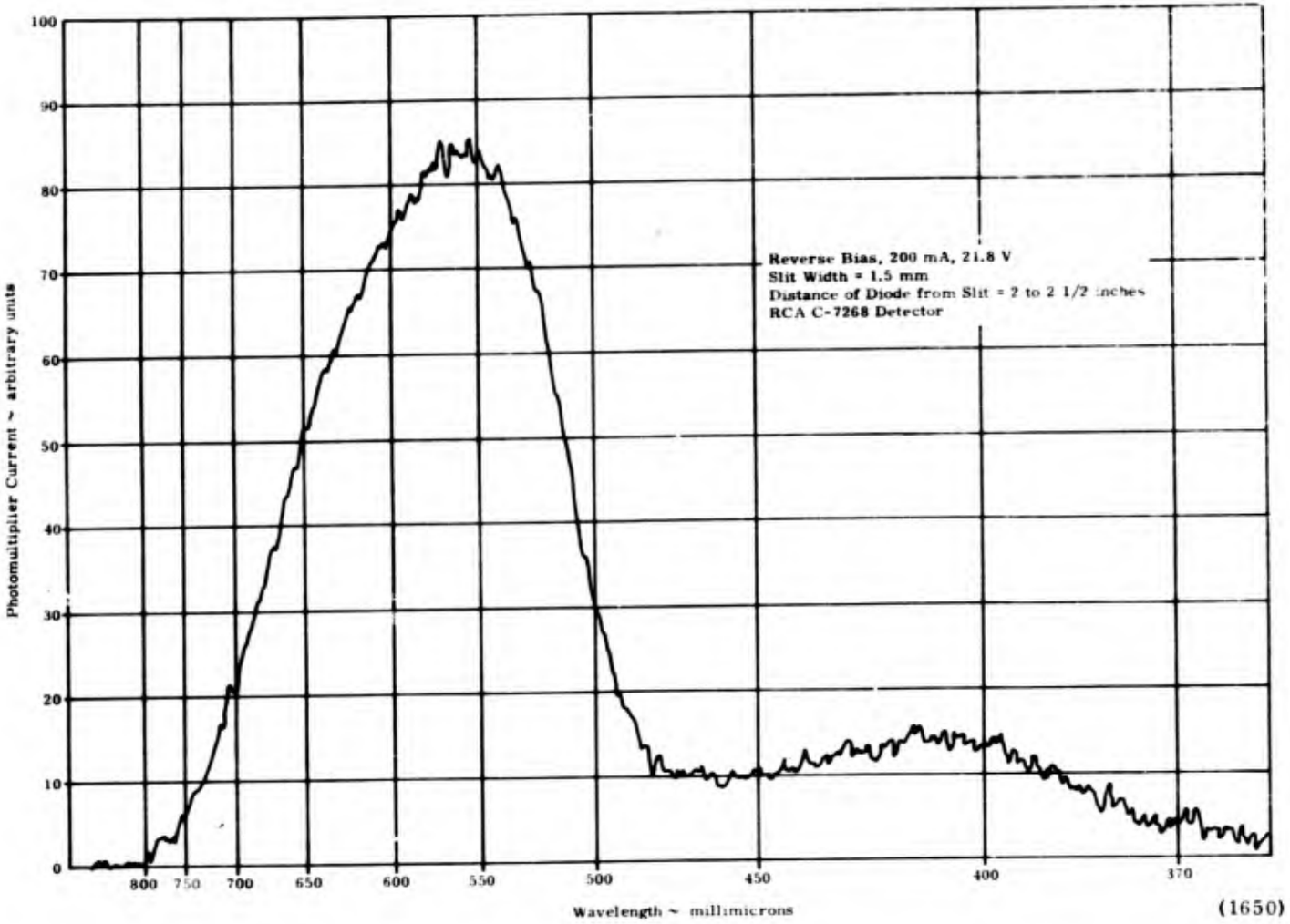

Figure 27. Spectrum of L-113, Water Cooled

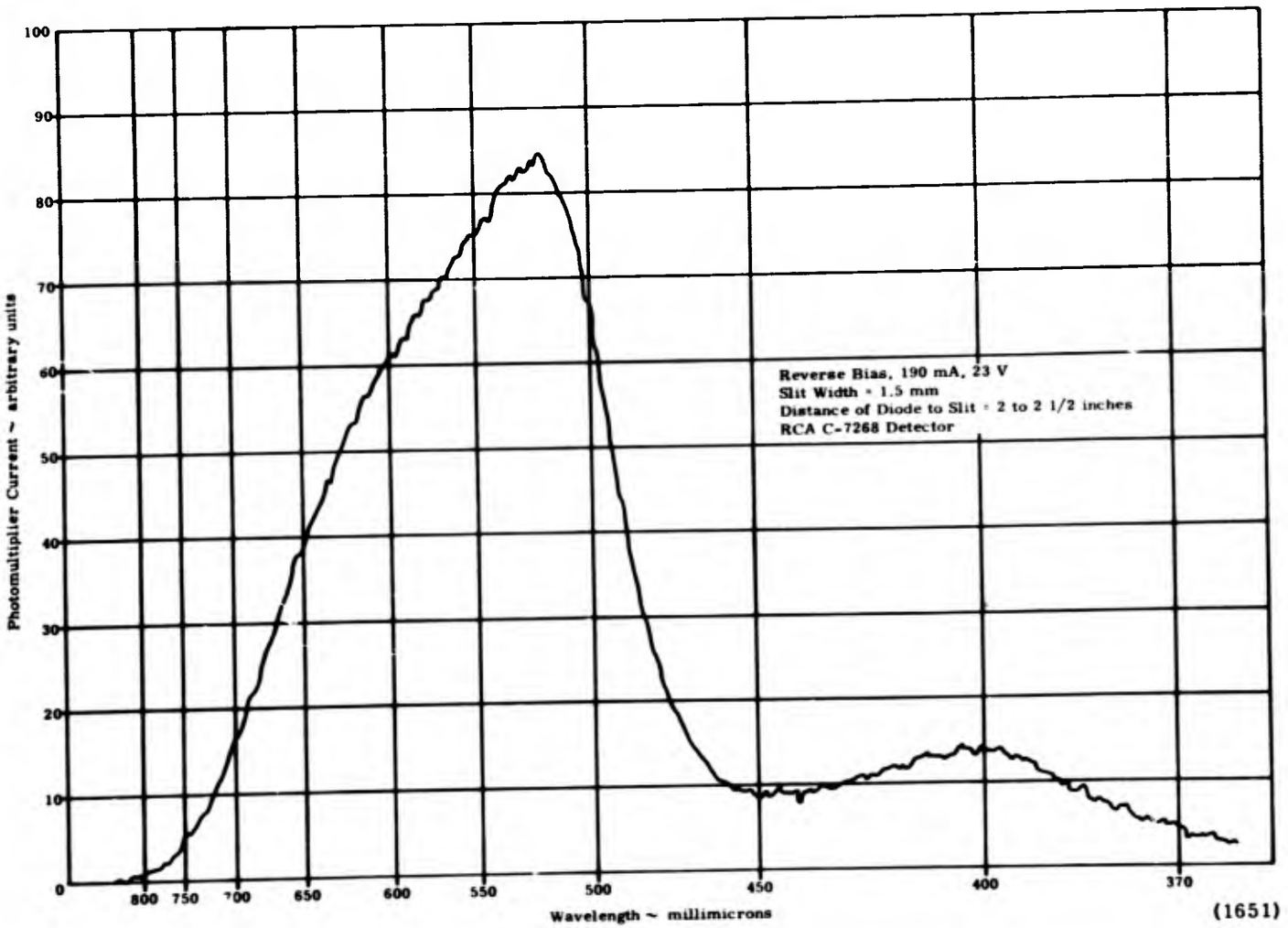

Figure 28. Spectrum of L-113, Liquid Nitrogen Cooled

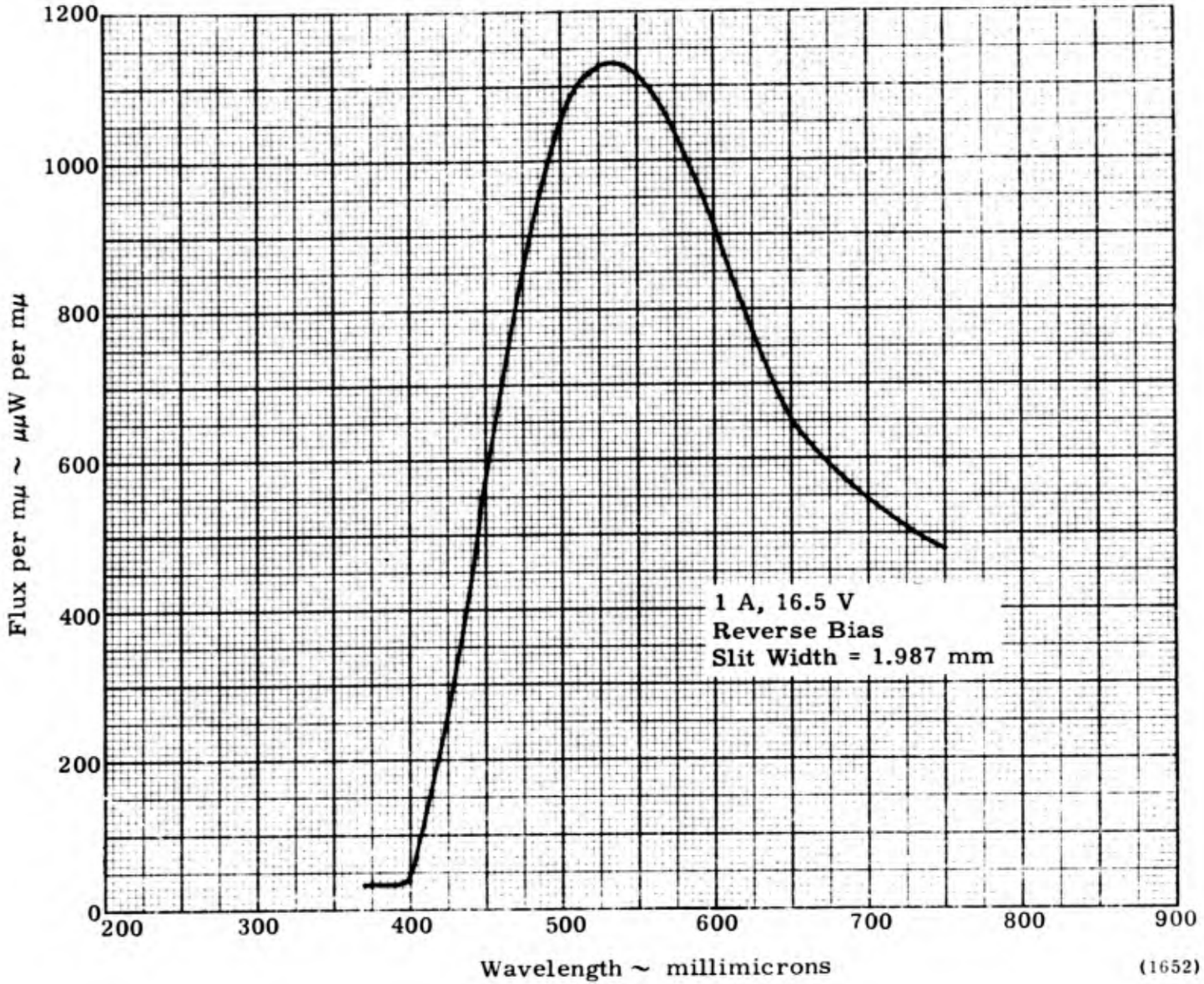

Figure 29. Spectral Irradiance of L-104

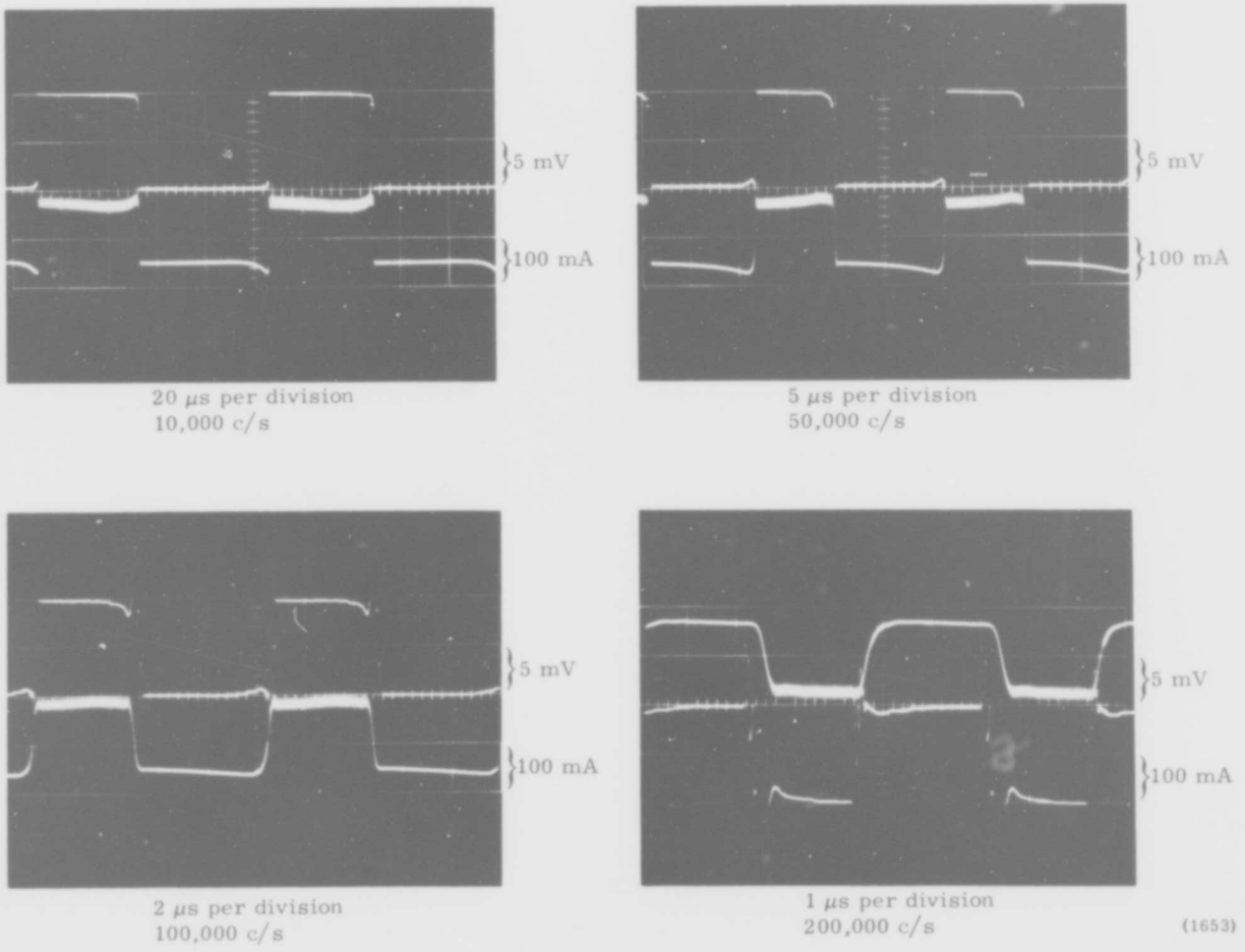

Figure 30. Square Wave Modulation of L-109

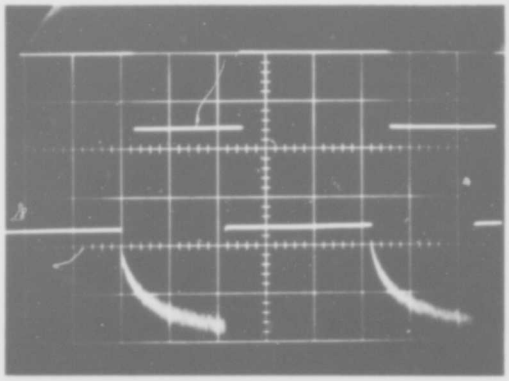

5 μs per division
60 c/s (1654)

Figure 31. Square Wave Modulation of L-119, Forward Bias

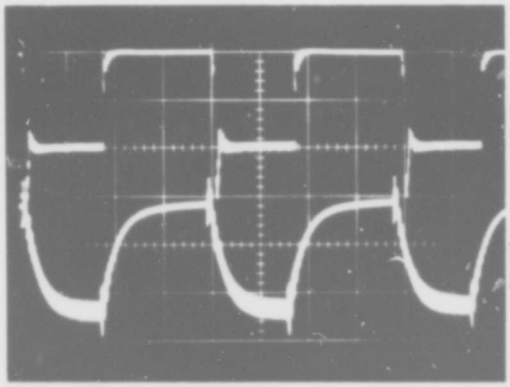

5 μs per division
50,000 c/s (1655)

Figure 32. Square Wave Modulation of L-119, Reverse Bias

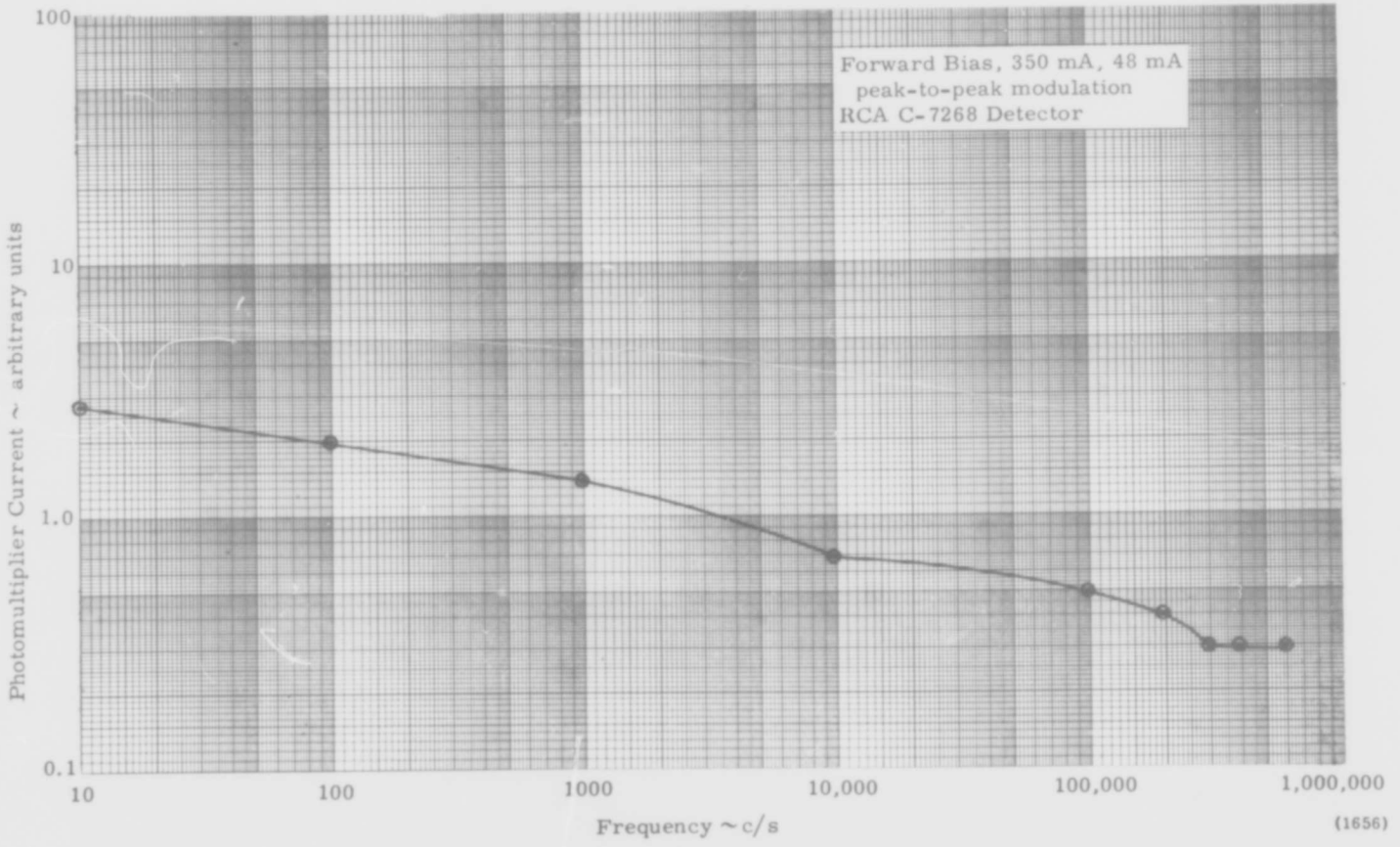

Figure 33. Sine Wave Modulation of L-120, Forward Bias

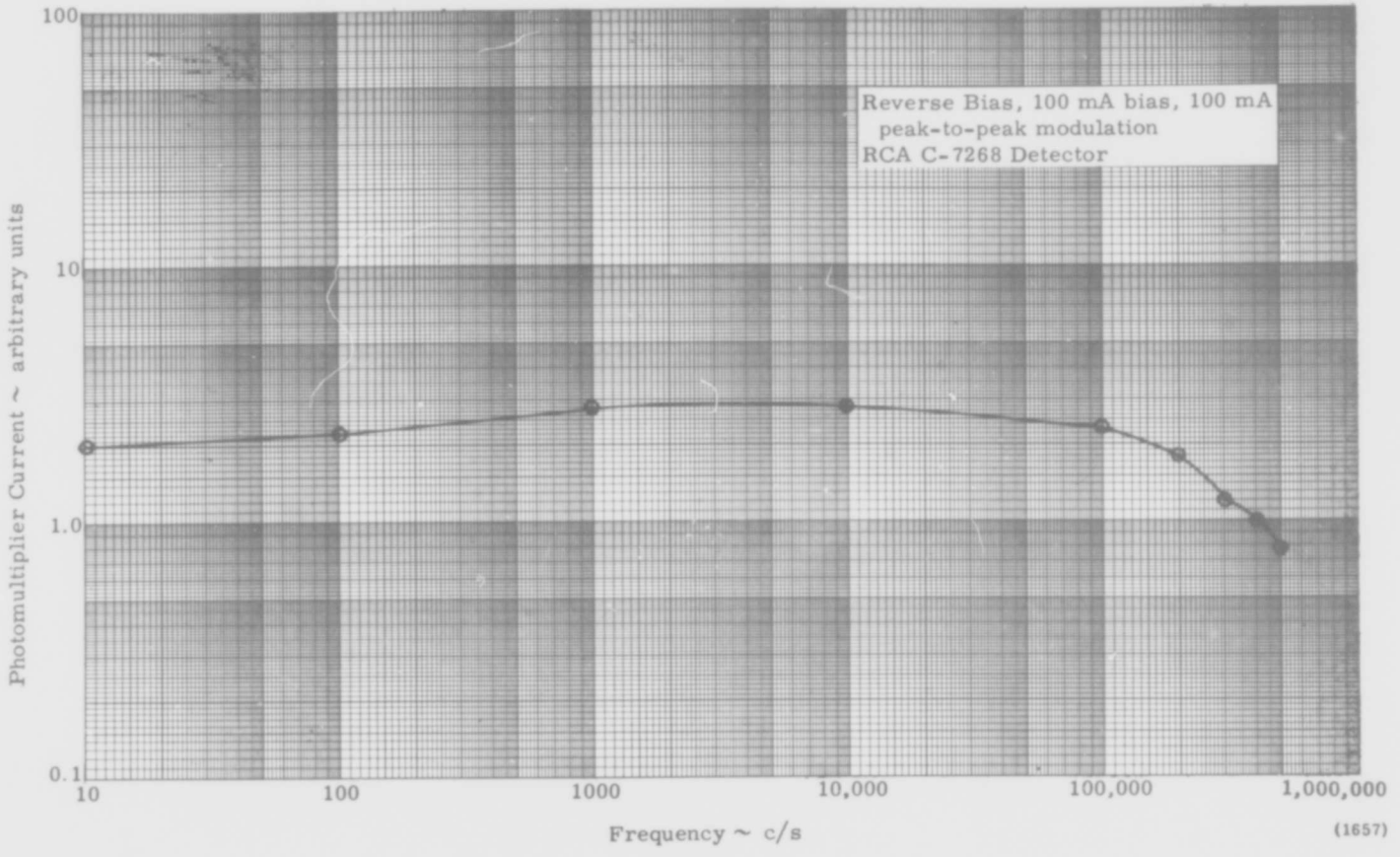

Figure 34. Sine Wave Modulation of L-120, Reverse Bias

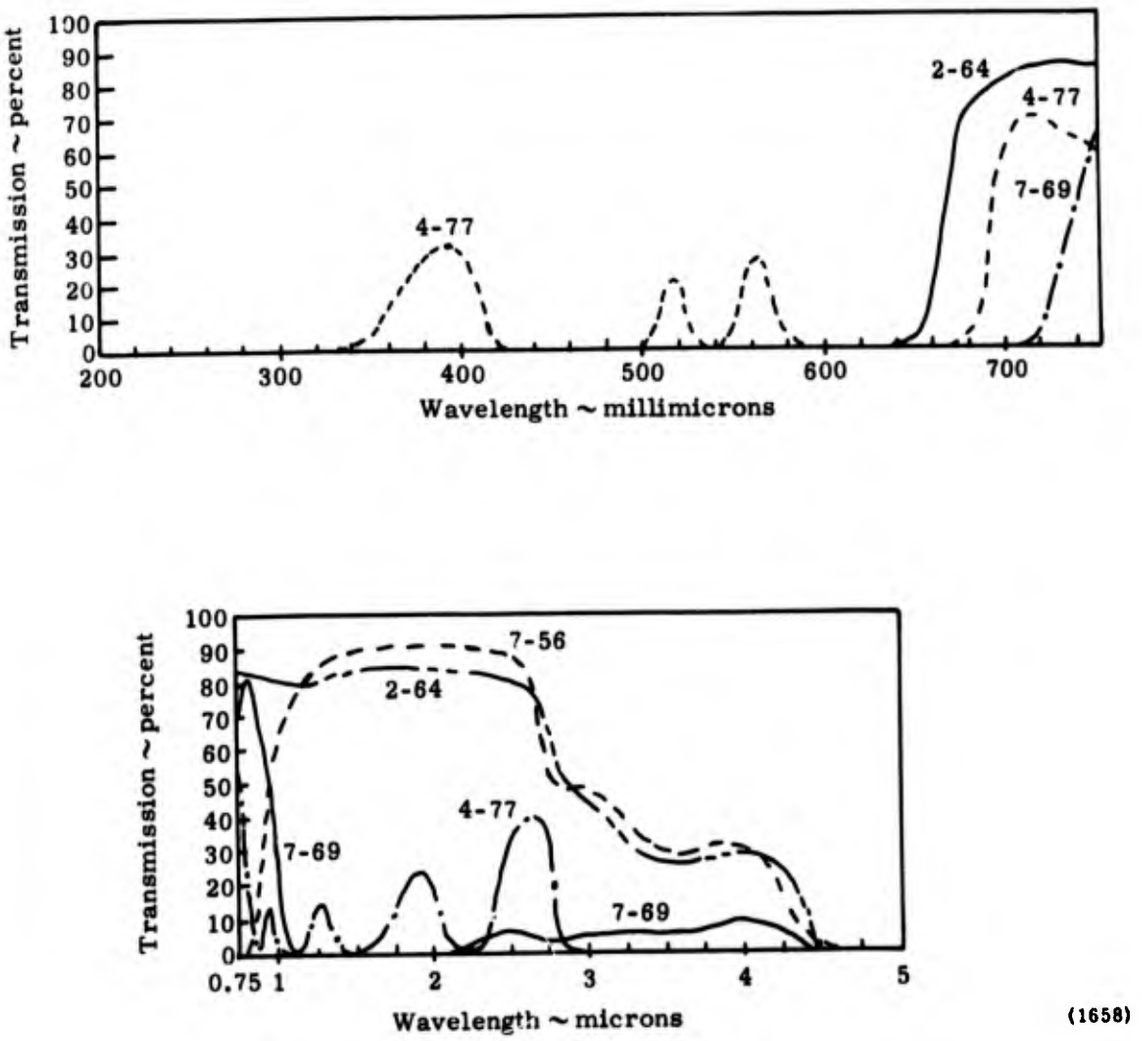

Figure 35. Corning Filter Transmission

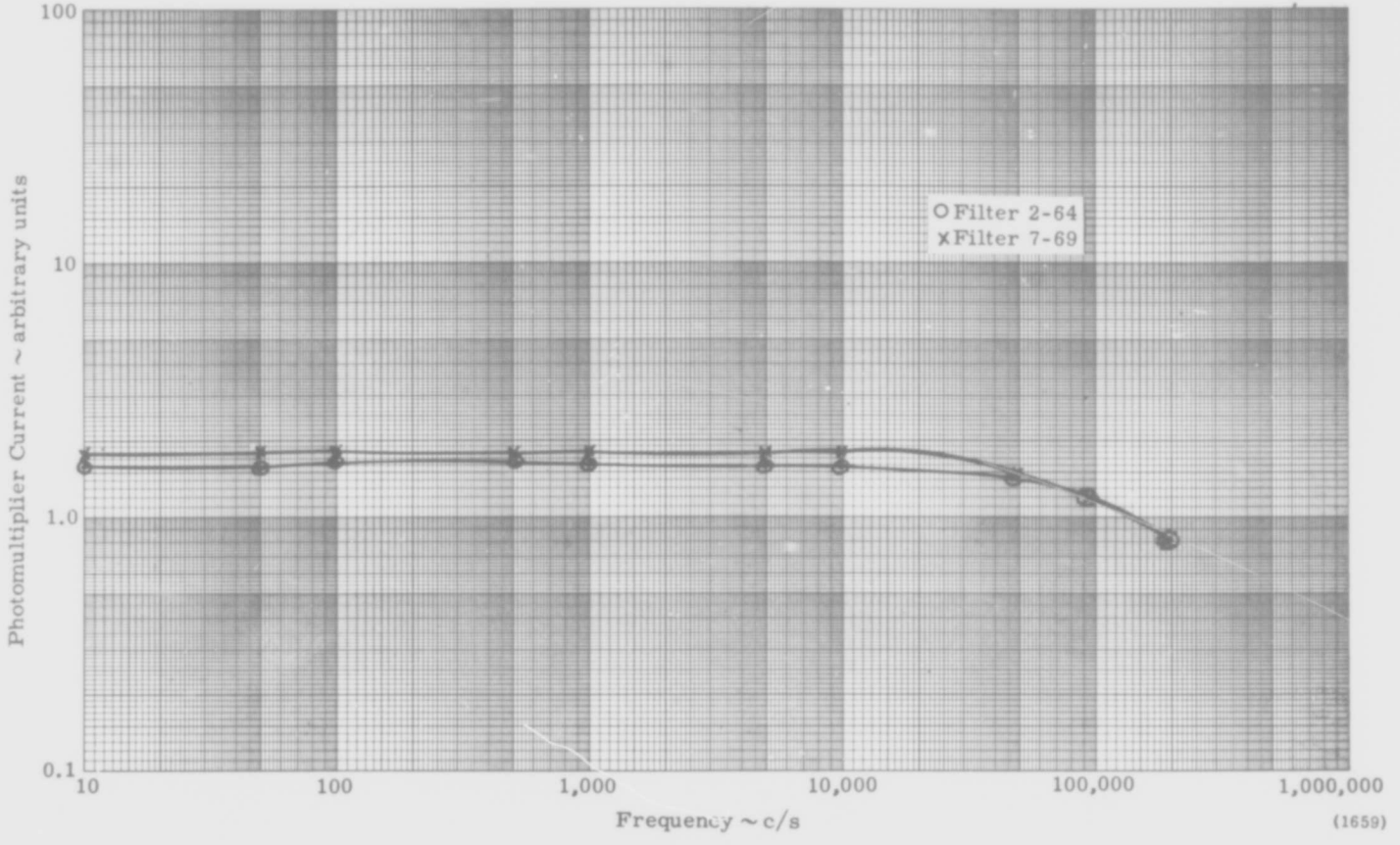

Figure 36. Sine Wave Modulation (Near Infrared) of L-104, Using Filters 2-64 and 7-69

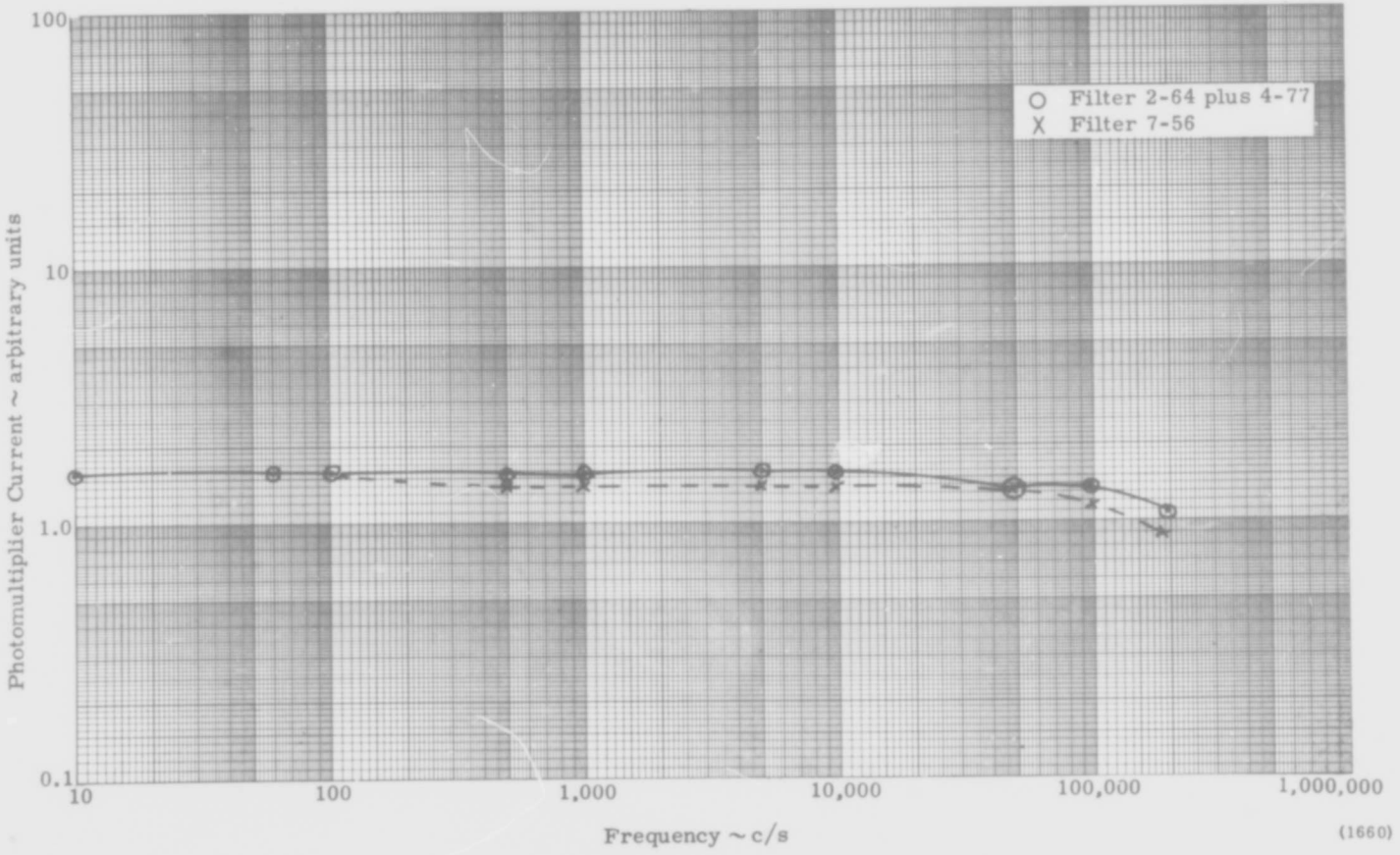

Figure 37. Sine Wave Modulation (Near Infrared) of L-104, Using Filters 2-64, 4-77, and 7-56

II. X-RAY ANALYSIS

To ascertain the crystal structure of the silicon carbide (β) under investigation, many simple rotation and normal beam, zero level Weissenberg patterns were taken. These patterns showed the structure to be of the cubic modification.

Although it was impractical to run X-ray patterns on all the crystals (some 80) used in the absorption measurements, many of them (such as 475, 78, 79) did have X-ray patterns taken. These all showed the β-cubic structure.

To check the crystallographic structure of the crystals used in the absorption studies, simple rotation, normal beam, zero-level Weissenberg and equi-inclination, n-level, Weissenberg diffraction patterns were taken. From these patterns it has been established that the crystals are β-SiC (zinc blend structure). Figure 38 is a rotation pattern indexed according to the FCC system. This photograph yields the interplanar spacing d_{hkl}, the extrapolated lattice parameter a_o, and the symmetry axes of the crystal. The d_{hkl} values are given in Table III.

TABLE III

Values for hkl, d_{hkl}, and a_{hkl}

hkl	d_{hkl}	a_{hkl}
111	2.496	4.323
200	2.159	4.318
220	1.536	4.344
311	1.312	4.351
222	1.251	4.334
400	1.087	4.348
331	0.9985	4.352
420	-	-
422	0.8879	4.350
333-511	0.8381	4.356

These data, when plotted according to the Jay-Bradley or Nelson-Riley method, yield an extrapolated lattice parameter of a_o = 4.357 Å.

The layer lines in Figure 38 have a spacing of 3.03 Å, which implies a < 110 > rotation axis for the sample in the Weissenberg camera. This can also be inferred from the fact that the (222) and (400) reflections are missing from the 1 = 1 layer line and that the (420) reflection is missing from the 1 = 0 layer line.

Figure 39 is a normal beam, zero-level Weissenberg pattern, of the same crystal as used in the Figure 38 pattern. Superimposed on the same pattern at the bottom is the zero-level of a simple rotation pattern. Figure 40 is a Weissenberg pattern, equi-inclination of the first layer line as observed in the simple rotation pattern.

From the latter two patterns it can be established that the crystal is FCC (zinc-blend structure) with a lattice parameter of a_o = 4.357 Å. Copper K_α radiation (filtered) was used for taking these patterns

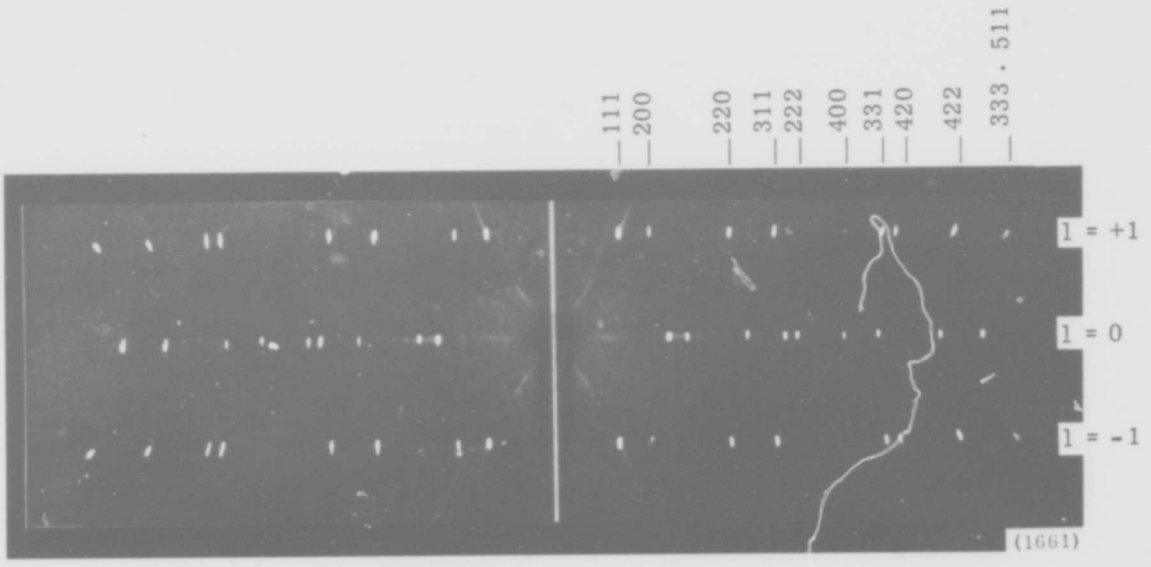

Figure 38. Simple Single Crystal Rotation Pattern About <110>

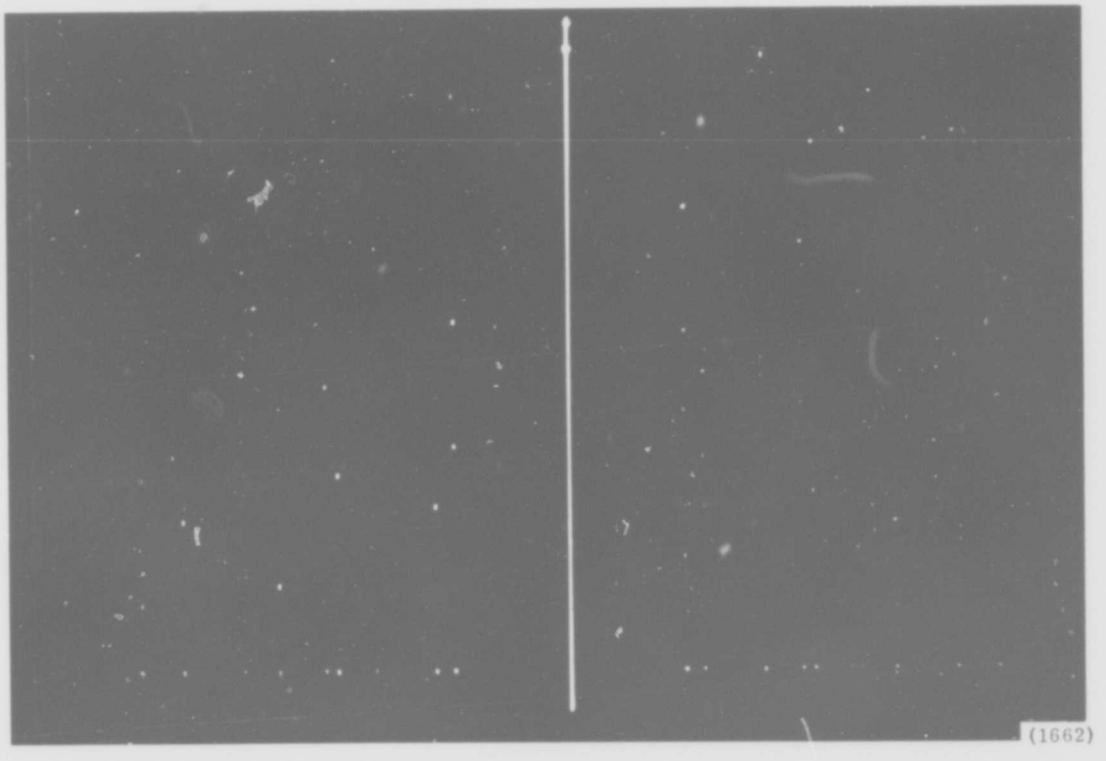

Figure 39. Normal Beam, Zero Level, Weissenberg Pattern About <110>

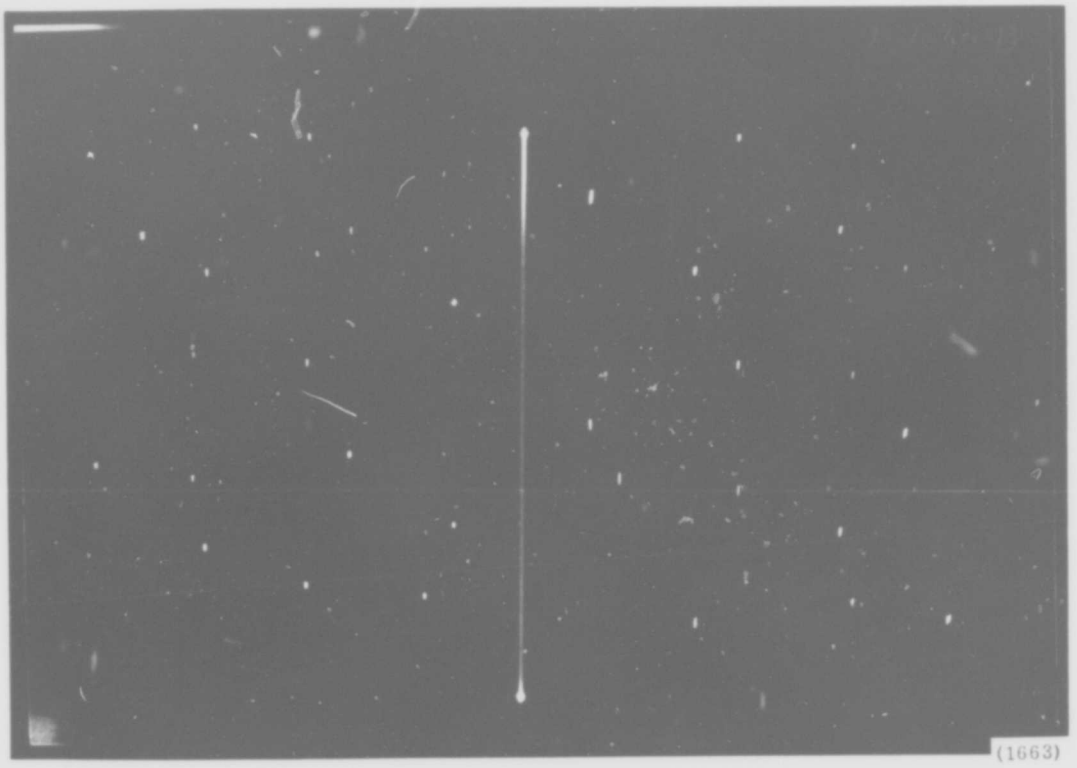

Figure 40. Equi-inclination Weissenberg Pattern of Level 1 = +1 Rotation About <110>

III. ABSORPTION SPECTRA

A. PREPARATION OF CRYSTALS AND EXPERIMENTAL PROCEDURE

The samples used in the absorption measurements in both the visible and infrared region of the spectrum had an effective diameter of approximately two millimeters. Experiments were carried out to determine the upper and lower limits for the thickness of the crystals that gave the best results for the instruments used. Experiments showed that optical paths through the crystal (thickness) can vary from 20 to 100μ; that is, a crystal can have as its lower limit a uniform thickness of 20μ to an upper limit of 100μ. Examination of the surface and parallelism of the faces was considered in an attempt to find ways of minimizing scattering. These results were then used as a basis for producing polished surfaces. It was found that polishing had to be done with very fine diamond paste (less than 0.5μ), followed by polishing with Linde "A", for satisfactory results. The results obtained with polished crystals agreed with those obtained with natural faces. However, in each case the crystals were etched with $HF\text{-}HNO_3$ solutions to remove surface contaminants. A final rinse was in triply distilled deionized water and then alcohol.

The samples used in these experiments were N type. The major dopant in these crystals is nitrogen. The number of carriers (electron) in these samples is estimated to be on the order of $10^{18}/cm^3$.

The absorption measurements were carried out on these crystals at temperatures between those of liquid nitrogen and 250°C using the Cary 14R spectrophotometer. The characteristics of this instrument were described in the first quarterly report (31 October 1965). Double beam operation was employed in the scan of each spectrum. To do this it was found necessary to attenuate the reference beam. This attenuation was accomplished by using neutral density filters (calibrated) supplied by the Applied Physics Corporation and also those supplied by the Limit Corporation. Although the suppliers furnished the optical densities of these filters it was felt that they should be calibrated with out own instrument. This was done. Furthermore, the Cary 14R spectrophotometer was checked for its zero line by scanning the spectrum without a sample in the sample compartment and no attenuation in the reference beam. If

the zero line was reasonably straight then preparations were made for obtaining the spectrum of the sample. If the zero line was not satisfactory the potentiometers would be adjusted to give the best zero line for the wavelength region of interest. Also, to make measurements at various temperatures, a thermostat equipped with a suitable sample holder was used. After a series of trial measurements the following procedure was evolved and employed routinely:

1 The optical density of the instrument with no reference beam attenuation and no sample was recorded. If this record was a reasonable straight line then,

2 The sample was placed in the thermostat and adjusted so that the direction of the incident beam was always normal to the < 110 > plane of the crystal and there this assembly was allowed to equilibrate.

3 When this condition was realized, attempts were made to determine the mode of scanning the spectrum of this particular sample. These attempts were those that correspond to determining what filters were to be used to obtain a measurable signal throughout the wavelength region of the instrument. The results of these attempts would be the subdivision of the whole wavelength region of the instruments into a set of wavelength intervals. For each interval a neutral density filter was used to give the best scan of the spectrum for that interval.

Once the spectrum of the sample was recorded, the same experiment was repeated on the following day to see if these results were reproducible. The number of samples employed in these experiments was about 80.

B. EXPERIMENTAL RESULTS AND DISCUSSION

From the results obtained from the above described measurements, only certain records were chosen for presentation in this report as representative of all the records taken. These results are presented graphically where the ordinate is the optical density and the abscissa is in electron volts. The range is restricted to those values from one to four electron volts. First in the order of presentation is a set of two records (optical density versus electron volts) for unpolished or natural crystals at room temperature with the direction of the incident beam perpendicular to the < 110 > face and these curves are given in Figures 41 and 42, respectively. Examination of these two curves reveals certain features: the shapes of the two curves are approximately the same; the intercepts on the electron volt axis of the maximum slope of the optical density are 2.78 and 2.?7 eV; both curves show a slight maximum at 3.12 eV. Second in the order of presentation is a set of curves for samples of crystals that have been ground and polished with half micron diamond paste and Linde "A" compound. The data displayed in these curves were obtained at room temperature. These curves are given in Figures 43 and 44. Examination of these curves reveals certain features: the shapes are not as similar as in the case of the first set; the intercepts on the electron volt axis of the maximum slopes of these curves have values of 2.58 and 2.44 eV, respectively; and both curves have a maximum at 3.15 and 3.12 eV, respectively. Furthermore, the maximum in Figure 44 is more defined than in Figure 43. The comparison of the two sets of curves reveals that the curves have approximately the same shape, the intercept of the maximum slope of the curve on the electron volt axis on the average is 2.55 eV, and a maximum at 3.10 eV. Examination of other curves than the one presented above shows the maximum at 3.1 eV. Thus, the above cited features are common for the unpolished and polished crystals.

The presence of the maximum at 3.1 eV suggested experiments on its temperature dependence. Measurements were made on some samples for three temperatures, i.e., liquid nitrogen, room temperature, and 250°C. Third in the order of presentation is a set of curves for a sample that has been ground and polished with half micron diamond paste and Linde "A" compound. The three curves are presented in the following figures: Figure 45 is the curve for room temperature; Figure 46 is the one for liquid nitrogen temperature; and Figure 47 has the one for 250°C. For the region between 1.5 eV to approximately 3.5 eV the optical densities show a trend given by the following inequality:

$$D_{250°C} > D_{\text{room temperature}} > D_{\text{liquid nitrogen temperature}}$$

where

$D_{250°C}$ is the optical density at 250°C, etc.

For the region from 3.5 eV and greater, the trend is given by the following inequality:

$$D_{\text{liquid Nitrogen}_2} > D_{250°C} > D_{\text{room temperature}}$$

Nevertheless, all three curves have a maximum at 3.10 eV. This maximum changes slightly with a change in temperature. So does the intercept of the maximum slope of the optical density curves. Their values are given below:

1 2.62 eV for 250°C

2 2.80 eV for room temperature

3 2.87 eV for liquid nitrogen temperature

The above paragraphs have listed the values of the intercept of the maximum slope of the optical density curves on the electron volt axis for the sole purpose of giving an intuitive idea of the onset of absorption of energy, and thus form a basis for speculating what the order of magnitude of the band gap may be. However, it must be realized that for the type of experiment discussed, the percent transmission or fraction of light transmitted through a slab of the crystal (parallelopiped)(optical path t) is given by

$$\frac{I}{I_o} = \frac{(1 - R)^2 \exp(-Kt)}{1 - R^2 \exp(-2Kt)}$$

here I is the intensity of the transmitted light, I_o is the intensity of the incident beam, R is the reflectivity and t is the thickness or the optical path. This equation is valid for multiple reflections inside the samples, and requires that t be large compared to the wavelength of light and that the beam be monochromatic. The equation is not valid when t is numerically comparable to the wavelength of light in such a way that interference effects among multiply reflected beams takes place. Furthermore, K is the the absorption coefficient of the material and is related to the absorption index k where $K = 4\pi k/\lambda$, and λ is the wavelength of light. Thus, since in any practical transmission measurements on semiconductors

$k^2 << n^2$ (refractive index), the average fraction transmitted is approximated by

$$\frac{I}{I_o \text{ avg}} \simeq (1 - R)^2 \exp(-Kt).$$

Here the 1 - R term is allowed for by calculating R if the index of refraction is known. To connect this relation of K with optical density D, one notes that $D \equiv \log_{10} (I_o/I)_{avg}$. Then the expression for the absorption coefficient becomes

$$K = \frac{2.303D + 2 \ln (1 - R)}{t}.$$

If R is small compared to one, the value of K will be dominated by D. Thus, the shape of the curve K versus $h\nu$ or λ will to a more or less extent be dominated by that of D. In general, the simplest expression which can be used to represent an absorption curve with an expoential edge is

$$K = K_\infty \left(1 + \exp\left[\alpha(E_o - h\nu)\right]\right)^{-1}$$

where α represents the steepness of the edge. Then if one consideres β-SiC as an ideal system, then according to Fan (Reference 1) the absorption is given by

$$K = \frac{\pi e^2}{nm} f_{ij} N(E)$$

where f_{ij} is the oscillator strength for the transition, N(E) is the density of states function which is the main parameter. For this case N(E) is discontinuous; being zero for the conduction band when E is below the bottom of the band and finite for E above it. But, for a practical material, N(E) is not discontinuous; it would seem reasonable to define the band edge as the point at which N(E) changes rapidly with E, thus implying that dN(E)/dE is a maximum. Then, correspondingly, the absorption edge is defined as the point where the slope of the absorption coefficient is a maximum. This implies that a value of E or λ is found for which dK/dE or $dK/d\lambda$ is a maximum. Some suggestion of this value of E in this report is given by specifying the value of the intercept of the maximum slope of the optical density curve on the electron volt axis. This value on the average is 2.5 eV and is higher than some of the values quoted by other investigators (e.g., Reference 2). Note that there are no data from photoconductivity experiments to support this estimate and that reflection correction was assumed not to affect the value of K greatly.

It is interesting to compare the value given with that obtained from theoretical considerations. Kobayashi (Reference 3) was the first to consider the band structure of β-SiC employing the orthogonal plane wave method. He predicted that the maximum of the valence band is at the center of the reduced Brillouni Zone, k = (000), labelled as $\Gamma^{(15)}$ and the minimum of the conduction band at k = $2\pi/a$ (100), labelled as X on the basis of the space group T^2d. He further predicted that there is allowed an indirect transition from the valence band to the conduction band ($\Gamma^{(15)}$ - X) assisted by an X type phonon with an energy change of 2.2 eV and a direct transition from the X point in the valence band to an X point in the conduction band corresponding to about 6 eV. Later, Bassani and Yoshimine (Reference 4) have extended his treatment to combinations of larger number of plane waves and obtained better convergence. They concluded that their results were qualitatively similar to Kobayashi, and they cited the energy change associated with the indirect transition as 2.86 eV. Next Chow and Liu (Reference 5) have taken the results of Bassani and Yoshimine and investigated the effects of relativistic interaction terms, and they found that the inclusion of the relativistic shifts of levels did not change significantly the band structure obtained by non-relativistic calculations (Reference 4). They found that these effects increase with the increase in the atomic numbers of the constituent atoms. They presented their results, which are given in the following table.

TABLE IV

Energy Gaps (in eV) for β-Sic

Indirect Gap	ΔE
$\Gamma^{(15)}_{val} \rightarrow X^{(1)}_{cond}$	2.8
Direct Gap at Γ	6.7
Direct Gap at X	5.8
Direct Gap at L	9.9

Then, on the basis of the theoretical considerations, the value of 2.5 eV is reasonable. As for the temperature variation of this "edge", the estimated value of $dEg/dT \simeq -5.0 \times 10^{-4}$ eV deg^{1}. Thus, the values of the absorption edge and the temperature coefficient of the edge, dEg/dT, are to be accepted as tentative.

So far the considerations have been restricted to the discussion of the absorption spectra in the visible region. For the region corresponding to 0.8 to 1.8μ, the optical density curve versus electron volts did not display any distinct features except for a slight maximum in the neighborhood of 1.4μ. The trace of the spectrum in this region is given in Figure 48. For the region of 1.8 to 2.5μ the preliminary tests indicated that more extensive modifications were required to obtain a measurable signal.

Next, absorption measurements in the region of 2.5 to 25μ were made on various samples. Here a microbeam condenser furnished by the Beckman Instruments Company was used and measurements were made at room temperature. Polished and unpolished samples were used. The trace given in Figure 49 is that of a polished sample and that in Figure 50 is for an unpolished, or natural faced, sample. The results given in these figures agree with those reported by Spitzer, Kleinman, Fresch, and Walsh (Reference 6).

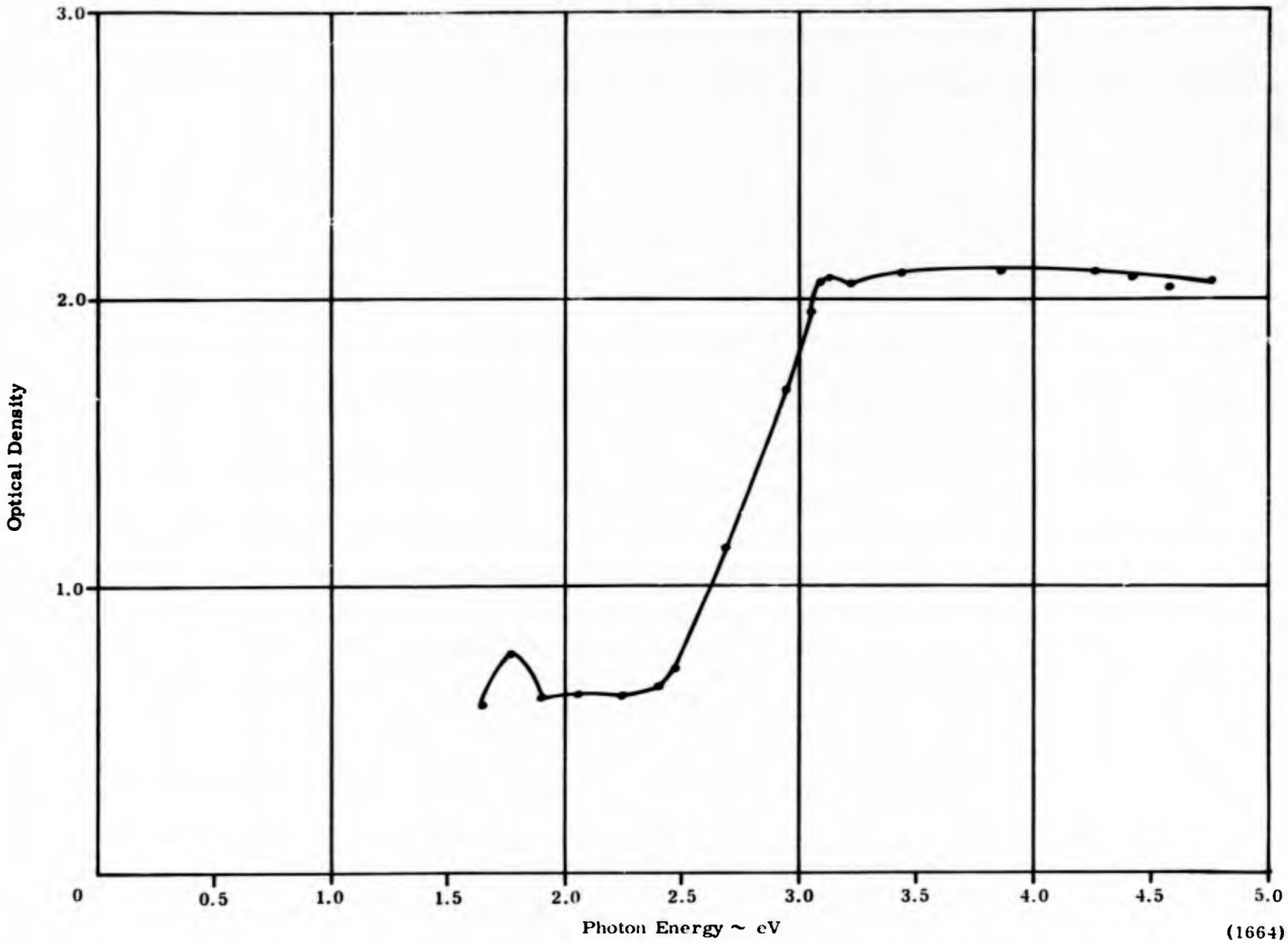

Figure 41. Crystal 78, Optical Density versus Photon Energy, Natural Faces

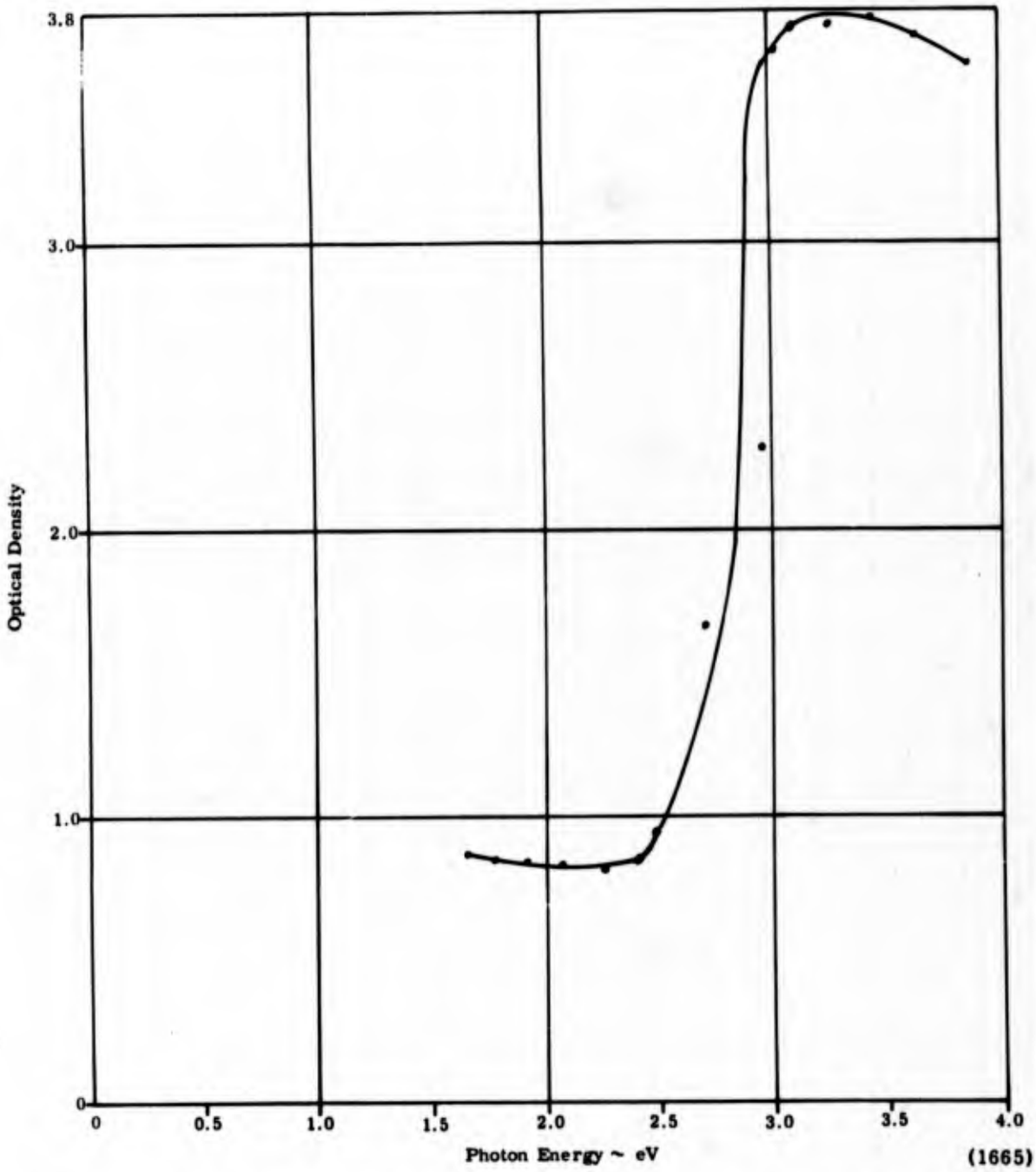

Figure 42. Crystal 75, Optical Density versus Photon Energy, Natural Faces

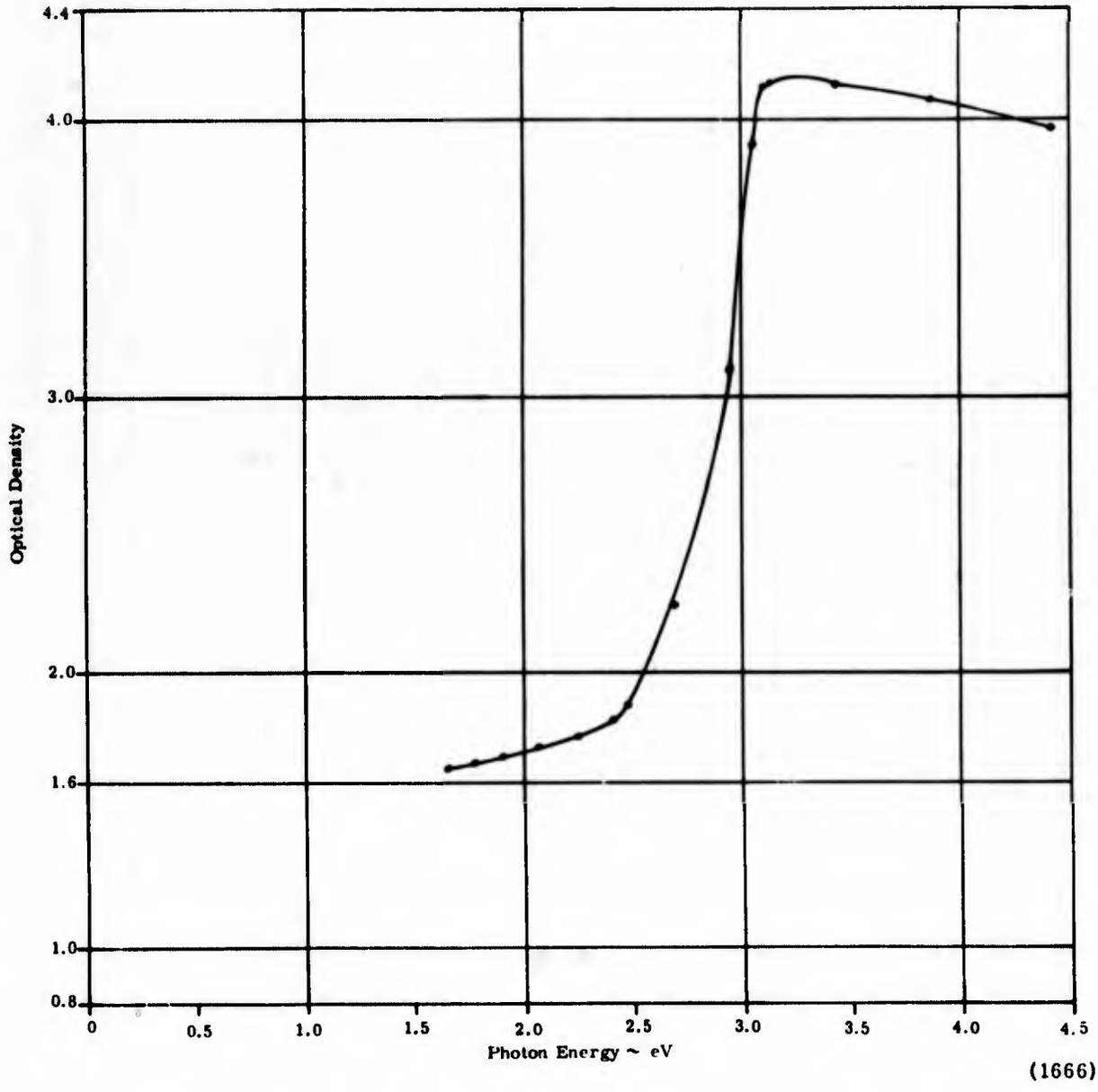

Figure 43. Crystal 35, Optical Density versus Photon Energy, Polished Faces

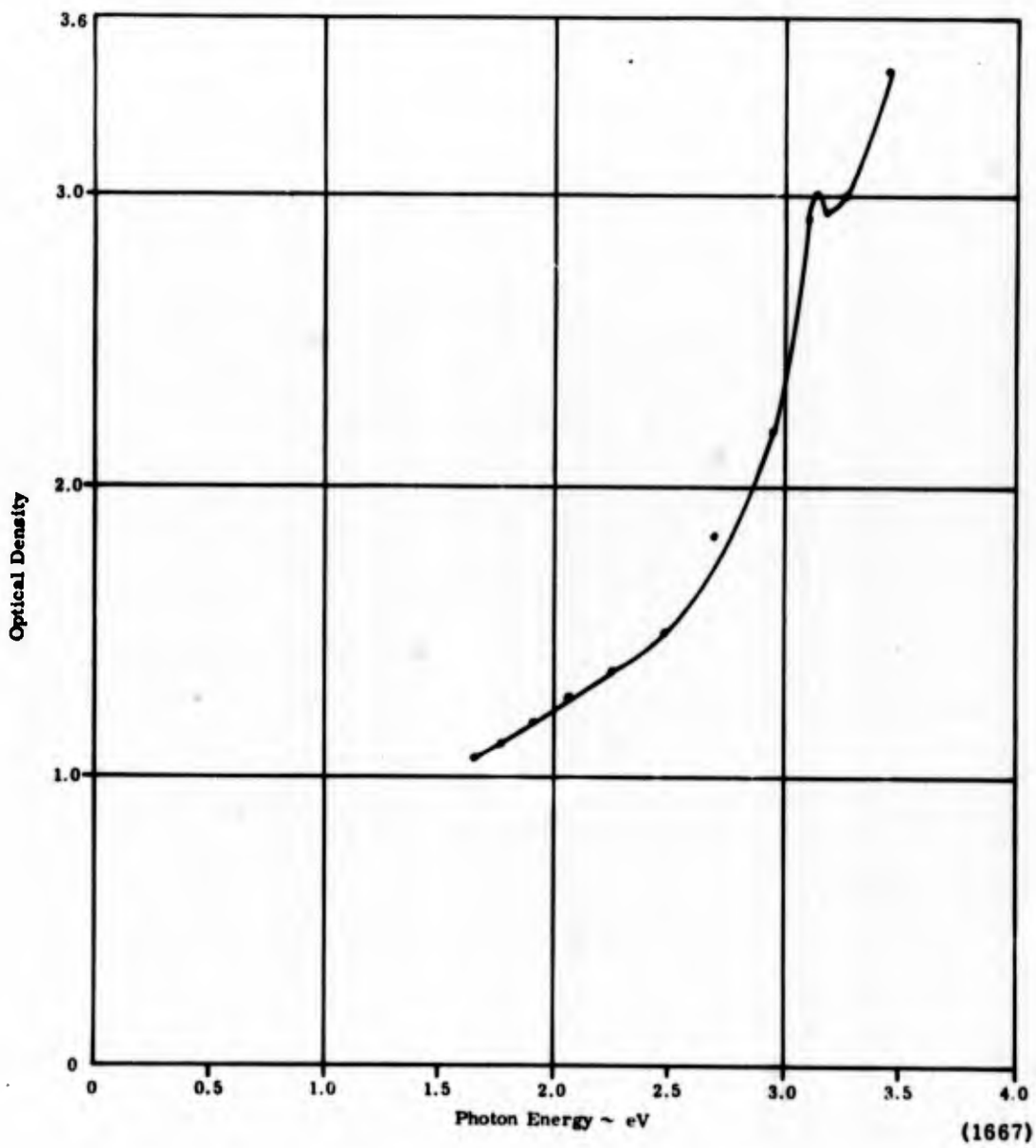

Figure 44. Crystal 79, Optical Density versus Photon Energy, Polished Faces

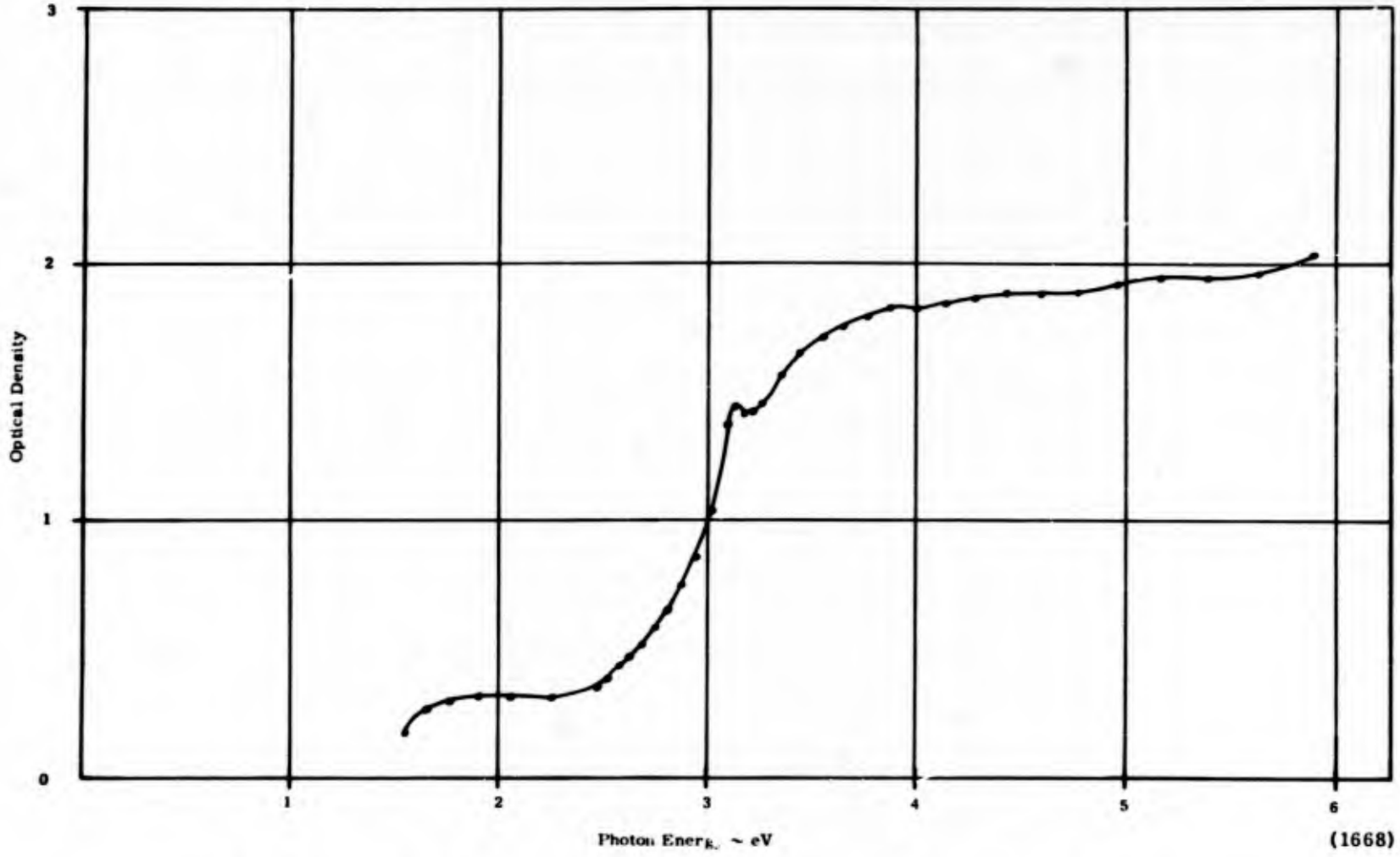

Figure 45. Crystal 19, Optical Density versus Photon Energy, Room Temperature

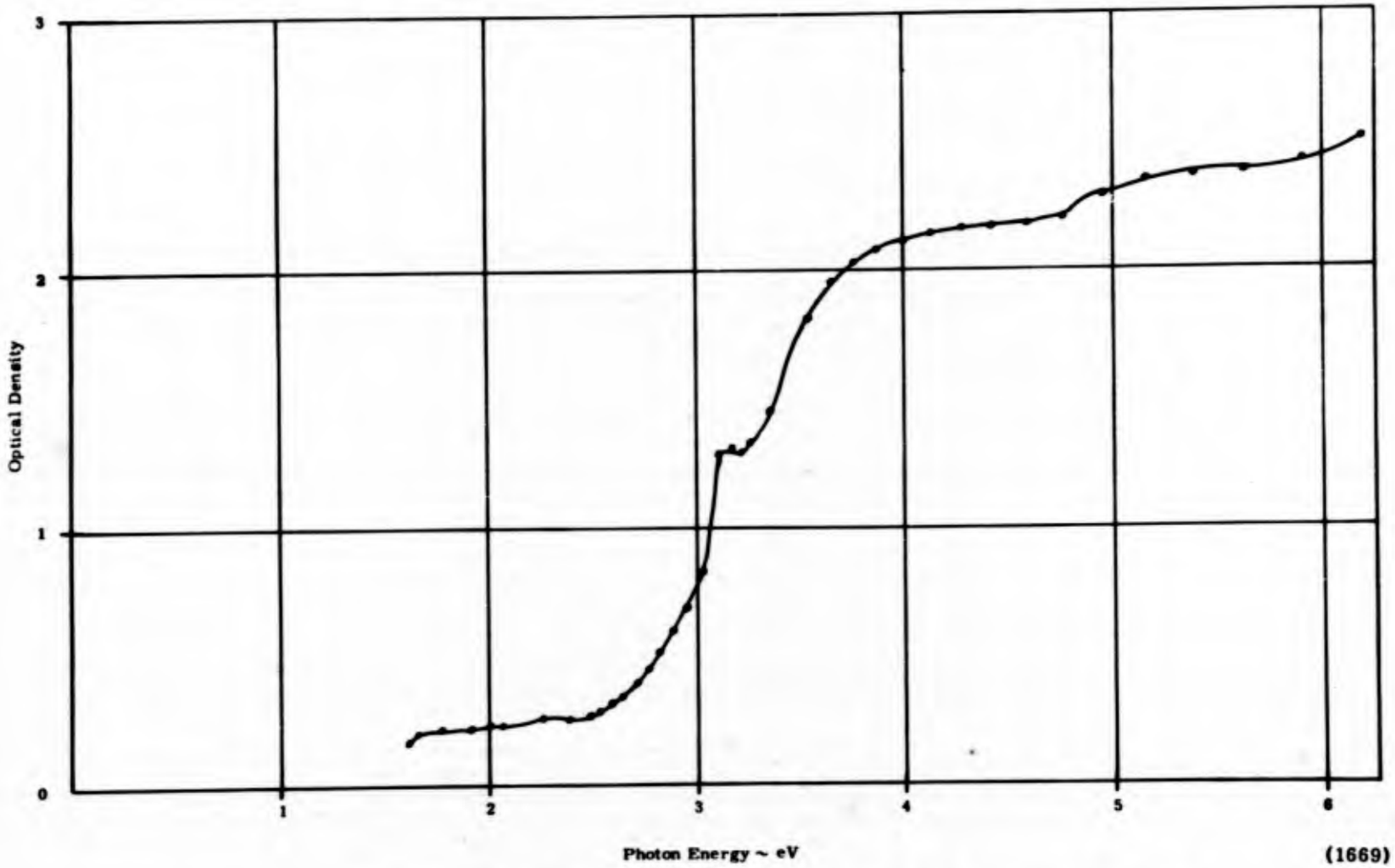

Figure 46. Crystal 19, Optical Density versus Photon Energy, Liquid Nitrogen Temperature

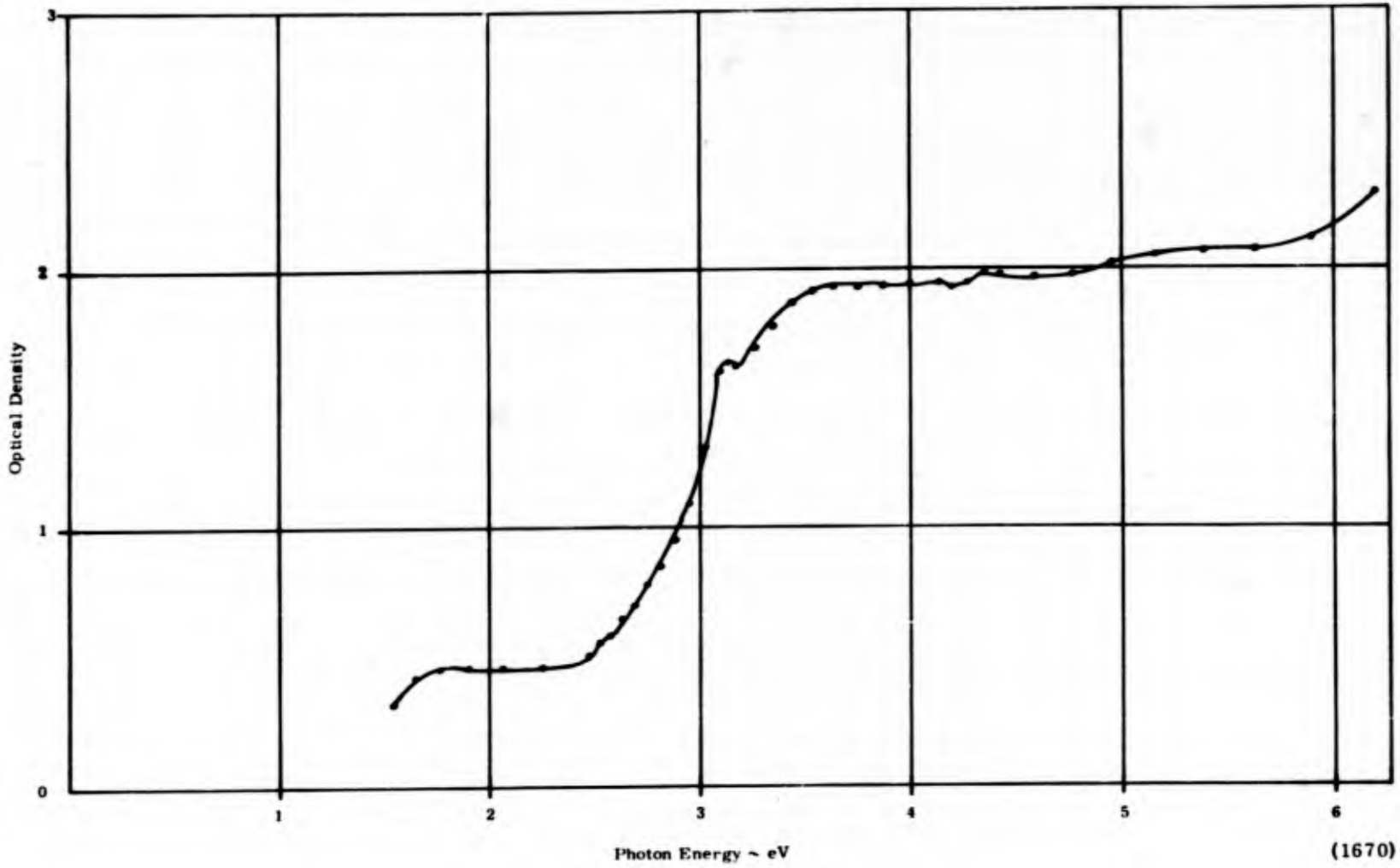

Figure 47. Crystal 19, Optical Density versus Photon Energy, 250°C

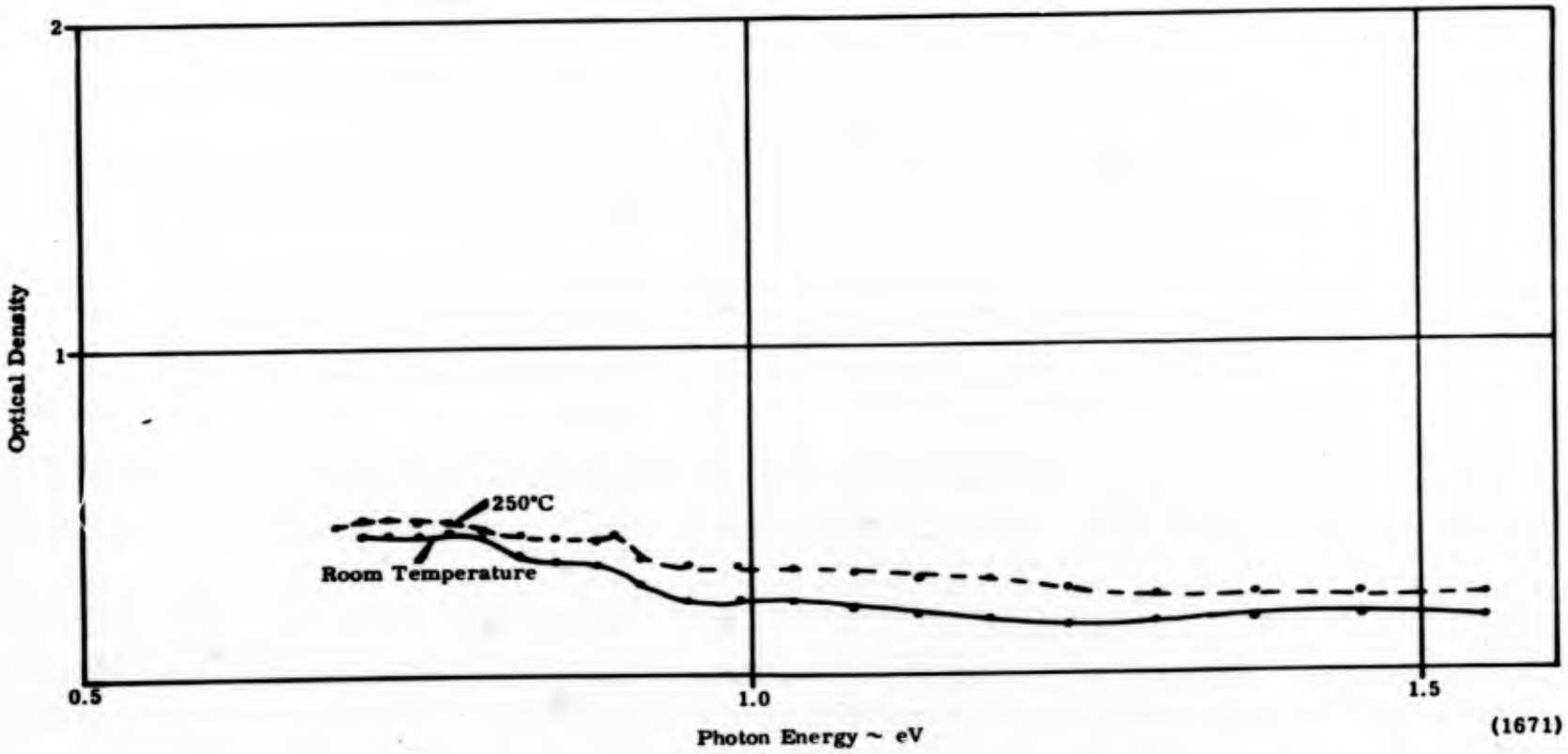

Figure 48. Crystal 19, Optical Density versus Photon Energy, Polished Faces, Near Infrared

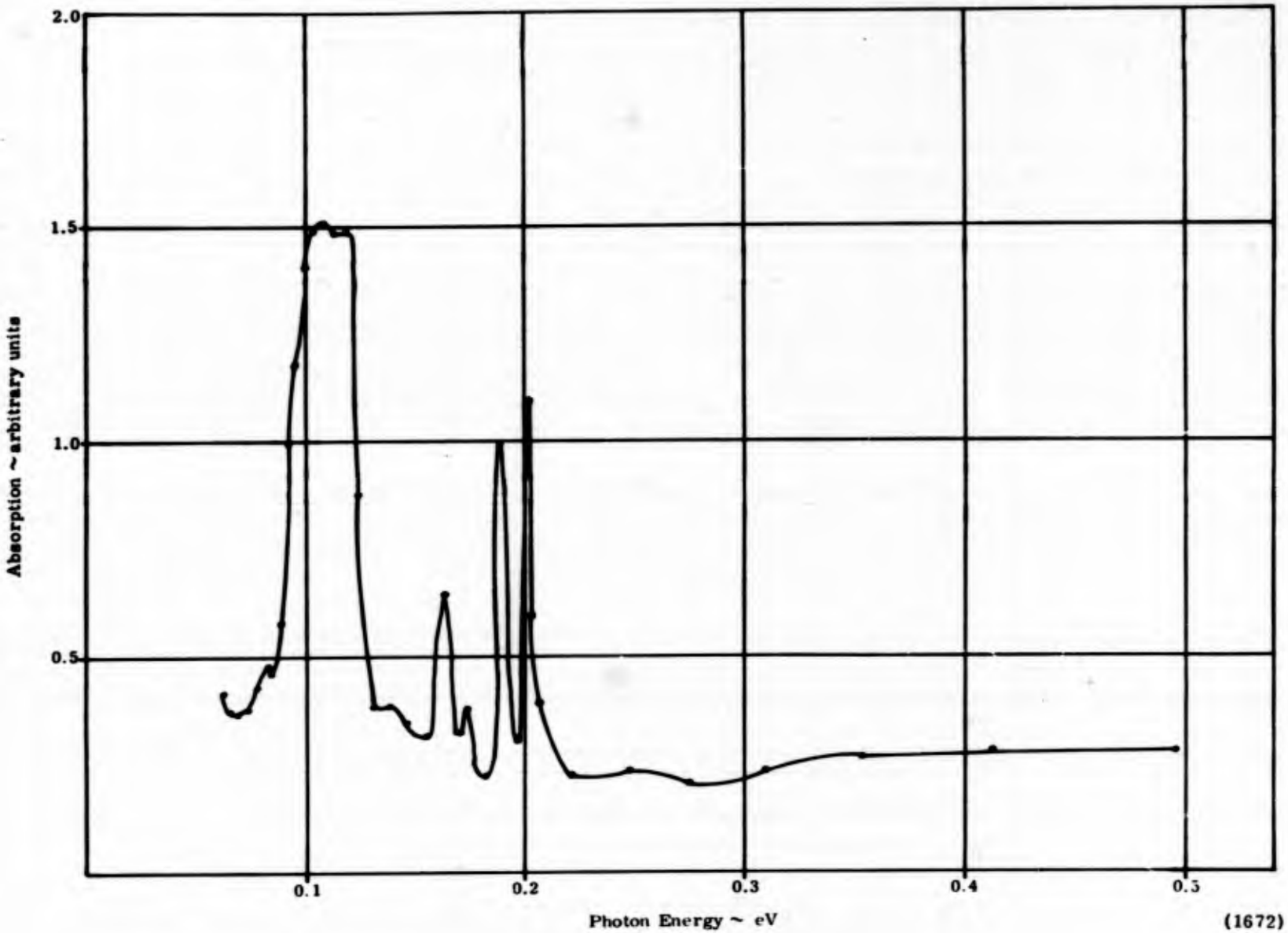

Figure 49. Crystal 58, Absorption versus Photon Energy, Polished Faces, Infrared

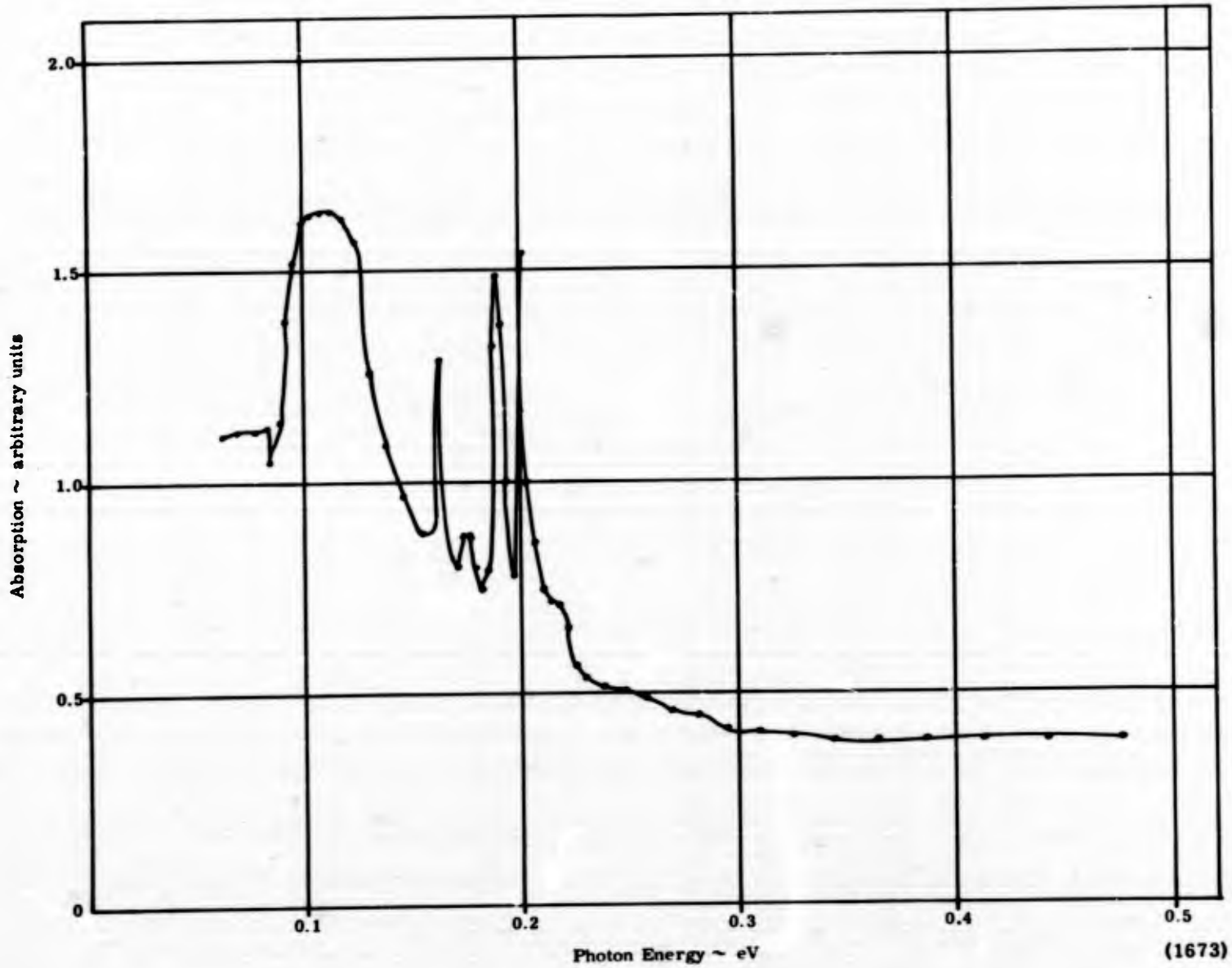

Figure 50. Crystal 54, Absorption versus Photon Energy, Natural Faces, Infrared

IV. REFLECTION SPECTRA

To determine precisely the value of the absorption coefficient K for a given wavelength, it is necessary to determine the reflectivity R given in the previous discussion. Furthermore, this information would serve to determine a more accurate value of the absorption edge if K is known as a function of wavelength. It is also possible to obtain optical constants, refractive index n and absorption index k, from measurements of reflected intensities by methods described by Avery (Reference 7) and others. In this regard it was decided to measure the reflection at various angles of incidence using plane polarized light and solve the Fresnel's equations for reflection. In this way it is possible to determine the refractive index and the absorption index of a material for a wavelength region of interest.

In this section a description of the work that has been done on reflection spectra in the visible is given.

The crystals selected for these investigations were thicker than those used for absorption measurements. These crystals were on the order of 2 millimeters in diameter and approximately 1 millimeter thick to reduce reflection from the backside of the crystal or reduce diffuse reflection. The same technique was used in preparing these crystals for study as that for the absorption measurements. Two faces of a crystal were first ground parallel with 6μ diamond paste. One of these faces was then polished with 0.5 diamond paste followed by a polishing with Linde "A" material. The crystals, just prior to use, were etched in a $HF\text{-}HNO_3$ solution followed by rinses in triply distilled deionized water and finally in alcohol.

The crystals used for these measurements were N type, with the electronic carrier concentration estimated to be on the order of $10^{18}/cm^3$.

To make reflection studies at various angles of incidence, a double crystal x-ray spectrometer was modified so as to mate with the Cary 14R instrument.

The beam from the 14R was collimated by means of a four inch long collimator with a 1 millimeter diameter hole in it. The collimator had a compartment machined into it to hold the polarizers used in the experiment.

The spectrometer was adapted with a jig for holding the crystal, which had three degrees of freedom. This jig was further adapted with a goniometer that held the crystal. The crystal was mounted on a blackened 1 millimeter post which was then inserted into the goniometer. With such an arrangement the crystal could easily be oriented with respect to the incident beam.

The detector was mounted on the stable arm of the spectrometer. A further innovation to the spectrometer was the addition of a driving motor on the tangent arm of the spectrometer. This permitted the crystal to be rotated with respect to the detector for intensity peaking purposes.

The whole spectrometer assembly was mounted in a light tight box, which in turn was mounted on a heavy steel table.

The results obtained to date are given in Figure 51. Here the curves are given for two angles of incidence, namely 50 and 60 degrees. For each angle of incidence two curves are given: one curve is for a given setting of the polarizer to give maximum intensity and the other is for the minimum so as to realize the condition that the plane of polarization for the maximum is perpendicular to the plane of polarization for the minimum. To solve the Fresnel equation the ratio of the reflectivity maximum to that minimum at these two angles of incidence was used. Thus, at 5000 Å for 50 and 60 degrees the ratios are 0.88 and 0.34, respectively. These values yield, on solving the Fresnel equations, $n = 2.27$ and $k = 0.72$. Now, $K = 4\pi k/\lambda = 1.81 \times 10^5 cm^{-1}$ at room temperature. Since time did not permit any further work, the value of the absorption coefficient at room temperature for 5000 Å is $1.81 \times 10^5\ cm^{-1}$ and the refractive index $n = 2.27$.

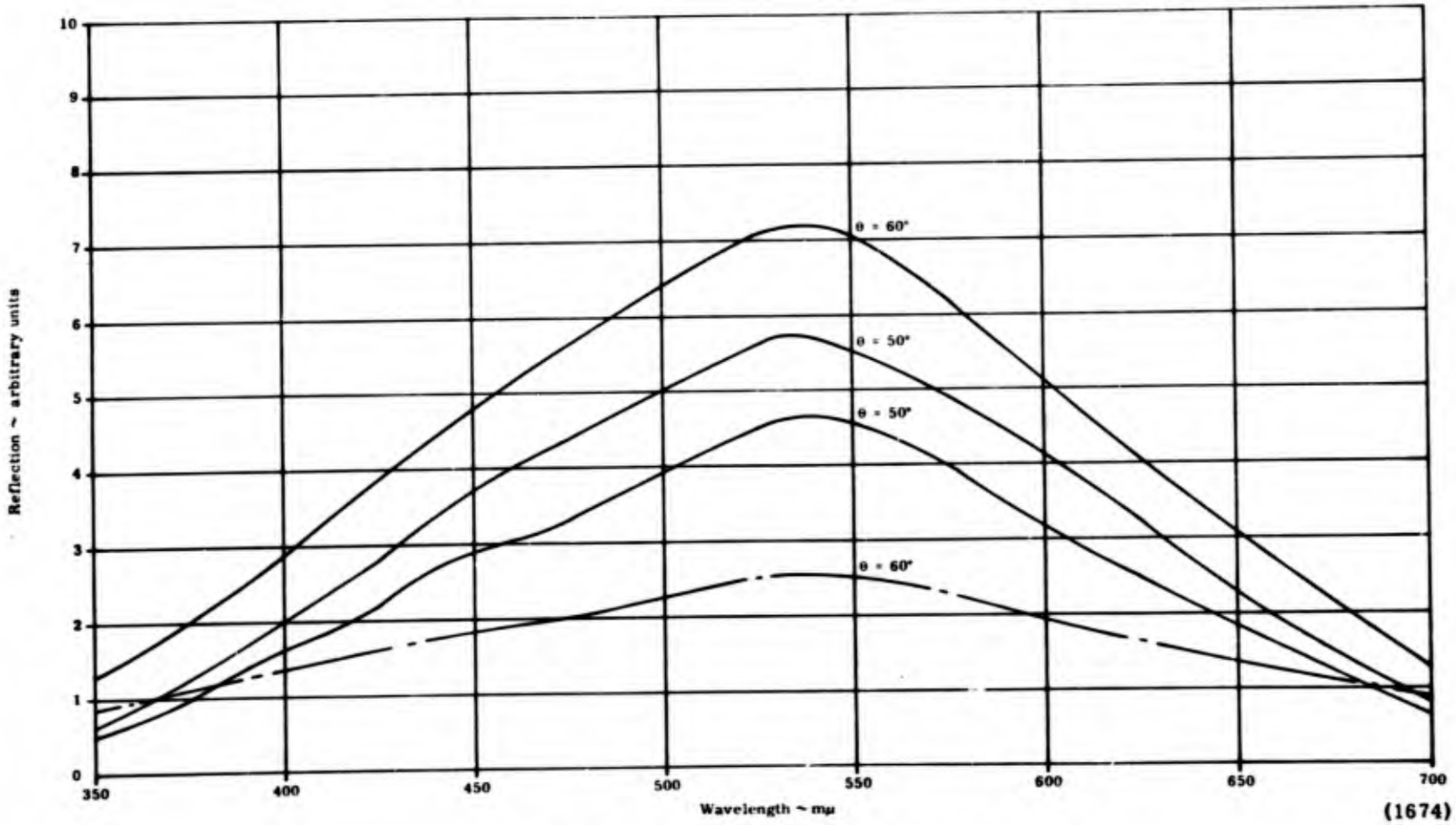

Figure 51. Crystal 84, Reflection Spectra

V. OTHER EXPERIMENTAL STUDIES

A. RADIATION STUDIES

1. Experimental Arrangement

Six β-SiC alloy diodes were fabricated and encapsulated in commercial " top hat " packages for radiation testing. The diodes were assembled, utilizing the latest techniques, but were limited in electrical performance by the low purity of the available crystals.

Three IN 536 and three IN 2974 silicon diodes were chosen as controls to be irradiated with the test diodes. The IN 536 diodes were selected because they were encapsulated in the same package as the β-SiC diodes. However, the PIV of the IN 536 diodes were much higher then the β-SiC diodes. The IN 2974 zener diodes were selected as silicon diodes having comparable breakdown voltage to the β-SiC diodes.

The diodes were irradiated by an advanced Triga type reactor owned by General Atomics located in San Diego, California. All units were electrically tested prior to irradiation.

The following electrical measurements were made on all diodes prior to irradiation and at each of 10 predetermined dosage levels:

1 Forward voltage drop (V_F) at 0.5, 5.0, and 20 mA (I_F);

2 Reverse voltage (V_R) at I_R = 100 μA;

3 Reverse leakage current (I_R) at 2 and 4 Vdc.

Ten dosage levels were selected between 5×10^{14} and 5×10^{17} nvt.

2. Experimental Results and Discussion

Figures 52, 53 and 54 show the average result of three units of each type and the effects of increasing radiation on these electrical parameters. A discrepancy is apparent in the IN 536 diodes, two units

terminating in an open condition while one shorted. Therefore, both results were plotted.

The stability of the β-SiC diodes up to a level of 10^{17} nvt is readily apparent. The IN 536 diodes were grossly affected at the first radiation level (5×10^{14} nvt).

The IN 2974 diodes show increasing degradation. The forward bias operation of diodes during irradiation had no effect on the results obtained.

The method of degradation appears to be the introduction of p-type acceptor levels by fast neutron bombardment. This is indicated by all units except the two IN 536 diodes which became electrically open. Therefore, final conclusions cannot be drawn until all the units are returned and extensively examined electrically and mechanically.

It is apparent from these preliminary results that the β-SiC diodes of this test remained stable to radiation dosage up to 1×10^{17} nvt, which is about two orders of magnitude greater than silicon or germanium diodes.

B. PHOTOLUMINESCENCE

Spectral measurements of the photoluminescence of β-SiC were made only for samples at liquid nitrogen temperatures, since no photoluminescence was visible from room-temperature samples. Measurements were made on two groups of five samples each; within a given group, the samples were required to be identical photoluminescent color as determined visually with 60X magnification.

In preparing to make measurements on a given group, the samples from that group were attached to a fused silica rod with a minute amount of styrene cement. This assembly was then immersed in liquid nitrogen in a fused silica dewar flask that had an unsilvered section for illumination and observation. Ultraviolet light from an Osram Hg (selected by Corning 5-57 and 7-60 glass filters in series) was focused by a quartz lens onto the samples. A portion of the photoluminescence was collected by a glass doublet lens and imaged on the slit of a Martin-built 1-m spectrograph. This spectrograph, with a 600 line/mm grating, was set up to record on Kodak 103a-F spectrographic film any emission between approximately 4000 Å and the film 's cutoff (approximately 6700 Å), with a resolution of better than 1 Å.

The results, shown in Figure 55, are derived from measurements of exposed film transmission by a Jarrell-Ash recording microdensitometer. These data are not corrected for film response. Resolution is better than 10 Å. Curves A and B in Figure 55 refer to a 2 1/2-hour exposure to the photoluminiscence from a group consisting of samples 3, 5, 6, 7 and 8. Curve A was taken from the midsection of the film strip and curve B from an edge. The "slit height" setting was 1.6 and the "slit width" setting 2.0. Curve C refers to a 6 1/2-hour exposure to the photoluminescence from a group consisting of samples 16, 17, 19, 21 and 22 taken from the center of the exposure. The slit height setting was 2.0 and the slit width setting 10.0.

The photoluminescence bands of β-Sic observed at liquid nitrogen temperatures do not correspond to those of W. J. Choyke, et al (Reference 8) at liquid helium temperature. This lack of comparison is consistent with the results of Lampert 's study of the exciton complexes, he suggested on the basis of his studies, that the luminescence of the nitrogen exciton complexes should be observable at liquid helium temperatures. Moreover, this was shown experimentally by Choyke et al. In the latter investigations, however, some lines have been seen at lower photon energy. These may agree with those we observed at liquid nitrogen temperature and thought were due to simultaneous emission of photons and two phonons and other bands that may appear to be due to one-phonon transitions which leave the nitrogen donor in the excited state. Nevertheless, they did not list these bands. Consequently, no comparison was possible.

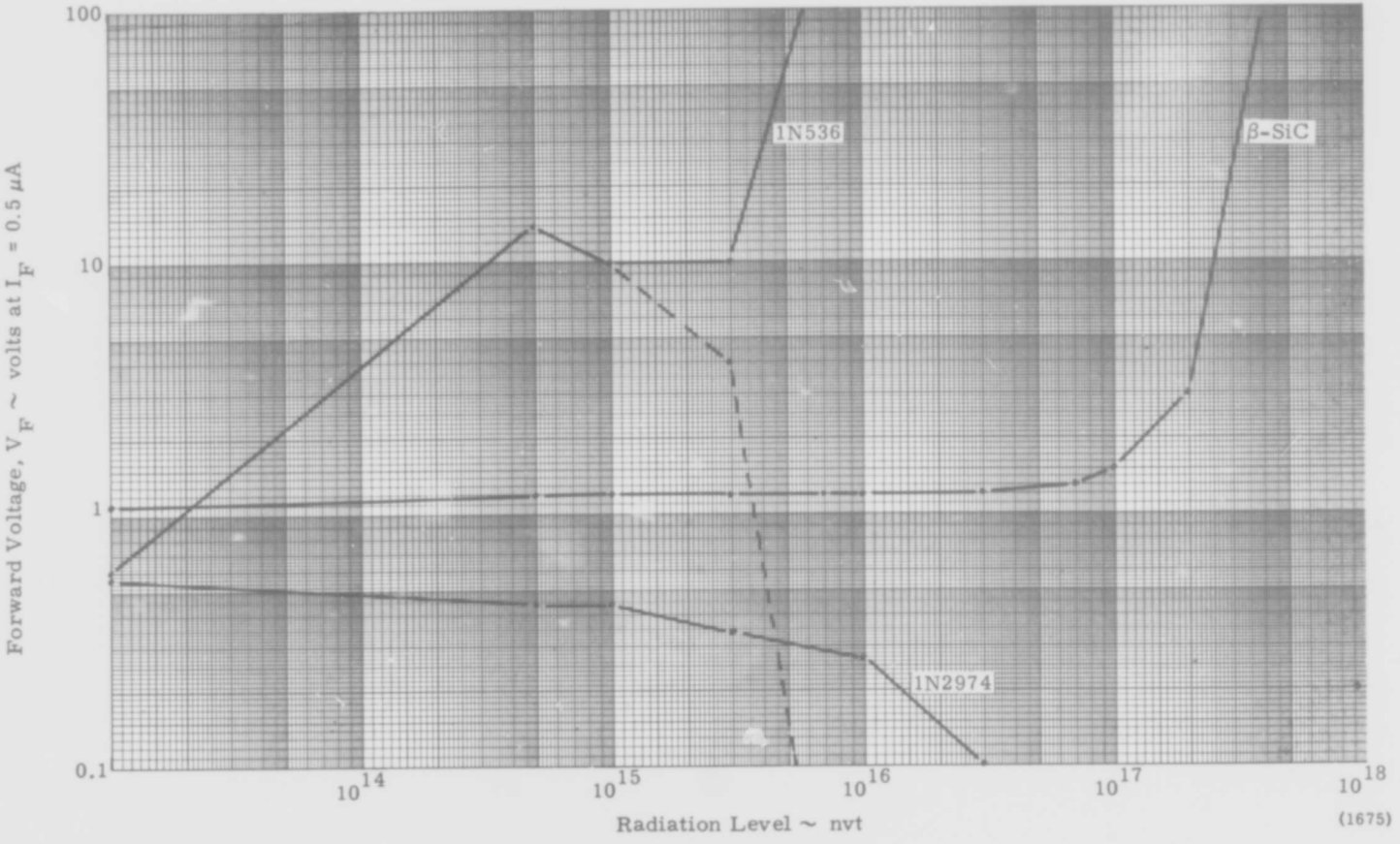

Figure 52. Radiation Effects on Forward Voltage

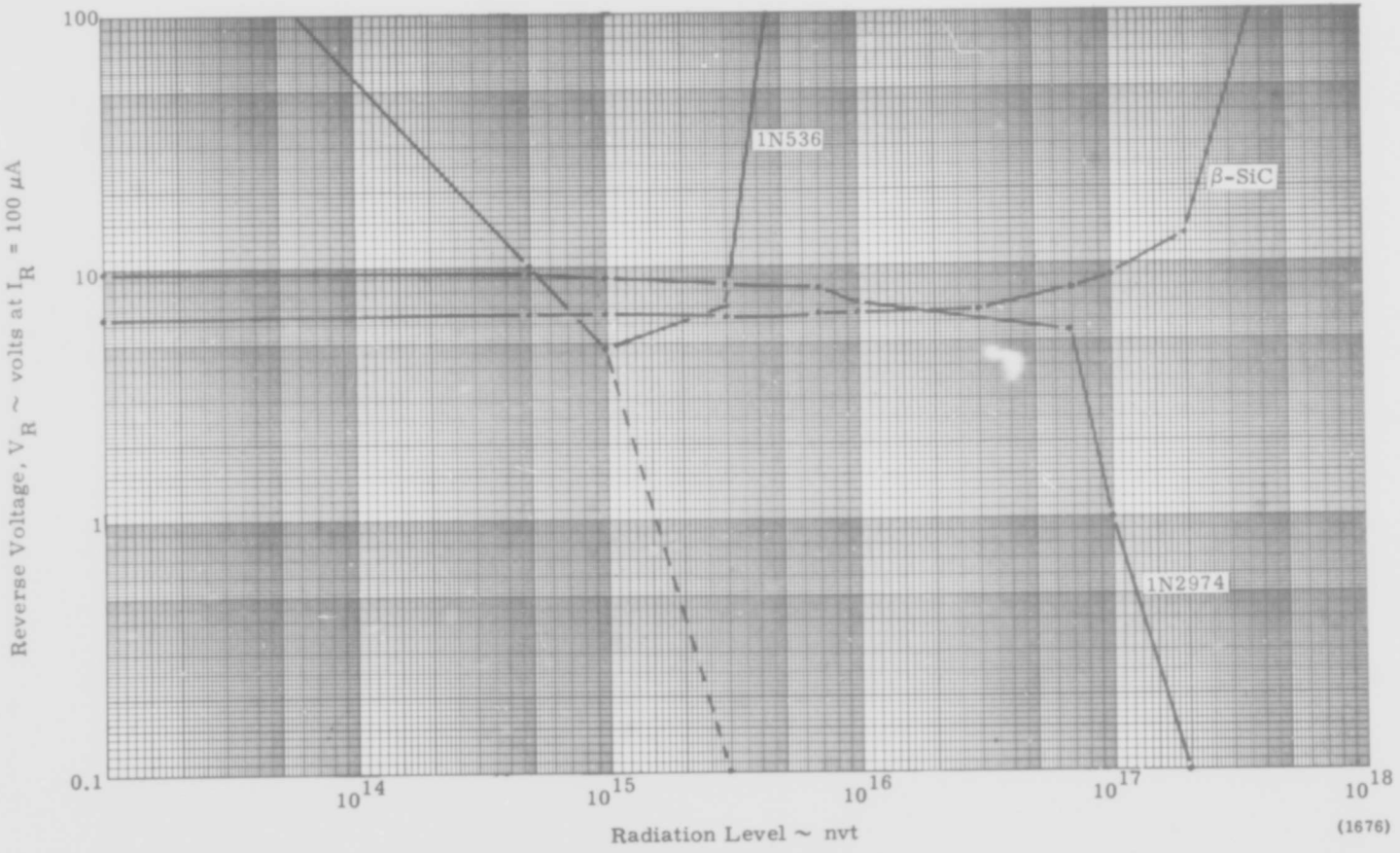

Figure 53. Radiation Effects on Reverse Voltage

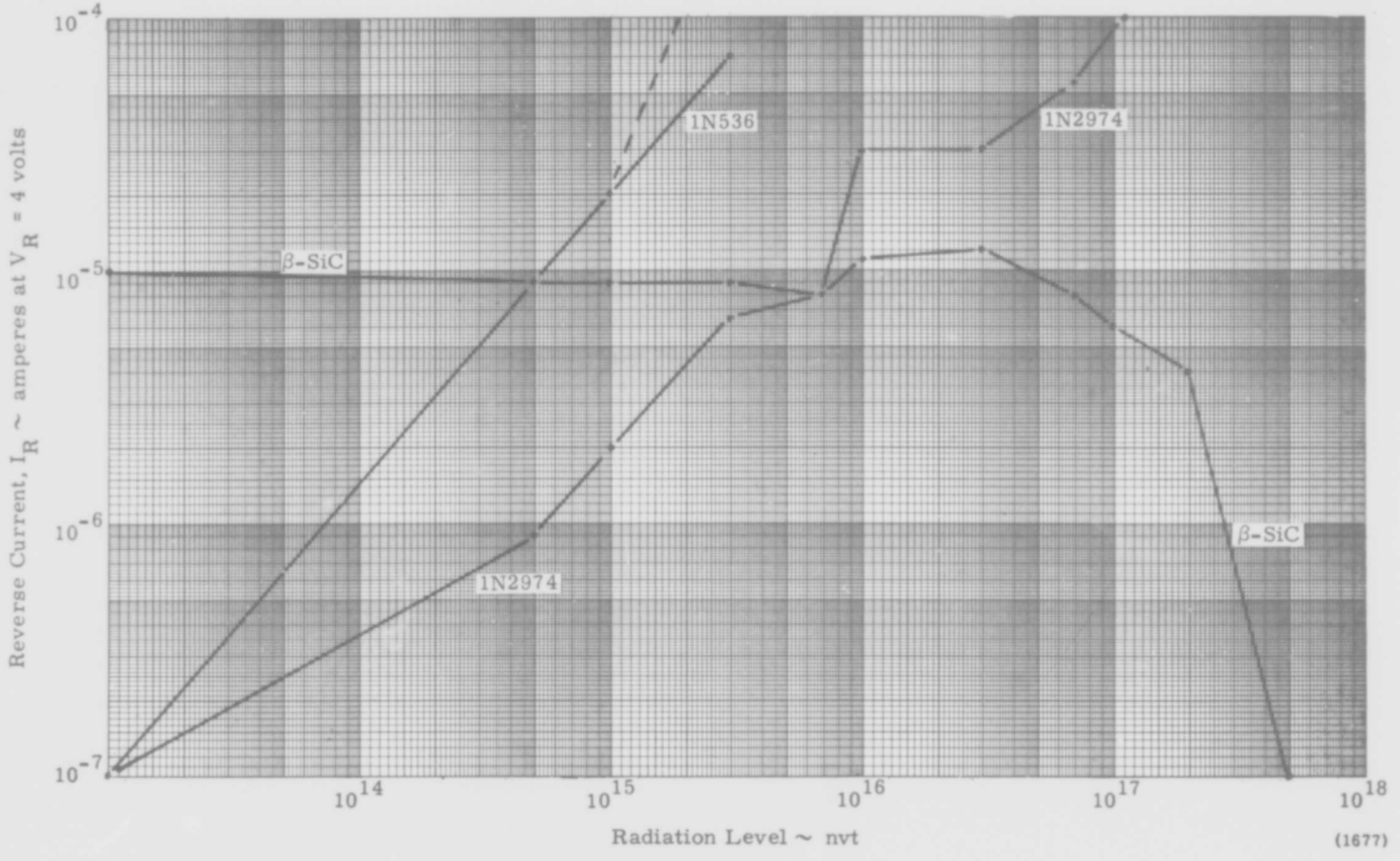

Figure 54. Radiation Effects on Reverse Leakage Current

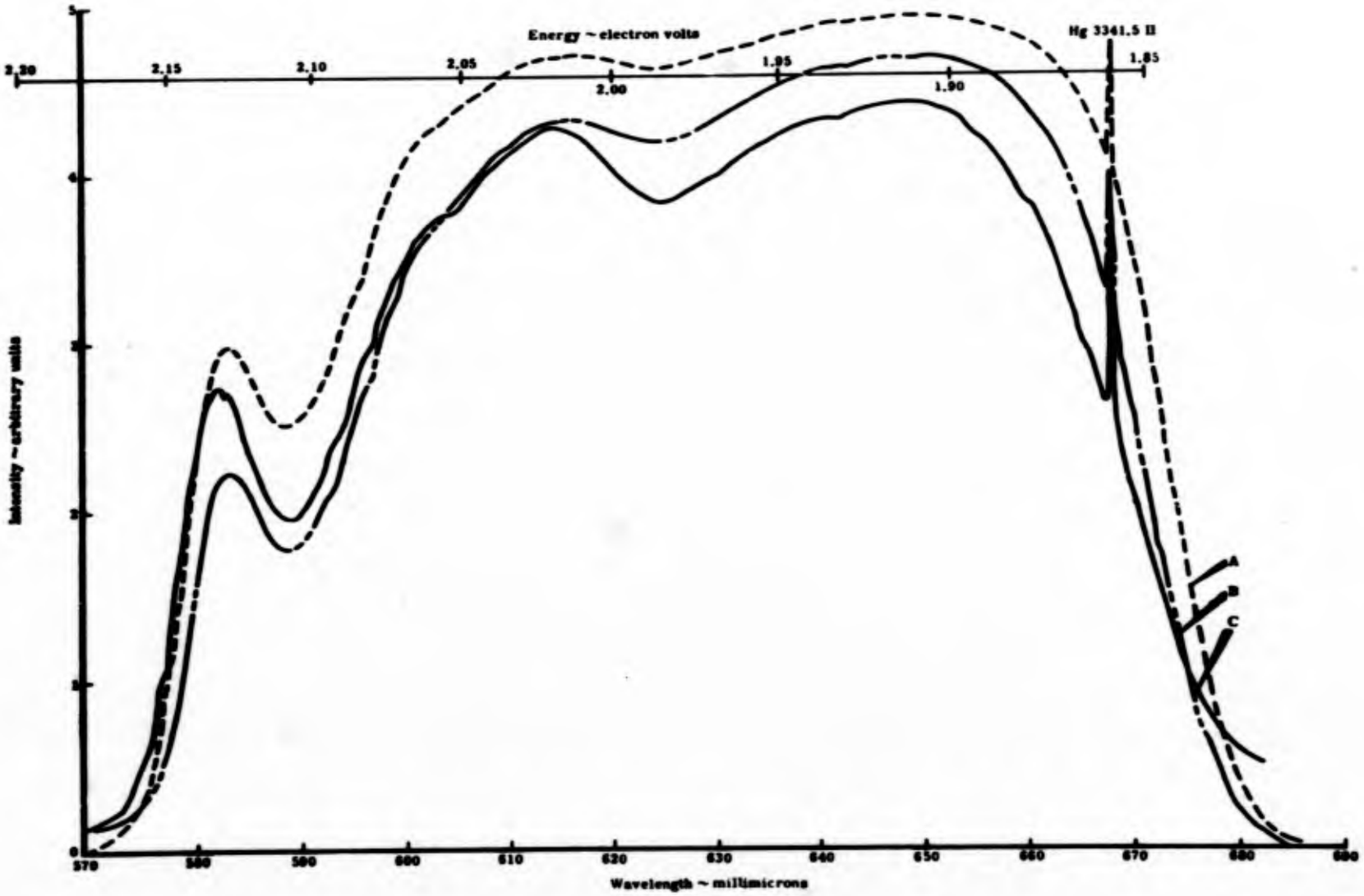

Figure 55. Photoluminescence at Liquid Nitrogen Temperature

APPENDIX

HALL EFFECTS

Hall effects studies were made using the standard techniques as well as the method of Van der Pauw (Reference 9) for samples of arbitrary shape. The electronic carrier concentrations were found to lie in the region of 10^{17} to $10^{19}/cm^3$, depending upon the conditions under which the crystals were grown. Hall coefficients were found to range from 50 to 75 cm^2/volt sec. Resistivities were found to range from 0.1 to 1.0 ohm-cm.

EFFECTIVE MASS

Best estimate of "effective mass" through courtesy of R. McMillan private communication.

Preliminary measurements employing cyclotron resonance show an effective mass given by $m^*/m = 0.41 \pm 0.04$. Measurements were made at 70 kMc; the magnetic field was perpendicular to the <110> planes during the measurements.

THERMAL CONDUCTIVITY

The thermal conductivity (Reference 10) at room temperature has been calculated to be

$$K_{(room)} = 0.1 \text{ to } 0.2 \text{ W/cm-deg.}$$

The dielectric constant is given as approximately 10.0 (Reference 11).

DEBYE TEMPERATURE

The Debye temperature (Reference 12) for β-SiC is approximately 1430°K.

REFERENCES

1. Fan, H. Y., Rep Prog Phys, Vol 19, p 107 (1956)
2. Dalven, R., J Phys Chem Solids, Vol 26, p 439 (1965)
3. Kobayasi, S., J Phys Soc (Japan), Vol 13, p 261 (1958)
4. Bassani, F., and Yoshimine, M., Phys Rev, Vol 130, p 20 (1963)
5. Chow, P. C. and Liu, L., Phys Rev, Vol 140A, p 1817 (1965)
6. Spitzer, W. G., et al, Phys Rev, Vol 113, pp 127 and 133 (1959)
7. Avery, D. G., Proc Phys Soc, Vol 65B, p 425 (1952)
8. Choyke, W. J. et al, Phys Rev, Vol 133A, p 1163 (1964)
9. Van der Pauw, L. J., Phillips Res Repts, Vol 13, p 1 (Feb 1958)
10. Slack, G. A., J Appl Phys, Vol 35, p 3460 (Dec 1964)
11. Silicon Carbide, Ed by O'Connor and Smiltens, W. G. Spitzer, et al, p 354, Pergamon Press (1960)
12. Silicon Carbide, Ed by O'Connor and Smiltens, A. Taylor and P. M. Jones, p 153, Pergamon Press (1960)